PB84-179886

Fundamental Study of Sulfate Aerosol Formation, Condensation, and Growth

Air Pollution Technology, Inc., San Diego, CA

Prepared for

Industrial Environmental Research Lab.
Research Triangle Park, NC

Mar 84

U.S. Department of Commerce
National Technical Information Service
NTIS

PB84-179886

EPA-600/7-84-049
March 1984

FUNDAMENTAL STUDY OF SULFATE AEROSOL FORMATION CONDENSATION AND GROWTH

by

Shui-Chow Yung, Cumbum N. Rangaraj, Benjamin L. Hancock,
Daniel Ugale, and Seymour Calvert

A.P.T., Inc.
5191 Santa Fe Street
San Diego, CA 92109

EPA Contract No. 68-02-3650
Project Officer: Leslie E. Sparks
Industrial Environmental Research Laboraory
Research Triangle Park, NC 27711
Prepared for:
U.S. Environmental Protection Agency
Office of Research and Development
Washington, D.C. 20460

INDUSTRIAL ENVIRONMENTAL RESEARCH LABORATORY
OFFICE OF RESEARCH AND DEVELOPMENT
U.S. ENVIRONMENTAL PROTECTION AGENCY
RESEARCH TRIANGLE PARK, NC 27711

REPRODUCED BY
NATIONAL TECHNICAL
INFORMATION SERVICE
U.S. DEPARTMENT OF COMMERCE
SPRINGFIELD, VA. 22161

TECHNICAL REPORT DATA

(Please read Instructions on the reverse before completing)

1. REPORT NO.
EPA-600/7-84-049

2.

3. RECIPIENT'S ACCESSION NO.
PB8[illegible] 179886

4. TITLE AND SUBTITLE
Fundamental Study of Sulfate Aerosol Formation, Condensation, and Growth

5. REPORT DATE
March 1984

6. PERFORMING ORGANIZATION CODE

7. AUTHOR(S)
S-C Yung, C. N. Rangaraj, B. L. Hancock, Daniel Ugale, and Seymour Calvert

8. PERFORMING ORGANIZATION REPORT NO.

9. PERFORMING ORGANIZATION NAME AND ADDRESS
A. P. T., Inc.
5191 Santa Fe Street
San Diego, California 92109

10. PROGRAM ELEMENT NO.

11. CONTRACT/GRANT NO.
68-02-3650

12. SPONSORING AGENCY NAME AND ADDRESS
EPA, Office of Research and Development
Industrial Environmental Research Laboratory
Research Triangle Park, NC 27711

13. TYPE OF REPORT AND PERIOD COVERED
Final; 10/80 - 9/82

14. SPONSORING AGENCY CODE
EPA/600/13

15. SUPPLEMENTARY NOTES
IERL-RTP project officer is Leslie E. Sparks, Mail Drop 61, 919/541-2925.

16. ABSTRACT

The report gives results of a study of the formation and growth of sulfate particles. Existing theoretical models on acid particle formation and growth were reviewed and evaluated. The formation and growth of sulfate particles during slow cooling, rapid cooling, and dilution cooling of flue gas were experimentally determined and compared with theories. The experimental results show that the temperature at which the self-nucleation of sulfuric acid occurs is lower than the acid dew point temperature. Thus, if the flue gas is slowly cooled to between dew point and nucleation temperatures, it is possible to force the sulfuric acid to condense out on surfaces, rather than form fine particles. The theories, experimental methods, and results are described.

17. KEY WORDS AND DOCUMENT ANALYSIS

a. DESCRIPTORS	b. IDENTIFIERS/OPEN ENDED TERMS	c. COSATI Field/Group
Pollution Flue Gases Sulfates Aerosols Particles Condensing Cooling	Pollution Control Stationary Sources Particulate	13B 21B 07B 07D 14G 20M

18. DISTRIBUTION STATEMENT
Release to Public

19. SECURITY CLASS *(This Report)*
Unclassified

20. SECURITY CLASS *(This page)*
Unclassified

21. NO. OF PAGES
187

22. PRICE

EPA Form 2220-1 (9-73)

NOTICE

This document has been reviewed in accordance with U.S. Environmental Protection Agency policy and approved for publication. Mention of trade names or commercial products does not constitute endorsement or recommendation for use.

Abstract

A theoretical and experimental program was performed to study the formation and growth of sulfate particles. Existing theoretical models on acid particle formation and growth were reviewed and evaluated. The formation and growth of sulfate particles during slow cooling, rapid cooling, and dilution cooling of flue gas were experimentally determined and compared with theories.

The experimental results show that the temperature at which the self-nucleation of sulfuric acid occurs is lower than the acid dew point temperature. Thus, if the flue gas is slowly cooled to between dew point and nucleation temperature, it is possible to force the sulfuric acid to condense out on surfaces rather than forming fine particles.

The theories, experimental methods, and results are described in this report.

TABLE OF CONTENTS

Page

Abstract iii
Figures v
Tables ix
Nomenclature xi
Acknowledgment xvii

Sections

1. Summary and Conclusions 1
   Summary 1
   Comparison Between Theory and Experiments 5
   Control Strategy Implications 6
   Conclusions 7
2. Introduction 8
3. Literature Review 10
4. Experimental Approach 45
   Flue Gas Simulator 46
   Sampling and Analysis Methods 53
   Instrument Calibration 66
5. Experimental Results 79
   Rapid Quenching Experiments 79
   Dilution Cooling Experiments 94
   Slow Cooling Experiments 104
6. Comparison Between Theory and Results 119
   Nucleation Temperature 119
   Slow Cooling Theory 125
7. Discussion and Recommendations 140
   Control Strategy Implications 140
   Future Research Recommendations 147
References 148

Appendix "A" 157

FIGURES

Figure Page

1 The free energy ΔG required to form a liquid drop of radius r in a vapor with partial pressure p 16

2 Mole fraction of Sulfur (IV) species in equilibrium at 25°C as a function of solution pH . 32

3 Experimental system design 47

4 Process flow diagram of flue gas simulator 48

5 Schematic diagram of the acid vapor generator . . 50

6 Water vapor generator 52

7 Fly ash particle generator 54

8 Predicted acid particle diameter 56

9 Acid concentration and particle size distribution sampling system 60

10 Diffusion battery (D.B.) calibration set-up . . . 67

11 Calibration of D.B. made up of 325 mesh screens . 70

12 Calibration of D.B. made up of 400 mesh screens . 71

13 Acid particle size distribution 77

14 Rapid quenching experimental set-up 80

FIGURES (continued)

Figure		Page
15	Measured acid particle size distribution	87
16	Measured acid particle size distribution	87
17	Effect of acid vapor concentration on acid particle size distribution	88
18	Effect of quench water temperature on nucleated acid particle size distribution	90
19	Effect of quench water temperature on nucleated acid particle size distribution	90
20	Effect of water vapor concentration on nucleated acid particle size distribution	91
21	Effect of water vapor concentration on nucleated acid particle size distribution	91
22	Effect of sulfur dioxide on nucleated acid particle size distribution	92
23	Effect of flyash on nucleated acid particle size distribution	92
24	Effect of flyash and SO_2 on nucleated acid particle size distribution	93
25	Dilution cooling experimental apparatus	95
26	Effect of SO_2 on nucleated acid particle size distribution	100

FIGURES (continued)

Figure		Page
27	Effect of SO_2 on nucleated acid particle size distribution	100
28	Effect of flyash on nucleated acid particle size distribution	101
29	Effect of flyash on nucleated acid particle size distribution	101
30	Effect of flyash and SO_2 on nucleated acid particle size distribution	102
31	Effect of flyash and SO_2 on nucleated acid particle size distribution	102
32	Effect of water vapor on nucleated acid particle size distribution	103
33	Effect of acid concentration on nucleated acid particle size distribution	105
34	Effect of dilution air temperature on nucleated acid particle size distribution	105
35	Slow cooling experimental set-up	106
35	Wall loss experimental set-up	115
36	Effect of SO_2 on nucleated acid particle size distribution	116

FIGURES (continued)

Figure Page

37 Effect of injected flyash on nucleated acid particle size distribution 116

38 Effect of sampling location on acid particle size distribution 117

39 Effect of acid vapor concentration on particle size distribution 118

40 Effect of water vapor concentration on nucleated particle size distribution 118

41 Predicted nucleation temperature 124

42 Dew point of sulfuric acid in flue gas (Lisle and Sensenbaugh, 1965) 143

43 Dew points for dilute mixtures of sulfur trioxide in stack gases with various water contents (Martin, et al. 1974) 144

44 Acid dew point in flue gas (Muller, 1969) 145

45 Dew point and acid nucleation temperatures 146

TABLES

Number Page

1 Gas-to-particle conversion mechanisms 12

2 Equilibrium constant for the SO_2-water system as a function of temperature 31

3 Rate expressions for the uncatalyzed oxidation of SO_2 in aqueous solutions 34

4 Rate expressions for the catalyzed oxidation of SO_2 in aqueous solutions 36

5 Summary of SO_2 oxidation processes in power plant plumes 42

6 Results of field measurements on the rates of SO_2 oxidation in power plant plumes 43

7 Some characteristics of aerosol measurement devices 57

8 Measured penetration of 325 mesh screens 68

9 Measured penetration of 400 mesh screens 69

10 Comparison data between diffusion battery model predictions and data 73

11 Sample data reduction calculations 76

12 Summary of rapid quenching experimental conditions 82

TABLES (continued)

Number Page

13 Acid particle size frequency distribution 84

14 Acid particle size frequency distribution 86

15 Summary of dilution cooling experimental conditions 97

16 Acid particle size distribution 98

17 Typical temperature profile 99

18 Nucleation temperature measurement 108

19 Effect of gas temperature on acid nucleation . . . 109

20 Wall loss experimental results 112

21 Summary of slow cooling experimental conditions . 113

22 Acid particle size frequency distribution 114

23 Source of physical property data for sulfuric acid-water solution 123

24 Nucleation temperature measurement 126

25 Slow cooling sampling calculation 139

NOMENCLATURE

A = fundamental molecule

A_C = cross-sectional area of target critical nuclei, m^2

A_i = wall area tranversed by flue gas during time interval i, m^2

A_r = the rotated angle of the principal axis, degree

a = constant, dimensionless

a_A = activity of "A", dimensionless

a_B = activity of "B", dimensionless

a_c = accommodation coefficient, dimensionless

B_A = molecular flux of acid molecules on to a given surface, /m^2-s

b = constant, dimensionless

b_A = number of molecules that arrive at the embryo, number/m^2-s

b_B = number of molecules that arrive at the embryo, number/m^2-s

b_D = correction for size regime dependence (Davies, 1979)

C' = Cunningham slip factor, dimensionless

C_{PG} = flue gas specific heat capacity, J/kg-K

C_p = heat capacity of the particle, cal/kg

C_p = particle concentration, g/Nm^3

C_{pp} = heat capacity of the particle, J/kg

D = diffusivity of the condensing species in the gas phase, m^2/s

D_A^o = given value of the diffusivity of H_2SO_4 in air, m^2/s

D_i = diffusivity of particle "i", m^2/s

D_p = particle diffusivity, cm^2/s

D_p = diffusivity of particle, m^2/s

D_W^o=a given value of diffusivity of steam in air, wire diameter, cm

d_i = inside tube diameter

d_{lm} = logarithmic-mean diameter of the tube wall, m

d_p^* = critical diameter of the drop or particle, m

d_p = particle diameter, m

NOMENCLATURE (continued)

d_{pa} = aerodynamic diameter, μmA = μm $(g/cm^3)^{0.5}$

d_{pc} = cut diameter, μm or μmA

d_{pi} = diameter of particle "i", m

e_d = well depth of Lennard-Jones potential, J

H_x = Henry's constant, atm/mol-fraction of total dissolved SO_2

h = heat transfer coefficient, cal/°C-m^2-s

h_i = inside tube heat transfer coefficient, W/m^2-K

h_o = outside heat transfer coefficient, W/m^2-K

ΔG^* = Gibbs free energy of formation of a critical size drop, J/drop

ΔG = Gibbs free energy of formation, J/drop

I = nucleation rate, number/m^3-s

I^* = rate of critical nucleus formation, /m^3-s

J_{AS} = mass transfer flux of acid onto the wall, mol/m^2-s

J_{WS} = flux of condensing water vapor on the wall, mol/(m^2-s)

K = kinetic factor defined by equation (10)

K_A = vapor-equilibrium partition coefficient for H_2SO_4, dimensionless

K_{ij} = hetermolecular coagulation constant, m^3/s

K_w = vapor-equilibrium partition coefficient for H_2O, dimensionless

k = Boltzmann's constant, J/K

k_A = mass transfer coefficient for sulfuric acid vapor, m/s

k_G^o = thermal conductivity of the flue gas at the given conditions, W/(m-K)

k_G = thermal conductivity of gas, W/m-K

k_{ps} = mass transfer coefficient for particles to the inside tube surface, m/s

k_s = thermal conductivity of the wall material, W/m-K

k_w = mass transfer coefficient for water vapor, m/s

L = latent heat of vaporization, cal/kg

L_t = total tube length, m

l_m = mean free path of gas, m

NOMENCLATURE (continued)

M = molecular weight, kg/mol
M_A = molecular weight of "A", kg/mol
M_B = molecular weight of "B", kg/mol
M_G = flue gas molecular weight, kg/mol
M_i = molecular weight of species "i", kg/mol
M_w = molecular weight of water, kg/mol
m = mass per molecule, kg
m_B = mass per molecule of species "B", kg
m_d = mass of the critical size drop, kg
m_h = mass of the hydrate which has "h" H_2O molecules, kg
N_i = stoichiometric coefficient for species "i" in the reaction
N_G = flue gas flow rate, mol/s
N_{Kn} = Knudsen number, dimensionless
N_{Pe} = Peclet number, dimensionless
N_{Pr} = Prandtl number, dimensionless
N_{Re} = Reynolds number, dimensionless
N_{SCA} = Schmidt number for acid vapor, dimensionless
N_{SCW} = Schmidt number for water vapor, dimensionless
n = number of molecules in a drop, number
n = number of screens, number
n^* = number concentration of critical size embryo, number/m^3
n_w = concentration of water molecules, /m^3
n_A = number of molecules of component "A" in the drop, number
n_B = number of molecules of component "B" in the drop, number
n_{Bh} = number concentration of hydrates which consist of one acid molecule and "h" water molecules, number/m^3
n_{GA} = number concentration of species "A" in gas phase, number/m^3
n_{GB} = number concentration of species "B" in gas phase, number/m^3

NOMENCLATURE (continued)

n_{Bh} = number density of hydrate containing "h" H_2O molecules, number/m^3

n_G = total number concentration of molecules of condensing species, number/m^3

n_i = number concentration of particles of size d_{pi}, m^{-3}

Oμ = collision integral (see Bird et al, 1960, Table B-1)

P = second order partial derivative of "ΔG" with respect to rotated axis "n_A".

P_A = equilibrium vapor presure of H_2SO_4 above sulfuric acid solution, Pa

$\overset{\circ}{P}_{AS}$ = equilibrium vapor pressure of "A" over a flat surface of solution "A" nd "B", Pa

P_{AS} = equilibrium vapor pressure of acid over the acid solution at the wall, Pa

$\overset{\circ}{P}_{BS}$ = equilibrium vapor pressure of "B" over a flat surface of solution "A" and "B", Pa

P_{ws} = equilibrium pressure of water vapor over the acid solution at the wall, Pa

Pt_d° = penetration, fraction

p = partial pressure, Pa or mmHg

$\overset{\circ}{p}_A$ = equilibrium vapor pressure of "A" over a flat surface of pure "A", Pa

$\overset{\circ}{p}_B$ = equilibrium vapor pressure of "B" over a flat surface of pure "B", Pa

p° = saturated vapor pressure above plane surface of the same liquid at the same temperature, Pa or mmHg

p° = pressure at which the standard property is known, Pa

p_d = equilibrium vapor pressur above the particle at the particle temperature, P_a or mmHg

p_w = equilibrium vapor pressure of H_2O above sulfuric acid solution, Pa

Q = second order parial derivative of "ΔG" with respect to the rotated axis "n_B"

R = universal gas constant, J/K-mol

NOMENCLATURE (continued)

r = radius of the drop, m

r = reaction rate

r^* = critical rdius of drop, m

r_h = radius of the hydrate which has "h" H_2O molecules, m

S = saturation ratio, dimensionless

S = Solidity factor of screens, dimensionless

S_A = relative humidity of "A", dimensionless

S_B = relative humidity of "B", dimensionless

T = temperature, K

T^o = absolute temperature at which the property is known, K

T_d = temperature of the particle, K or °C

T_i = vapor temperature at the inlet of time interval i, °C or K

T_{i+1} = vapor temperature at the end of time interval i, °C

T_{oi} = outside cooling gas temperature on interval i, °C or K

T_p = temperature of the particle, K

T_s = wall temperature, °C, or K

t = time, s

U = overall heat transfer coefficient for heat transfer through the wall, $W/(m^2-K)$

u_s = superficial gas velocity, cm/s

V_A = molar volume of "A", m^3/mol

V_B = molar volume of "B", m^3/mol

V_i = average thermal velocity of particle "i", m/s

V_p = volume of particle, m^3

x_w = wall thickness, m

x_A = mole fraction H_2SO_4 in liquid condensate, fraction

x_B = critical molar fraction of "B", fraction

Y_B = net rate of acid hydrates striking a critical size drop, $/m^2-s$

y_B^* = critical mass fraction of "B", fraction

y^* = mass fraction of "B" in the drop, fraction

NOMENCLATURE (continued)

Greek

σ = surface tension, N/m

μ_L = chemical potential of single molecule in liquid phase, J/molecule

μ_V = chemical potential of single molecule in vapor phase, J/molecule

ρ_L = density of drop, kg/m³

P_ϱ = particle density, kg/m³

η = single cylinder collection efficiency, dimensionless

ρ = density of the sulfuric acid solution drop, kg/m³

σ_G = Lennard-Jones zero potential diameter, m

μ_G = viscosity of flue gas, Pa-s

ACKNOWLEDGMENT

A.P.T., Inc. greatly appreciates the guidance and contribution by Dr. Leslie E. Sparks, Project Officer, EPA, IERL/RTP during this study.

SECTION 1
SUMMARY AND CONCLUSIONS

SUMMARY

Objectives

This research was a theoretical and experimental study of sulfate aerosol formation and growth under conditions that exist in industrial smoke stacks and the near stack plumes. The objectives were to develop the fundamental data and mathematical models necessary to design emission control strategies and devices for sulfate condensation aerosols.

Approach

The general approach was first to define the mechanisms by which sulfur oxide and sulfur trioxide are converted to sulfate particles and then use this knowledge to develop optimum control.

Sulfur dioxide and sulfur trioxide can convert to sulfate particles by the following mechanisms:

1. Condensation of sulfuric acid vapor (or water vapor associated sulfur trioxide) to form sulfuric acid drops.
2. Condensation of sulfuric acid vapor on pre-existing particles such as fly ash, liquid drops, and acid drops.
3. Sorption of SO_2 by liquid or solid particles followed by oxidation of SO_2 to sulfate.
4. Gas phase oxidation of SO_2 to SO_3 which is subsequently condensed by mechanisms 1 and 2.
5. Chemical reaction of acid vapor with solid or liquid particles.

This study emphasizes the sulfate formation by mechanism 1 and 2. Mechanism 4 is not significant in most industrial smoke stacks and mechanisms 3 and 5 are system dependent.

Sulfate formation due to condensation is a physical process in which the gas temperature must be below the acid dew point. Gas cooling can be the result of heat transfer to the surroundings, quenching (such as by introducing water sprays), and mixing with cold gas. All three cooling processes could occur in industrial smoke stacks and in near-stack plumes. Therefore, sulfate formation in typical flue gas mixtures during slow cooling, rapid quenching, and dilution cooling was experimentally studied. The results obtained in this study plus published data were then used to verify sulfate formation models and develop emission control technologies.

Experiments

Apparatus

The basic design for all experiments was the same. It consisted of a flue gas simulator for supplying acid-laden gas for various cooling apparatus. Major components of the flue gas simulator included an acid vapor generator, a steam generator, a fly ash particle generator, and a SO_2 gas cylinder.

Sulfuric acid and water vapors were generated by vaporizing dilute sulfuric acid and water at controlled rates. Fly ash particles were produced by re-dispersion. SO_2 was metered into the flue gas simulator from a gas cylinder. Room air was used as the carrier gas because the amount of oxygen in the flue and the presence of carbon dioxide and nitrogen oxides have no effect on sulfate particle formation in the stack.

The following cooling apparatus was used in the experiments:

1. Slow cooling - double pipe heat exchanger
2. Rapid quenching - packed bed column
3. Dilution cooling - parallel stream dilution chamber.

Measurement Methods

Gas samples at the cooling apparatus inlet and outlet were obtained simultaneously to determine:

1. Inlet acid vapor, water vapor, SO_2, and fly ash particle concentrations.

2. The amount of acid vapor condensed on existing particles.
3. Concentration of newly formed acid particles.
4. The amount of acid vapor condensed on walls.
5. Particle size distribution.

The sampling train used at the inlet consisted of a cascade impactor (or quartz filter) followed by a condensation coil, a quartz filter, three impingers, and gas metering and moving instruments. The outlet sampling train consisted of an impactor (with final filter removed) connected in series with a screen diffusion battery, a quartz filter, a condensation coil, another quartz filter, 3 impingers, and the gas metering and moving instruments. The instruments upstream of the condensation coil were heated to and maintained at gas temperature. The condensation coil was water cooled and its temperture was controlled at 60°C to 90°C when SO_2 was injected.

The acid collected by the impactor, diffusion battery, and filter was analyzed by extraction and titration. Acid collected by the condensation coil and impinger was determined by washing followed by titration.

Results

Rapid Quenching

Rapid quenching experiments were for simulating the sulfate particle formation in a scrubber. The quencher used in this study was a randomly packed bed of Berl saddles. The effects of acid vapor concentraiton (10 to 100 ppmv), water vapor concentration (5 to 15% by volume), SO_2 concentration (0 to 1,000 ppmv), fly ash particle concentration (0 to 1.3 g/m^3), and quench water temperature (20°C to 60°C) on nucleated acid particle size distribution were determined experimentally. The results are:

1. Higher water temperature and lower acid and water vapor concentrations resulted in higher concentration of fine particles. Low water temperature decreased the gas temperature and caused additional water vapor condensation on the nucleated particles. Decreasing

the acid and water vapor concentrations reduced the particle growth.

2. The presence of SO_2 had no effect on acid particle nucleation.
3. In the presence of fly ash particles, acid particles were larger because of condensation of acid vapor on the particles. Rapid quenching caused local high supersaturation of acid vapor, and therefore large quantity of ultra-fine acid particles were nucleated.
4. After the quencher, particle growth due to agglomeration was negligible.

Dilution Cooling

Dilution cooling experiments were done to simulate the sulfate particle formation in the near-stack plume. The cooler was a concentric parallel stream dilution chamber with the dilution air forming a sheath around the flue gas. The effects of dilution air temperature, water and acid vapor concentrations, and the presence of SO_2 and fly ash particles on acid nucleation were studied. The results are:

1. The concentration of fine acid particles decreased with increasing dilution air temperature, decreasing acid vapor concentration, and increasing water vapor concentration.
2. SO_2 had no effect on acid particle nucleation.
3. The concentration of fine acid particles decreased in the presence of fly ash particles.

Slow Cooling

Slow cooling experiments were for studying the acid particle nucleation which could occur in industrial smoke stacks, dry pollution control devices such as ESP's and baghouses. The experiments were performed on a co-current double pipe heat exchanger with the flue gas flowing in the center pipe. Acid particle samples were taken at the location where nucleation was observed to start. The experimental findings are:

1. Over 80% of the acid vapor was condensed on preexisting fly ash particles.
2. Higher acid vapor and lower water vapor concentrations resulted in the formation of a large quantity of ultrafine acid particles.
3. SO_2 had no effect on acid particle nucleation.
4. Large quantity of acid vapor was condensed on walls upstream of nucleation starting point.

Comparison Between Theory and Experiments

Nucleation Temperature

The nucleation of sulfuric acid particles involves two condensible species - water and sulfuric acid vapors. For a given water and acid vapor concentration combination, the temperature at which nucleation of sulfuric acid particles starts can be predicted from thermodynamics and classical kinetic theories. In the present study, the simplified equation by Kiang and Stauffer (1973) was used to predict the nucleation temperature, which was defined as the temperture which gives a nucleation rate of $1/cm^3$-s.

The calculations indicate that nucleation, once started, goes to completion quickly. Acid vapor is depleted in a very short time. The predicted nucleation temperature increases with increasing water vapor and acid vapor concentrations. This means less cooling of flue gas is needed to initiate the formation of acid particles if the acid vapor and water vapor concentrations are high.

The measured acid particle nucleation temperatures varied around the predictions. By considering the uncertainties in vapor pressure and surface tension data, the agreement between theory and experiment is considered to be good.

Slow Cooling

A mathematical model was developed to characterize the nucleation, condensation, and growth of sulfuric acid particles in a flow system. The model accounts for gas cooling, vapor loss to the wall, homogeneous binary nucleation, heterogeneous condensation on existing particles, diffusional loss of nucleated particles and coagulation. A computer program was written for applying the model to slow cooling experiments. The program uses a quasi-steady state approach, and follows a small element of fluid through the pipe, and computes changes in temperature, vapor concentration, and particle concentration due to the above mentioned mechanisms in successive increments of distance along the pipe.

The measured gas cooling rate and wall condensation of acid vapor were compared to that predicted from heat and mass transfer. Because of entrance effect, the measured cooling rate and wall condensation of acid vapor were much higher than calculated.

Capture Strategy Implications

The flue gas dew point temperature has been measured and predicted by numerous investigators. Although there are differences in dew point temperature given by different investigators, they are all much higher than the acid particle self nucleation temperature found in this study and predicted from classical nucleation theory. Thus, if the flue gas is slowly cooled to between dew point and nucleation temperature, it is possible to force the sulfuric acid to condense out on surfaces, such as on fly ash particles and walls, rather than forming fine particles. The experimental results obtained in this study show this control method is feasible.

Rapid cooling of the flue gas should be avoided to minimize the chance for acid particle nucleation. In cases where the flue gas must be quenched, then the quench water should be as cold as possible. It would also be helpful if additional water vapor, such as waste steam, is introduced into the gas stream.

CONCLUSIONS

The conclusions from this study are as follow:

1. The temperature at which the self-nucleation of sulfuric acid particles starts can be predicted from theory and it agrees with our experimental results. Thus, the sulfuric acid nucleation temperature for flue gas can be predicted, providing that the gas pressure, water vapor concentration and sulfur trioxide concentration are known.
2. To minimize the chance for fine acid particle formation, rapid cooling of the flue gas should be avoided.
3. While the presence of SO_2 has no effect on acid nucleation, fly ash particles have great effect. Most of the acid vapor condenses on ash particles if the gas is cooled slowly.
4. Increasing the water vapor concentration in the gas stream increases the acid particle diameter by additional condensation or solution induced particle growth.

SECTION 2

INTRODUCTION

Primary sulfates are known to contribute to the formation of acid rain, reduced atmospheric visibility, and human respirable diseases. To illustrate the magnitude of the sulfate impacts, it is estimated that over 1/3 of the airborne respirable particles in the Eastern U.S. are in the form of sulfate (Homolya and Cheney, 1978).

A major source of atmospheric sulfate particles is the chemical reaction of SO_2 and particles in the ambient air. However, reduction of SO_2 emissions has not generally resulted in a noticeable decrease in atmospheric sulfate. Additionally, near stack condensation of sulfate aerosols are known to be a major cause of high plume opacity. Therefore, it is worthwhile to consider control techniques for reducing primary sulfate emissions.

Existing particle control systems are not effective at removing condensible aerosols because the aerosol precursors are often in the vapor state when they pass through the control device. Although the vapors usually will condense in a wet scrubber, they often form ultrafine particles which are very difficult to capture.

The first step toward developing acceptable technology for reducing condensible aerosol emissions is to obtain an adequate data base and understanding of the mechanisms involved. Specifically, this means understanding the condensation, formation, and growth of sulfate aerosols in a simulated flue gas environment. Some of the basic questions to be answered are listed below.

1. How are sulfate aerosols formed? What design and environmental parameters promote their formation?

2. What are the effects of factors such as: residence time, gas and particle composition, temperature, water vapor concentration, water drop size and pH, fly ash particle size and concentration, cooling rate, and sunlight intensity?

3. What control options are available? What is needed to develop adequate control technology for primary sulfates?

A theoretical and experimental program was performed to study the formation and growth of sulfate particles. Existing theoretical models on acid particle formation and growth were reviewed and evaluated. The formation and growth of sulfate particles during slow cooling, rapid cooling, and dilution cooling of flue gas were experimentally determined and compared with theories. The theories, experimental methods, and results are described in this report.

SECTION 3

LITERATURE REVIEW

ACID VAPOR CONCENTRATION

When materials containing sulfur compounds, such as organic sulfur compounds in coal and petroleum, pyrite, hydrogen sulfide in sour natural gas, and metal sulfide ores, are burned (or roasted), the sulfur present is converted to sulfur dioxide. Part of the sulfur dioxide will oxidize further to sulfur trioxide at high temperature. The amount of sulfur dioxide oxidized to sulfur trioxide depends on furnace operation and the types and amounts of metal impurities present.

Sulfur trioxide exists in dissociated form at high temperature. As the flue gas mixture is cooled down, SO_3 associates with water vapor to form sulfuric acid vapor. This process is represented by the equation:

$$SO_3 + H_2O_{\,(gas)} \text{ ---> } H_2SO_4{}_{\,(gas)} + 29.83 \text{ kcal/mole} \qquad (1)$$

This reaction takes place in the gaseous phase; the reaction heat is absorbed by the gas.

The degree of association of sulfur trioxide with water vapor can be determined from the equilibrium constant for the above equation. The equilibrium constant is expressed by the equation:

$$K_p = \frac{p_{SO_3}\, p_{H_2O}}{p_{H_2SO_4}} \qquad (2)$$

where K_p = equilibrium constant, mmHg

p_{SO_3} = vapor pressure of SO_3, mmHg

p_{H_2O} = vapor pressure of water, mmHg

$p_{H_2SO_4}$ = vapor pressure of sulfuric acid, mmHg

The equilibruim constant depends only on temperature. This temperature dependency has been determined experimentally by various researchers and is expressed by the following formula:

$$\log K_p = 5.881 - \frac{5000}{T} + 1.75 \log T - 5.7 \times 10^{-4} \qquad (3)$$

where T = gas temperature, K

As an illustration, assume the gas temperature is 204°C (400°F), moisture content in the flue gas is 10% by volume, and the SO_3 concentration is 30 ppm by volume, then the equilibrium constant calculated from equation (3) is 0.652 mmHg and the degree of association of SO_3 with water to form sulfuric acid vapor is 99.1%

GAS-TO-PARTICLE CONVERSION

Gas-to-particle conversion, such as the condensation of sulfuric acid vapor to form acid drops, may result from homogenous gas phase processes, or it may be controlled by processes in the particulate phase. Table 1 summarizes the various gas-to-particle conversion mechanisms. Homogenous gas-phase chemical reactions such as the oxidation of SO_2 to SO_3 may generate condensible products. Once a condensible species has been formed in the gas phase, it may condense on existing particles or form new sites for condensation (condensation nuclei). Alternatively, molecules from the gas may be transported to the surface of a particle or drop and may react with the particle or drop. Literature on all these gas-to-particle conversion processes has been reviewed. A brief discussion of particle formation by nucleation is presented in the following sections.

TABLE 1 GAS-TO-PARTICLE CONVERSION MECHANISMS

- Gas-to-Particle Conversion
  - Nucleation
    - Homogenous
      - Single condensible species
      - Multicomponent condensation (heteromolecular)
    - Heterogeneous
      - Condensation on ions
      - Condensation on insoluble particles
      - Condensation on soluble particles
  - Heterogeneous Condensation (with chemical reaction)
    - Transport limited
    - Surface controlled chemical reaction
    - Particulate phase controlled chemical reaction
  - Homogeneous condensation (gas phase reaction to form condensible species).

Nucleation

Nucleation is defined as the conversion of several fundamental molecules in the gas phase into a stable liquid or solid particle. Nucleation and condensation occurs in three major steps:

1. Supersaturation
2. Nucleation
3. Particle growth

The necessary condition for nucleation is that the vapor pressure of the condensation species must be greater than the equilibrium vapor pressure, i.e. supersaturated. In mathematical form this becomes:

$$S = \frac{p}{p^o} \tag{4}$$

where p = partial pressure in gas phase, Pa
p^o = saturated vapor pressure above a plane surface of the same liquid at the same temperature, Pa

When the saturation ratio, S, is greater than 1 the vapor is supersaturated; $S = 1$, the vapor is saturated; and $S < 1$, unsaturated.

When the vapor is saturated, the vapor-liquid system is in equilibrium. The slightest increase in vapor pressure above the saturated vapor pressure will result in immediate condensation of vapor, whereas the smallest decrease in pressure will produce additional evaporation of liquid.

Supersaturation is the result of physical processes, such as cooling or mixing with cold gas. Once supersaturation occurs, condensation will occur. In the absence of "foreign" nuclei, molecules of the condensing species aggregate to form new particles or drops. This is termed homogeneous nucleation or condensation. Condensation may also take place on surfaces, on insoluble and soluble particles, on positive and negative ions. This is termed heterogeneous nucleation.

Nucleation, either homogeneous or heterogeneous, has been studied theoretically by a number of researchers such as Berker and Doring (1935), Zeldovich (1942), Frenkel (1955), Reiss (1950), Doyle (1961), Kiang and Stauffer (1973), Mirabel and Katz (1974), and Yue and Hamill (1979). They have shown that nucleation can be predicted from the thermodynamics and kinetics of the nucleation process. The thermodynamics determines the conditions under which new particles will form. Kinetics determines the nucleation rate.

According to these researchers, the nucleation rate (i.e. the number of particles or drops formed per unit volume of gas in one second) can be predicted by the equation:

$$I = K \exp\left(-\frac{\Delta G^*}{kT}\right) \tag{5}$$

where I = nucleation rate, number /m³-s

K = kinetic factor

ΔG^* = Gibbs free energy of formation of a drop which has a size and composition such that it is in equilibrium with the surrounding gas, J/drop

k = Boltzmann's constant, J/K

T = temperature, K

The equations for calculating "K" and "ΔG*" have been derived for different nucleation conditions. The following is a brief presentation of the derivations.

Homogeneous Nucleation

Homogeneous nucleation increases the particle number concentration in the gas and may involve a single condensible species such as water or several species to form a solution drop.

Single Condensible Species - The change in Gibbs free energy of formation for the condensation process is given by the expression:

$$\Delta G = n\,(\mu_L - \mu_V) + 4\pi r^2 \sigma \qquad (6)$$

where ΔG = Gibbs free energy of formation, J/drop
n = number of molecules in a drop, number
σ = surface tension, N/m
μ_L = chemical potential of single molecule in liquid phase, J/molecule
μ_V = chemical potential of single molecule in vapor phase, J/molecule
r = radius of the drop, m

Figure 1 is a graphical presentation of equation (3) for the cases of an unsaturated and a supersaturated vapor. For the unsaturated case, $p > p^\circ$, the free energy required for drop formation increases sharply with the drop radius. When the vapor is supersaturated, $p > p^\circ$, the free energy attains a maximum when "r" is equal to a certain critical value "r*". A drop (or an embryo in homogeneous condensation) of critical radius, r*, is therefore in equilibrium with the vapor. This equilibrium is unstable, i.e., a slight increase in drop radius (or an increase in supersaturation) lowers the free energy and the drop starts growing. A slight reduction in drop radius (or in supersaturation) raises the free energy and the drop vaporizes.

The Gibbs free energy of formation for a critical size drop is called the critical Gibbs free energy of formation, "ΔG*". It can be obtained by maximing "ΔG" in equation (6) with respect to "n" or "r". The result is:

$$\Delta G^* = \frac{16\pi\,\sigma^3 m^2}{3\,(\varrho_L k\,T \ln S)^2} \qquad (7)$$

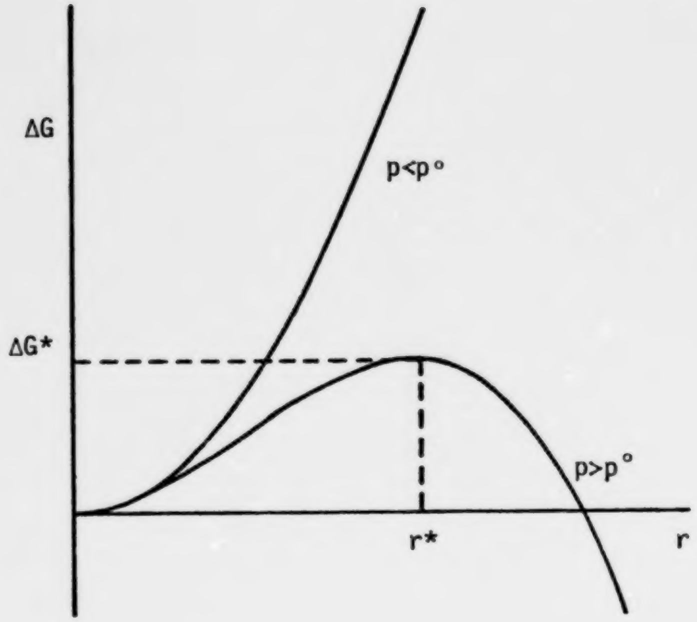

Figure 1. The free energy ΔG required to form a liquid drop of radius r in a vapor with partial pressure p.

where ΔG^* = free energy for forming a critical size embryo, J/drop
k = Boltzmann's constant, J/K
m = mass per molecule, kg
S = saturation ratio, dimensionless
T = temperature, K
σ = surface tension of drop, N/m
ρ_L = density of drop, kg/m³

The equation for the kinetic factor "K" is derived by analyzing the following drop formation:

$$A + A_n \rightleftarrows A_{n+1} \qquad (8)$$

$$A_n \rightleftarrows A_{n-1} + A \qquad (9)$$

where A = fundamental molecule
A_{n+1} = a drop which contains n+1 molecules of "A"
A_{n-1} = a drop which contains n-1 molecules of "A"
n = integer

Equations (8) and (9) show that "A_n", i.e. a drop containing "n" molecules of "A" can be formed by:

1. collision between a single molecule "A" and A_{n-1}, a drop containing "n-1" molecules of "A"
2. evaporation of a single molecule "A" from A_{n+1}, a drop containing "n+1" molecules of "A"

On the other hand, "A_n" is destroyed by the following two processes:

1. evaporation of a single molecule of "A" from "A_n"
2. collision between a single molecule "A" and "A_n"

Collision and evaporation can occur between multi-molecule drops. However, their rate is small compared to single molecule collision and evaporation and therefore can be neglected. Becker and Doring (1935), Zeldovich (1942), and Frenkel (1955) assumed that the formation and destruction of "A_n" reached a steady state. Under these conditions, the kinetic factor takes the form:

$$K = \frac{4\pi \, (r^*)^2 \, p \, n_G \, a_c \, Z}{(2\pi \, mkT)^{0.5}} \tag{10}$$

$$Z = \frac{\rho_L \, \ln^2 S}{8\pi m} \left(\frac{kT}{\sigma} \right)^{3/2} \tag{11}$$

where K = Kinetic factor
r^* = critical radius of the drop, m
p = vapor pressure, Pa
m = mass per molecule, kg
k = Boltzmann's constant, J/K
T = temperature, K
n_G = total number concentration of molecules of condensing species, number /m³
a_c = accommodation coefficient, dimensionless
σ = surface tension, N/m
S = saturation ratio, dimensionless
ρ_L = density of drop, kg/m³

The critical radius of the drop is calculated from Kelvin's equation:

$$r^* = \frac{2 \, \sigma \, M}{R \, T \, \rho_L \, \ln S} \tag{12}$$

where r^* = critical radius of the drop, m
σ = surface tenstion, N/m
M = molecular weight, kg/mol
R = universal gas constant = 8.35 J/K-mol
T = absolute temperature, K
ρ_L = density of the drop, kg/m³
S = saturation ratio, dimensionless

Substituting equations (7), (10), (11), and (12) into equation (5), the nucleation rate becomes:

$$I = 2\, a_C \left(\frac{m}{\varrho_L}\right)^{2/3} n_G^2 \left(\frac{k}{2\pi m}\right)^{0.5} \left[\frac{\sigma\left(\frac{m}{\varrho_L}\right)^{2/3}}{kT}\right]^{1/2} \exp -\left\{\frac{16\pi}{3}\left[\frac{\sigma\left(\frac{m}{\sigma_L}\right)^{2/3}}{kT}\right]^3 \ln^{-2} S\right\} \tag{13}$$

where I = nucleation rate, number /m³-s
m = molecular mass, kg
ϱ_L = density of the drop, kg/m³
n_G = total number concentration of condensing species, number /m³
k = Boltzmann constant, J/K
σ = surface tension, N/m
S = saturation ratio, dimensionless
a_C = accommodation coefficient, dimensionless
T = gas temperature, K

Multicomponent Condensation - The Gibbs free energy of drop formation from two vapor species is (Flood, 1934; Reiss, 1950; Doyle, 1961; Winkler, 1973; Kiang and Stauffer, 1973; Mirabel and Katz,1974; Takahashi et al., 1975; Nair and Vohra, 1975; Yue et al., 1979):

$$\Delta G = n_A\,(\mu_{AL} - \mu_{AV}) + n_B\,(\mu_{BL} - \mu_{BV}) + 4\pi\, r^2\, \sigma \tag{14}$$

where ΔG = Gibbs free energy of formation, J/drop
n_A = number of molecules of component 'A' in the drop, number
n_B = number of molecules of component 'B' in the drop, number
μ_{AL} = chemical potential of component 'A' in liquid phase, J/molecule

μ_{AV} = chemical potential of component 'A' in vapor phase, J/molecule

μ_{BL} = chemical potential of component 'B' in liquid phase, J/molecule

μ_{BV} = chemical potential of component 'B' in vapor phase, J/molecule

r = radius of embryo, m

σ = surface tension, N/m

Heist and Reiss (1974) plotted "ΔG" versus "n_A" and "n_B" in three dimensional space and found a saddle point which corresponds to the minimum height of the free energy barrier "ΔG^*". The radius and composition at this point are called the critical radius and the critical composition.

At the saddle point, the following equations hold:

$$\left(\frac{\Delta G}{n_A}\right)_{n_B} = 0 \qquad \text{and} \qquad \left(\frac{\Delta G}{n_B}\right)_{n_A} = 0 \tag{15}$$

Substituting equation (14) into equation (15) and expressing "n_A" and "n_B" in terms of partial molar volumes "V_A" and "V_B", the following equations are obtained:

$$RT \ln \frac{S_A}{a_B} = \frac{2\ \sigma\ V_A}{r^*} - \frac{3\ x_B^*\ V}{r^*}\ \frac{d\ \sigma}{d\ x_B}\bigg|_{x_B = x_B^*} \tag{16}$$

$$RT \ln \frac{S_A}{a_B} = \frac{2\ \sigma\ V_B}{r^*} - \frac{3\ (1\ x_B^*)V}{r^*}\ \frac{d\ \sigma}{d\ x_B}\bigg|_{x_B = x_B^*} \tag{17}$$

where R = universal gas constant, J/K-mol

T = temperature, K

V = molar volume of solution, m³/mol

V_A, V_B = molar volume of "A" or "B", m³/mol

x_B^* = critical molar fraction of "B", fraction

r^* = critical radius of drop, m
σ = surfacc tension, N/m
S_A, S_B = relative humidity of "A" or "B", dimensionless
a_A, a_B = activity of "A" or "B", dimensionless

Relative humidities and activities are defined as follows:

$$S_A = \frac{p_A}{p_A^\circ} \tag{18}$$

$$S_B = \frac{p_B}{p_B^\circ} \tag{19}$$

$$a_A = \frac{p_{AS}^\circ}{p_A^\circ} \tag{20}$$

$$a_B = \frac{p_{BS}^\circ}{p_B^\circ} \tag{21}$$

where p_A°, p_B° = equilibrium vapor pressure of "A" or "B" over a flat surface of pure "A" or "B", Pa
$P^\circ{}_{AS}$, $P^\circ{}_{BS}$ = equilibrium vapor pressure of "A" of "B" over a flat surface of solution of "A" and "B", Pa

Equations (16) and (17) are called the generalized Kelvin's equations. Kelvin's equations can also be expressed in terms of density instead of molar volume. In this case, Kelvin's equations are:

$$\ln \frac{S_A}{A} = \frac{2\, M_A\, \sigma}{RT\, \rho_L r} \left[1 + \frac{y_A}{\rho_L} \left. \frac{d\, \rho_L}{d\, y_B} \right|_{y_B = y_B^*} - \frac{3}{2} \frac{y_B}{\sigma} \left. \frac{d\, \sigma}{d\, y_B} \right|_{y_B = y_B^*} \right] \tag{22}$$

$$\ln \frac{S_B}{A} = \frac{2\ M_B\ \sigma}{RT\ \varrho_L\ r^*} \left[1 - \frac{(1-y_B^*)}{\varrho_L} \left.\frac{d\varrho_L}{dy_B}\right|_{y_B=y_B^*} + \frac{3(1-y_B^*)}{2\ \sigma} \left.\frac{dr}{dy_B}\right|_{y_B=y_B^*} \right] \tag{23}$$

where M_A, M_B = molecular weight of "A" or "B", kg/mol
y_B^* = critical mass fraction of "B", fraction
ϱ_L = density of drop, kg/m³
y^* = mass fraction of "B" in the drop, fraction

For a given condition (T, p_A, and p_B known), equations (16) and (17) can be solved for "r*" and "x_B^*" ("r*" and "y_B^*" if equations (22) and (23) are solved). Since a_A, a_B, ϱ_L, σ, V_A, and V_B are implicit functions of "x_B" or "y_B", analytic solutions cannot be obtained. It is necessary to solve these equations by trial and error, numerical, or graphical methods.

Once the critical radius "r*" and composition are found, "a_A", "a_B", and "σ" at the critical composition can be obtained from tabulated data. The critical free energy of formation "ΔG*" can then be calculated by combining equations (17) and (12):

$$\Delta G^* = \frac{4\pi}{3}\ \sigma\ r^{*2} \tag{24}$$

Reiss (1950) assumed that each drop is able to grow or shrink by acquiring or losing single molecules and obtained the following expression for the kinetic factor (Mirabel and Katz, 1974):

$$K = \frac{b_A\ b_B}{b_A \sin^2 A_r + b_B \cos^2 A_r}\ n_{GA} + n_{GB}\ 4\pi\ (r^*)^2 \left(-\frac{P}{Q} \right)^{0.5} \tag{25}$$

where K = kinetic factor
b_A, b_B = number of molecules that arrive at the embryo of species A and B, number /m²-s
n_{GA}, n_{GB} = number densities of species A and B in gas phase, number /m³

A_r = the rotated angle of the principal axis, degree

r^* = critical radius of the embryo, m

P, Q = second order partial derivative of "ΔG" with respect to the rotated axis "n_A" and "n_B"

The angle of rotation is given by the equation

$$\tan 2A_r = \frac{\dfrac{\partial^2(\Delta G)}{\partial n_A \; \partial n_B}}{\dfrac{\partial^2(\Delta G)}{\partial n_A^2} - \dfrac{\partial^2(\Delta G)}{\partial n_B^2}} \tag{26}$$

In terms of the unrotated second derivatives and angle of rotation, "P" and "Q" are given by the equations:

$$P = \frac{\partial^2(\Delta G)}{\partial n_A{}^2} \cos^2 A_r + 2 \frac{\partial^2 n(\Delta G)}{\partial n_A \partial n_B} \cos A_r \sin A_r + \frac{\partial^2(\Delta G)}{\partial n_B^2} \sin^2 A_r \tag{27}$$

$$Q = \frac{\partial^2(\Delta G)}{\partial n_A^2} \cos^2 A_r + 2 \frac{\partial^2(\Delta G)}{\partial n_A \partial n_B} \sin A_r \cos A_r + \frac{\partial^2(\Delta G)}{\partial n_B^2} \cos A_r \tag{28}$$

If species "B" is present in low concentration compared to "A", then $b_B << b_A$, $n_{GB} << n_{GA}$, and "K" simplifies to:

$$K = \frac{4\pi (r^*)^2 \, b_B}{\sin^2 A_r} \, n_{GA} \left(- \frac{P}{Q} \right)^{0.5} \tag{29}$$

Kiang and Stauffer (1973) approximated equation (29) with the following equation which is much simpler for calculating the nucleation rate:

$$K = \frac{4\pi(r^*)^2 \, n_{GA} \, n_{GB} \, kT}{(2\pi \, m_B \, kT)^{0.5}} \qquad (30)$$

where
K = kinetic factor
k = Boltzmann's constant, J/K
m_B = mass per molecule of species "B", kg
n_{GA}, n_{GB} = number concentration of species "A" and "B" in gas phase, number /m^3
r^* = critical radius of embryo, m
T = temperature, K

The hetermolecular homogeneous nucleation theories presented in the above paragraphs have been used by a number of researchers (e.g. Kiang and Stauffer (1973), Mirabel and Katz (1974)) to predict the formation of $H_2O - H_2SO_4$ particles in the atmosphere. However, they ignored the formation of $H_2O - H_2SO_4$ hydrates. Giaugue et al. (1960) have published a phase diagram indicating the existence of six distinct solid hydrate phases. These are $H_2SO_4 \cdot H_2O$, $H_2SO_4 \cdot 2H_2O$, $H_2SO_4 \cdot 3H_2O$, $H_2SO_4 \cdot 4H_2O$, $H_2SO_4 \cdot 6.5\ H_2O$, and $H_2SO_4 \cdot 8H_2O$, the last being speculative. The formation of hydrates will reduce the rate of nucleation because it lowers the partial pressure of the free H_2SO_4 molecules, i.e. lowers the saturation ratio of sulfuric acid vapor.

The effect of hydrate formation on nucleation rate has been examined by Heist and Reiss (1974), Shugard et al. (1974), and Shugard and Reiss (1976). They derived a new equilibrium distribution for the critical size nuclei "n^*" in terms of "n_{GB}", the number concentration of acid molecules (hydrated or not) and the sum of the number concentrations for the hydrate species "n_{Bh}" (containing one acid molecule and "h" water molecules). The critical size nuclei, "n^*" is given by:

$$n^* = n_{GA}\left(1 - \frac{n_{Bh}}{n_{GB}}\right)\exp\left(-\frac{\Delta G^*}{kT}\right) \qquad (31)$$

where n^* = number concentration of critical size embryos, number $/m^3$

n_{GA} = number concentration of water molecules, number $/m^3$

n_{GB} = total number concentration of acid molecules, number $/m^3$

n_B^* = number of acid molecules in the critical size drop number

n_{Bh} = number concentration of hydrates which consist of one H_2SO_4 molecule and "h" water molecules, number $/m^3$

ΔG^* = critical Gibbs free energy of formation, J/drop

k = Boltzmann's constant, J/K

T = temperature, K

The net rate of acid hydrates striking a critical size drop is:

$$Y_B = (8\pi kT)^{0.5} \sum_h \frac{(r^* + r_h)^2 \, n_{Bh}}{\left(\frac{1}{m_d} + \frac{1}{m_h}\right)^{-0.5}} \qquad (32)$$

where Y_B = net rate of acid hydrates striking a critical size drop, $/m^2$-s

r^* = radius of the critical size drop, m

r_h = radius of the hydrate which has "h" H_2O molecules, m

m_d = mass of the critical size drop, kg

m_h = mass of the hydrate which has "h" H_2O molecules, kg

n_{Bh} = number density of hydrate containing "h" H_2O molecules, number $/m^3$

Finally, the rate of nucleation accounting for hydrate formation is predicted by:

$$I = \frac{Y_B}{\sin^2 A_r} n_{GB} \left(1 - \frac{n_{Bh}}{n_{GB}}\right)^{n_B^*} \exp\left(- \frac{\Delta G^*}{kT}\right) \qquad (33)$$

where I = nucleation rate, number /m³-s

Heterogeneous Condensation

When large concentrations of particles are present and the saturation ratio is low, condensation takes place on the existing particles without formation of new particles. This process is called heterogeneous condensation.

The rate of heterogeneous condensation depends on the exchange of mass and heat between a particle and the gas phase. When the particle diameter is large compared to the mean free path of the gas, diffusional theory can be used to calculate the transport rate of the condensible species toward the particle. The rate of diffusional condensation is given by the Maxwell equation:

$$\frac{dn_A}{dt} = \frac{2\pi d_p D_p}{kT} (p - p_d^o) \qquad (34)$$

or

$$\frac{d\, d_p}{dt} = \frac{4 D_p M}{RT\, d_p} (p - p_d^o) \qquad (35)$$

where d_p = particle diameter, m

D_p = diffusivity of the condensing species in the gas phase, m²/s

n_A = quantity of vapor in gas, mol

R = universal gas constant, m³-mmHg/K-mol

T = temperature, K

p = vapor pressure, mmHg

p_d^o = equilibrium vapor pressure above the particle at the particle temperature, mmHg

t = time, s

M = molecular weight, kg/mol

For particles with diameter much smaller than the mean free path of gas, the rate of condensation can be calculated from kinetic theory of gas (Friedlander, 1977):

$$\frac{dn_A}{dt} = \frac{a_c \ (p - p_d^\circ) \ \pi d_p^2}{(2\pi m \ kT)^{0.5}} \tag{36}$$

where
k = Boltzmann's constant, J/K
a_c = accommodation coefficient, dimensionless
m = mass per molecule, kg

For particles with diameters in the intermediate range, there is no simple analytical equation for predicting the condensation rate. Fuchs and Sutugin (1971) proposed the following approximate interpolation formula for predicting the rate of condensation:

$$\frac{dn_A}{dt} = 2\pi \ MD_p \ d_p \frac{(p - p_d^\circ)}{kT} \left[\frac{1 + N_{Kn}}{1 + 1.71 N_{Kn} + 1.333 N_{Kn}^2} \right] \tag{37}$$

where $N_{Kn} = \frac{2 \ l_m}{d_p}$ = Knudsen number, dimensionless
l_m = mean free path of gas, m

When $N_{Kn} << l_m$, i.e. particles are large, equation (37) reduces to equation (35). When $N_{Kn} >> l_m$, equation (37) is about 1.2 times equation (36) with $a_c = 1$.

The equilibrium vapor pressure, "p_d°", in equations (35) through (37) is a function of particle diameter and particle temperature. When vapor condenses on the surface of a particle, the latent head of condensation is released and the temperature of the particle becomes higher than the temperature of the gas. The temperature of the particle can be predicted by performing an energy balance around the particle. The resulting equation is:

$$\frac{1}{6} \pi d_p \rho_p C_p \frac{d T_d}{dt} = \frac{dn_A}{dt} L - 2\pi d_p h (T_d - T) \qquad (38)$$

where T_d = temperature of the particle, °C
C_p = heat capacity of the particle, cal/kg
h = heat transfer coefficient, cal/°C-m²-s
ρ_p = particle density, kg/m³
L = latent heat of vaporization, cal/kg
n_A = quantity of vapor in gas, mol

Once the particle temperature is calculated from equation (38), the equilibrium vapor pressure can be calculated from Kelvin's equation by assuming the particle behaves like a pure drop of the condensing species:

$$p_d^{\circ} = p^{\circ} \exp\left(\frac{d_p^{*} \ln S}{d_p}\right) \qquad (39)$$

where p° = equilibrium vapor pressure over a flat surface of liquid, Pa
d_p^{*} = critical diameter of the drop or particle, m
S = saturation ratio, dimensionless

The homogeneous nucleation theories and the heterogeneous condensation theories presented in the above can be applied to industrial stacks to predict the formation of sulfate particles. These processes together with particle growth, diffusion, coagulation, convection, and sedimentation determine the time rate of change of the particle size distribution function. A population balance equation (or general dynamic equation) can be set by performing a material balance. By solving the equation for different initial and boundary conditions, the size distribution function can be calculated for geometries and flow conditions of interest.

Oxidation in Liquid Drop

Gases such as SO_2, NH_3, CO_2, and Cl_2 dissolve in water and hydrolyze to produce a variety of ionic species. The sulfur dioxide-water system is discussed in the following sections because it leads to the formation of sulfate particles.

When SO_2 is in equilibrium with sulfur(IV) sulfur(IV) stands for the sum of H_2SO_3, HSO_3^-, and $SO_3^{=}$) in water, the following equations describe the equilibrium:

$$SO_2\ (gas) + H_2O \rightleftarrows H_2SO_3 \tag{40}$$

$$H_2SO_3 \rightleftarrows H^+ + HSO_3- \tag{41}$$

$$HSO_3^- \rightleftarrows H^+ + SO_3^{=} \tag{42}$$

$$H_2O \rightleftarrows H^+ + OH^- \tag{43}$$

The corresponding equilibrium relationships are:

$$P_{SO_2} = H_x [H_2\ SO_3] \tag{44}$$

$$K_1 = \frac{[H^+][H\ SO_3^-]}{[H_2\ SO_3]} \tag{45}$$

$$K_2 = \frac{[H^+][SO_3^{=}]}{[H\ SO_3^-]} \tag{46}$$

$$K_3 = [H^+]\ [OH^-] \tag{47}$$

where K_1, K_2, K_3 = equilibrium constants
H_x = Henry's constant, atm/mol fraction
$[H^+]$ = hydrogen ion concentration in the water, mol
$[HSO_3^-]$ = bisulfite ion concentration, mol

$[SO_3^{2-}]$ = sulfite ion concentration, mol
$[OH^-]$ = hydroxyl ion concentration, mol
$[H_2SO_3]$ = physically dissolved concentration of SO_2, mol

The Scrubber Handbook (Calvert et al., 1970) approximated the Henry's constant tabulated in International Critical Table (1928) by the following equation:

$$\ln H_x = 2.518 + 0.4263\ t - 0.0001235\ t^2 \tag{48}$$

where H_x = Henry's constant, atm/mol fraction of total dissolved, SO_2
t = temperature, °C

In Table 2, some values for the thermodynamic constants H_x, K_1, and K_2 are given as a function of temperature. Figure 2 shows the mole fraction of the three sulfur (IV) species in equilibrium as a function of solution pH at 25°C. As can be seen, the bisulfite ion, HSO_3^-, is the most abundant sulfur (IV) species in the pH range of 3 to 6. At $pH > 8$, sulfite ion, SO_3^{2-}, is the dominant species.

The sulfate formation due to the heterogeneous SO_2-oxidation in the drop has the following three steps occurring in series:

1. Transfer of SO_2 in bulk gas-phase to the vicinity of drop surface
2. Absorption of SO_2 into the water drop
3. Oxidation of SO_2 to sulfate

Steps (1) and (2) can be predicted from mass transfer. Step (3) depends on how SO_2 is oxidized and it is the rate determining step for sulfate formation in liquid phase (Beilke and Gravenhorst, 1978).

TABLE 2. EQUILIBRIUM CONSTANT FOR THE SO_2-WATER SYSTEM AS A FUNCTION OF TEMPERATURE.

Temperature °C	H_x, mol/l-atm	K_1, molar	K_2, molar
5	2.72	2.78×10^{-2}	1.0×10^{-7}
15	1.76	2.19×10^{-2}	7.9×10^{-8}
25	1.24	1.74×10^{-2}	6.24×10^{-8}
Author	Gmelin(1963)	Sillen(1964)	Sillen(1964)

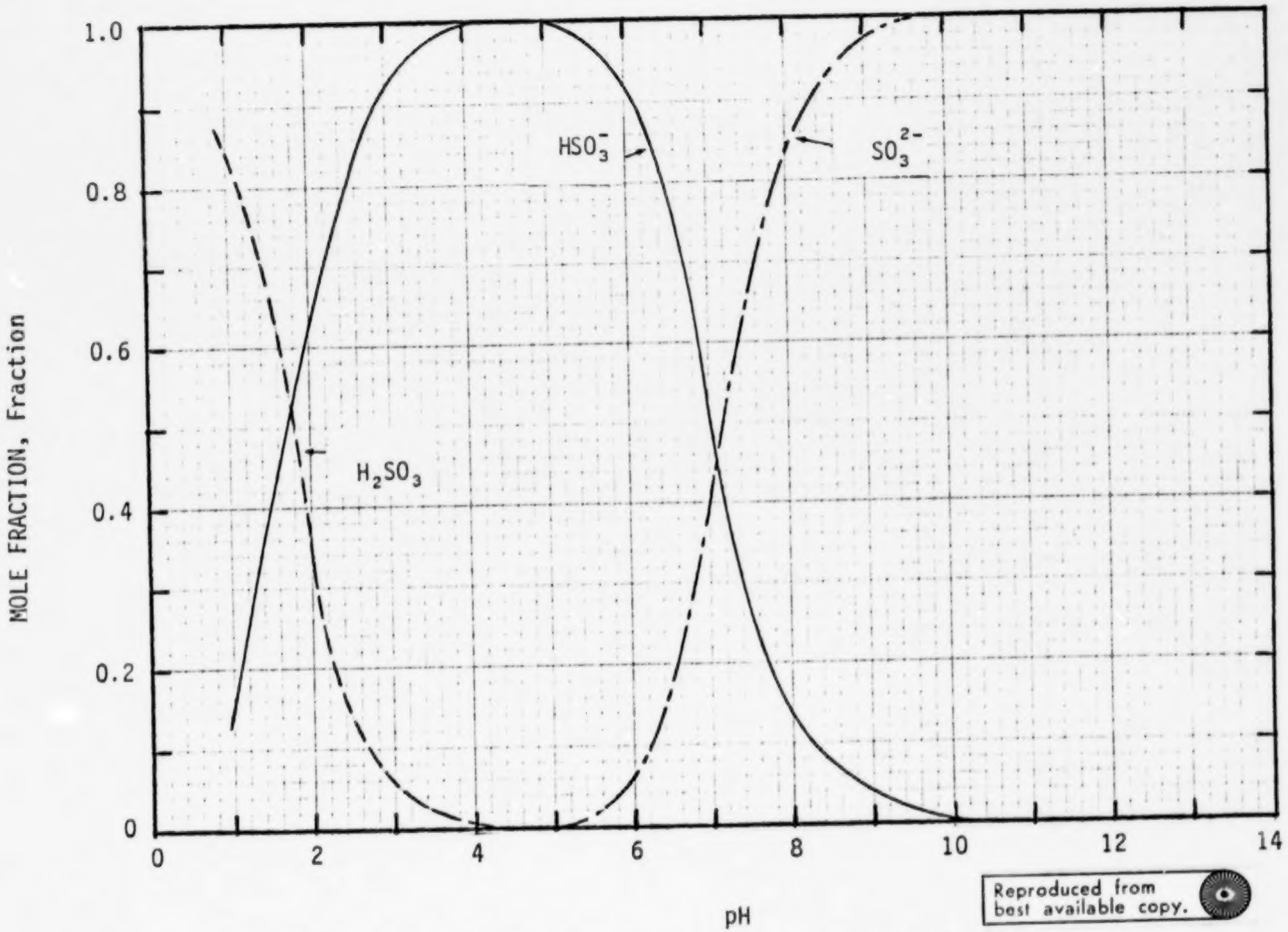

Reproduced from best available copy.

Figure 2. Mole fraction of Sulfur (IV) species in equilibrium at 25°C as a function of solution pH.

Liquid phase SO_2-oxidation can occur according to one or more of the following processes:

1. Oxidation by O_2 in the absence of catalysts
2. Oxidation by O_2 in the presence of catalysts
3. Oxidation by strong oxidizing agents

Oxidation By O_2 In The Absence of Catalysts

One of the most important questions in the oxidation of SO_2 in liquid phase is whether the bisulfite ion or the sulfite ion is the oxygen carrier or both. A great many discrepancies in the literature concerning the pH dependence of SO_2-oxidation and sulfate formation could be removed if there were a clear answer to this question since in a water drop in equilibrium with a fixed SO_2 concentration $[HSO_3]$ varies with $1/[H^+]$ and $[SO_3^{2-}]$ with $1/[H^+]^2$.

The more widely accepted view is that SO_3^{2-} is the oxygen carrier and the oxidation follows the simple overall reaction:

$$SO_3^{2-} + 1/2\ O_2 \longrightarrow SO_4^{2-} \qquad (49)$$

Table 3 summarizes the rate expressions which emerge from some of the principal laboratory experiments which have been carried out on the uncatalyzed oxidation of SO_2 by oxygen. It can be seen that most investigators have expressed the production rate of SO_4^{2-} as a function of sulfite concentration in the aqueous solution and that this rate varies linearly with the concentration of SO_3^{2-}. The production rate of SO_4^{2-} is independent of oxygen concentration for acidic solutions ($3 < pH < 7$) but it varies linearly with concentration of oxygen at high pH's ($pH > 9$).

The temperature dependence of the uncatalyzed liquid phase oxidation rate of SO_2 by oxygen in the acidic region is fairly weak. Larson et al. (1978) reported an activation energy of only 7.1×10^3 J/mol in this region. However, for $7 \leq pH \leq 9.5$, Larson et al. (1978) reported an activation energy of 8.9×10^4 J/mol.

Table 3: Rate Expressions for the Uncatalyzed Oxidation of SO_2 in Aqueous Solutions

Author	Rate Expression	Rate Constants	pH Range	Temp. °C
Fuller and Crist(1941)	$\frac{d[SO_4^{2-}]}{dt} = (k_1+k_2[H^+]^{0.5})[SO_3^{2-}]$	$k_1 = 1.3\times10^{-2}$, 1/s $k_2 = 6.6$, $1/M^{0.5}s$	5.09-7.82	25
Winkelmann (1955)	$\frac{d[SO_4^{2-}]}{dt} = k_1[SO_3^{2-}]$	$k_1 = (4\pm1.5)\times10^{-3}$, 1/s	7.0 to 10.3	25
Schroeter (1963)	$\frac{d[SO_4^{2-}]}{dt} = k_1[SO_3^{2-}]+k_2[HSO_3^-][H^+]^{-0.5}$	$k_1 = 2.9\times10^{-3}$, 1/s $k_2 = 2\times10^{-6}$, $M^{0.5}/s$ $k_3 = 32$, $1/M^{0.5}$-s	6.95 to 8.20	25
Scott & Hobbs (1967)	$\frac{d[SO_4^{2-}]}{dt} = k_1[SO_3^{2-}]$	$k_1 = 1.6\times10^{-3}$, 1/s	?	25
Miller & de Pena (1972)	$\frac{d[SO_4^{2-}]}{dt} = k_1[SO_3^{2-}]$	$k_1 = 3\times10^{-3}$, 1/s	2 to 4	25
Beilke, et al (1975)	$\frac{d[SO_4^{2-}]}{dt} = k_1[H^+]^{-0.16}[SO_3^{2-}]$	$k_1 = 1.2\times10^{-4}$, $M^{0.16}/s$	3 - 6	25
Larson, et al. (1978)	$\frac{d[SO_4^{2-}]}{dt} = (k_1+k_2[H^+]^{0.5}+k_3P_{O_2}[H^+]^{-1})[SO_3^{2-}]$	$k_1 = (4.8\pm0.6)\times10^{-3}$, 1/s $k_2 = (8.9\pm1.0)$, /s-$M^{0.5}$ $k_3 = (3.9\pm0.6)\times10^{-2}$, M/s-atm	4 - 12	25

A special type of SO_2-oxidation by O_2 in the absence of catalysts is the oxidation in the presence of ammonia (NH_3). It has been accepted by many scientists that the SO_2 - NH_3 - H_2O mechanism was the effective SO_2-oxidation process in atmospheric drops. The effect of ammonia is to keep the drop pH high when sulfur (IV) is oxidized to sulfate. This effect was investigated by many scientists, for example by Junge and Ryan (1958), Van den Heuvel and Mason (1963), Scott and Hobbs (1967), McKay (1971), Miller and de Pena (1972), Easter and Hobbs (1974), and Tomasi et al. (1975).

SO_2-Oxidation By O_2 in the Presence of Catalysts

Catalysts are mainly transition metals of the 4th period, especially manganese and iron. Table 4 shows a summary of rate expressions by various investigators. It can be seen that most workers have found that the rate of production of SO_4^{2-} varies linearly with the sulfur species which they have chosen to use. Also, most studies suggest that the production rate is dependent on the concentration of SO_3^{2-} or HSO_3^- .

The dependence of the rate of sulfate production on the concentration of the catalyst is most difficult to resolve from the available data. The difficulty arises because of the variety of catalysts employed, the differences in the concentrations of both catalyst and sulfite employed in various studies, and the different anions of the catalyst salts. The general results indicated by the catalyzed studies summarized in Table 4 are that the sulfate production rate appears to be linearly dependent on the concentration of the catalyst. However, there is considerable disagreement on the relative efficiencies of the catalysts and the maximum amounts to catalyze the reaction.

Barrie and Georgii (1976) reported an interesting catalytic effect in using "mixed salt" catalyst. They found that equimolar concentrations (on the order of 10^{-5} M) of $Mn\,Cl_2$ and $Fe\,Cl_3$ (or $Fe\,Cl_2$) produced an oxidation rate about one order of magnitude greater than that for the same molar concentration of $Mn\,Cl_2$ or $Fe\,Cl_3$ alone. If this "mixed salt" effect were to occur under

Table 4: Rate Expression for the Catalyzed Oxidation of SO_2 in Aqueous Solutions

Author	Rate Expression	Rate Constant	pH Range	Remarks
Fuller & Crist(1941)	$\frac{d[SO_4^{2-}]}{dt} = (k_1+k_2[Cu^{2+}])[SO_3^{2-}]$	$k_1=0.013$, /s $k_2=2.68\times10^2$, /s-M	≤ 10.6	Cupric ion conc. 10^{-9} to 10^{-4}M
Karraker (1963)	$\frac{-d[SO_4^{2-}]}{dt} = k_1\frac{[Fe^{3+}]}{[H^+]}\left(1-k_2\frac{[Fe^{2+}]}{[O_2]}\right)[H_2SO_3]$	-	1.39-2.6	$10^{-4}M<[Fe^{3+}]<10^{-1}M$, $[SO_2]_{ag} = 10^{-3}M$ $T = 10°C$
Barron & O'Hern (1966)	$\frac{-d[O_2]}{dt} = k_1[Cu^{2+}]^{0.5}[SO_3^{2-}]^{1.5}$	$k_1=1.2\times10^3$, /s-M	7-9	$10^{-7}M<[Cu^{2+}]<10^{-4}M$
Bracewell & Gall(1967)	$R_o = \frac{[SO_2]_o^{2.2}\,[MnSO_4]^2}{k_1[MnSO_4]^2+k_2[SO_2^-]_o^{2.2}}$	$k_1=1.32\times10^{-3}$, s/M $k_2=3.2\times10^{-4}$, s/M	-	$1\times10^{-5}M<[SO_2]<3.4\times10^{-5}M$ $1\times10^{-6}M<[Mn^{2+}]<7.5\times10^{-5}M$
Matteson et. al.(1969)	$\frac{d[SO_2]_{aq}}{dt} = k_1[Mn^{2+}][SO_2]_{aq} + k_2([Mn^{2+}]_o - Mn^{2+})$	$k_1=4.2\times10^3$, /s-M $k_2=0.17$, /s	-	
Cheng et al. (1971)	$\frac{d[SO_4^{2-}]}{dt} = k_1[\text{Mass of } Mn^{2+}][SO_2]$	-	-	-
Brimblecombe & Spedding (1974)	$\frac{d[S(IV)]}{dt} = k_1[Fe^{3+}][S(IV)]$	$k_1 = 100$, /s-M	≤ 4.9	$T = 25°C$ $10^{-7}M<[SO_3]<10^{-2}M$ $5\times10^{-8}M<[Fe^{3+}]<5\times10^{-6}M$

Table 4: Continued

Author	Rate Expression	Rate Constant	pH Range	Remarks
Freiberg (1974)	$\frac{d[SO_4^{2-}]}{dt} = (k_1 + k_2[Fe^{3+}])[Fe^{3+}][H^+][SO_3^-]^2$	$k_1 = 3.8 \times 10^{16}$, /s-M^3 $k_2 = 5.7 \times 10^{18}$, /s-M^4	1.39 to 2.6	-
Barrie & Georgii (1976)	$\frac{d[SO_4^{2-}]}{dt} = k_1[SO_3^{2-}]$	$k_1 = 9.4 \times 10^2$, s with $[MnCl_2] = 10^{-4}M$	1.8 to 3.0	
Sutherland (1977)	$\frac{d[SO_4^{2-}]}{dt} = \frac{[HSO_3^{2-}][H^+]^n[Fe^{3+}]}{k_1 + k_2[HSO_3^-]}$	$n \leq 1.0$ $k_1 >> k_2[HSO_3^-]$ for small $[HSO_3^-]$	<4.5	

atmospheric conditions, it could be of great importance in the oxidation of SO_2 in the atmosphere.

With regard to the temperature dependence of the catalyzed reaction, an activation energy of 7.7×10^4 J/mol is most often quoted (Barron and O'Hern, 1966). This measurement was made on mildly alkaline solutions ($7 \leq pH \leq 9$). Hoather and Goodeve (1934) reported a "critical increment" for the overall process of 11.4×10^4 J/mol ± 4% in acidic solutions with $MnCl_2$ as catalyst, and Sutherland has reported an activation energy of $(14.2 \pm 0.8) \times 10_4$ J/mol for $pH \leq 4.5$ with Fe^{3+} as catalyst. The higher values in the acid region cast some doubt on the importance of the catalyzed reaction in the atmosphere. Barrie and Georgii found that their "mixed salt" catalyst displayed a negligible temperature dependence, although the activation energies for the single salts were similar to that found by Hoather and Goodeye (1934).

Uncatalyzed Liquid Phase Oxidation of SO_2 By Strong Oxidizing Agents

Most important oxidizing agents are O_3 and H_2O_2. SO_2 oxidation in solution by ozone has been studies by Penkett (1972, 1974), Penkett et al. (1979), and Larson et al. (1978). The rate expressions derived by them are:

$$\text{Penkett:} \quad \frac{d[SO_4^{2-}]}{dt} = k_3 \, [O_3]_{aq} \, [H\,SO_3^-] \qquad (50)$$

where $k_3 = 3.3 \times 10^5$, (Penkett, 1972)

$k_3 = 2 \times 10^8$, (Penkett, 1974)

$k_3 = 7.13 \times 18^5$ at pH = 4, (Penkett, 1979)

$k_3 = 1.79 \times 10^6$ at pH = 5, (Penkett, 1979)

$k_3 = 4.5 \times 10^6$ at pH = 6, (Penkett, 1979)

Larson:

$$\frac{d[SO_4^{2-}]}{dt} = (4.4 \pm 2.0) \times 10^4 \; K_{HO_3} \, P_{O_3} \, [HSO_3^-] \, [H+]^{-0.1 \pm 0.02} \qquad (51)$$

where $K_{HO_3} = 0.0123$ M/atm

As can be seen, the rate of production of SO_4^{2-}, derived by both of these workers, varies linearly with the concentration of ozone and bisulfite. Larson et al. (1978) observed a weak dependence on the explicit hydrogen ion concentration, and Penkett et al. (1972, 1974, 1979) observed no dependence on explicit hydrogen ion concentration. These results suggest that the liquid phase oxidation of SO_2 by ozone will be less prone to retardation in acid solutions than oxidation by oxygen. It is noteworthy that the rates derived from these studies agree within a factor of two.

The temperature dependence of the ozone oxidation reaction is relatively weak. Larson et al. (1978) measured an activation energy of 1.6×10^4 J/mol over a pH range of 4 to 6. This is not significantly different from the activation energy for oxidation by oxygen; therefore, the relative importance of two oxidizing agents should not vary greatly with temperature.

Another oxidizing agent of importance SO_2-oxidation in liquid phase is H_2O_2 due to its high solubility in water. Penkett et al. (1979) performed experiments to measure the reaction rate and derived the following rate expression:

$$\frac{d[SO_4^{-}]}{dt} = k_4 \, [H_2O_2] \, [HSO_3^{-}] \qquad (52)$$

where $k_4 = 1.3 \times 10^3$ m^3/mol-s at pH = 4.3
$k_4 = 5.4 \times 10^2$ m^3/mol-s at pH = 5.4
$k_4 = 2.7 \times 10^1$ m^3/mol-s at pH = 6.6
$[H_2O_2] = 4.3 \times 10^{-5}$ mol/m^3 for 1 ppb H_2O_2

Significant discrepancies exist between the rate constants derived by various researchers. It is necessary to evaluate the experimental techniques used by these researchers to resolve the discrepancies between the measured values of the rate constants. It should be determined whether the SO_3^{2-} ion or the HSO_3^- ion (or both) is the oxygen carrier. This question is of fundamental importance for the pH dependence of sulfate formation.

Heterogeneous Condensation with Chemical Reaction

Sulfuric acid vapor or sulfur trioxide can transport to a drop or solid particle and react with the drop or the particle to form sulfates. The chemical reaction occurs either on the surface or inside the drop or particle. Depending on the types of chemical reaction, the gas-to-particle conversion occurs in the following steps.

Chemical Reaction on the Surface

1. Diffusion of the vapor from the main body of gas through the gas film to the surface of the drop or particle.
2. Reaction on the surface between the vapor and the particle.

Chemical Reaction Occuring Inside the Particle

1. Diffusion of vapor through the film surrounding the particle to the surface of the solid.
2. Penetration and diffusion of the adsorped vapor into the particle.
3. Reaction inside the particle.

Each of the above steps could be gas-to-particle conversion rate determining steps. For diffusional control, the conversion rate is the same as that predicted from equation (34). For surface reaction control, the conversion rate depends on reaction species, reaction order, and amount of reaction materials present.

The particle will grow if the reaction product remains on the surface or in the particle. The growth rate will be equal to the conversion rate. Friedlander (1977) gave the following equation for particle growth due to internal chemical reaction.

$$\frac{dV_p}{dt} = \frac{d_p^3}{6\rho_p} (\Sigma M_i N_i) r \tag{53}$$

where

V_p = volume of particle, m^3
M_i = molecular weight of species "i", kg/mol
N_i = stoichiometric coeficient for species "i" in the reaction
r = reaction rate

Homogeneous Gas Phase Reaction and Heterogeneous Reaction (Ex-stack)

The SO_2 to SO_4^{2-} conversion is the major sulfate particle formation mechanism in the atmosphere. It has been widely studied in power plant plumes over the last two decades. A list of the mechanisms that have been proposed for SO_2 to SO_4^{2-} conversion in power plant plumes is shown in Table 5 and a list of the conversion rates that have been measured in field studies is given in Table 6.

The rate of conversion of sulfur dioxide to sulfate aerosol in power plant plumes is low near the point of emission, but increases to several percent per hour as ambient air mixes with the plume (Wilson, 1978). Hegg and Hobbs (1980) reported conversion rates ranged from 0 to 5.7% ± 2% of SO_2 per hour for travel times of 10 to 162 min. They reported that both homogeneous nucleation rate to the rate of formation of particle volume was 2.7×10^2 to 3.9×10^5 particles/cm^3 in different plumes, with a mean of $7.4 \times 10^4 \pm 1.2 \times 10^5$ particles/cm^3. The relationship between the rates of formation of particle surface area and particle volume in the plumes was reported to be in fair agreement with the relationship suggested by McMurry and Friedlander (1978).

Sulfate aerosol formation in near stack plume could be due to reaction with condensed water drops. The reaction rate depends on the pH of the drop. Junge and Ryan (1958) have found that the oxidation of SO_2 in aqueous solutions decreases markedly as the pH is lowered, becoming negligible at pH values of about 2.

TABLE 5. SUMMARY OF SO_2 OXIDATION PROCESSES IN POWER PLANT PLUMES

Process	Rate based on reactant concentrations in the atmosphere ($\% h^{-1}$)	Reference
(a) Homogeneous Gas Phase		
$SO_2 + OH + (M) \rightarrow HSO_3 (+M)$	0.4–2.7	Davis *et al.* (1974) Calvert *et al.* (1978)
$SO_2 + HO_2 \rightarrow OH + SO_3$	0.2–2.0	Calvert *et al.* (1978)
$SO_2 + CH_3O_2 \rightarrow CH_3O + SO_3$	0.02–2.0	Calvert *et al.* (1978)
$SO_2 + CH_3CHOO \rightarrow SO_3 + CH_3CHO$	0.01–0.3	Cox and Penkett (1972) Calvert *et al.* (1978)
(b) Homogeneous Liquid Phase		
$SO_3^{2-} + O_2 \xrightarrow{Fe^{+3}} SO_4^{2-} + O$	~0.13	Brimblecombe and Spedding (1974)
$SO_3^{2-} + O_3 \rightarrow SO_4^{2-} + O_2$	0.4	Penkett (1972) Larson *et al.* (1978)
$SO_3^{2-} + O_2 \xrightarrow{Mn^{+2} \& Fe^{+3}} SO_4^{2-} + O$	2.2	Barrie and Georgii (1976)
$SO_2 \cdot H_2O + O_2 \xrightarrow{Soot} SO_4^{2-}$	Fast	Chang *et al.* (1977)
(c) Heterogeneous		
$SO_2 + Soot + O_2 \rightarrow SO_4^{2-}$	?	Novakov *et al.* (1974)
SO_2 + aerosol with various trace metals $\rightarrow SO_4^{2-}$	?	Urone *et al.* (1968)

Reproduced from
best available copy.

TABLE 6. RESULTS OF FIELD MEASUREMENTS ON THE RATES OF SO_2 OXIDATION IN POWER PLANT PLUMES

Power plant location	SO_2 oxidation rate ($\% h^{-1}$)	Method	Reference
Colbert Plant (Alabama)	0–30	SO_3 and SO_2 measurements	Gartrell *et al.* (1963)
330 MW Plant in (Eastern U.S.)	18–100	SO_2 decay relative to SF_6	Dennis *et al.* (1969)
Frankfurt am Main (West Germany)	100–300	SO_2 decay relative to CO_2	Weber (1970)
Crystal River (Florida)	36–83	SO_2 decay relative to sub-micron particles	Stephens and McCaldin (1971)
Keystone (Pennsylvania)	0–10	$^{32}S/^{34}S$ ratio, change with oxidation	Newman *et al.* (1975)
Labadie (Missouri)	0.41–4.9	Total change in particle volume	Cantrell and Whitby (1978)
Four Corners (New Mexico)	0.27–0.84	Sub-micron sulfate and SO_2 – change of ratio with ti	Ursenbach *et al.* (1977)
Labadie and Portage des Sioux (Missouri) Muscle Shoals (Alabama) Kyger Creek (Ohio)	0–5	Particulate sulfur to total sulfur ratio	Forrest and Newman (1977)
Labadie (Missouri)	0–3	Particulate sulfur to total sulfur ratio	Gillani *et al.* (1978)
Four Corners (New Mexico)	2–8	CCN production (CCN to SO_2 ratios)	Pueschel and Van Valin (1978)
Labadie (Missouri)	0–4	Particulate sulfur to total sulfur ratio	Husar *et al.* (1978)
Cumberland (Tennessee)	0–7	Particulate sulfur to total sulfur ratio	Meagher *et al.* (1978)
Great Canadian Oil Sands (Alberta, Canada)	0–3	Particulate sulfur to total sulfur ratio	Lusis *et al.* (1978)
Centralia (Washington) Four Corners (New Mexico)	0–6	Total change in particle volume	Hobbs *et al.* (1979)

Physical and chemical sorption of SO_2 and possible subsequent oxidation to sulfate, can be appreciable on the surface of particles which contain insoluble metal oxide as well as soot, even at low relative humidity (Urone et al., 1968; Smith et al., 1969); Corn and Cheng, 1972; Chun and Quon, 1973; Novakov et al., 1974). However, available information suggests that the heterogeneous oxidation of SO_2 at high relative humidities in either water droplets or films surrounding particles, and in the presence of certain catalytic metal salts (especially those of iron or manganese), is the dominant sulfate formation mechanism (Johnstone and Mall, 1958, 1960; Junge and Ryan, 1958; Cheng et al., 1971; Corn and Cheng, 1972; Foster, 1969; Freiberg, 1974; Newman et al., 1975). Sulfate formation by this latter mechanism has been estimated from laboratory data to be as great as 60% per hour (Johnstone and Coughanover, 1958; Cheng et al., 1971).

Rothenberg (1980) presented adsorption isotherm for fly ash particles. He showed that fly ash can absorb appreciable amounts of water. The absorbed water can speed up the SO_2 transformation process because reaction in solution is fast (Chang, 1977).

SECTION 4

EXPERIMENTAL APPROACH

The main objective of the experimental program was to study the sulfate aerosol formation and growth under conditions likely in industrial smoke stacks and near stack plume. Since the production of power from coal and oil accounts for about half the sulfur oxide emissions, the laboratory experiments were designed to model the flue gas in a power plant and covered the formation of sulfate aerosol in the flue gas downstream of the air preheater but not the formation of SO_2 and SO_3 inside the boiler.

Sulfate particle formation involves the following mechanisms:

1. Condensation of sulfuric acid vapor (or water vapor associated sulfur trioxide) to form sulfuric acid drops.
2. Condensation of sulfuric acid vapor on pre-existing particles such as fly ash, liquid drops, and acid drops.
3. Sorption of SO_2 by liquid or solid particles followed by the oxidation of SO_2 to sulfate.
4. Gas phase oxidation of SO_2 to SO_3 which is subsequently condensed by mechanisms 1 and 2.

Gas phase oxidation of SO_2 to SO_3 occurs in high temperature environments or due to light irradiation. Neither of these exists in the duct between the air pre-heater and the stack exit. Therefore, sulfate formation via gas phase oxidation of SO_2 to SO_3 was not studied in the experimental program.

Sulfate formation due to condensation is a physical process in which the gas temperature must be below the acid dew-point temperature. Gas cooling can be the result of heat transfer to the surroundings and quenching (such as by introducing water sprays), and mixing with cold gas.

These cooling processes could occur in industrial smoke stacks and in near-stack plumes. Therefore, experiments were performed in the laboratory to simulate the sulfate particle formation during:

1. Slow cooling,
2. Rapid quenching, and
3. Dilution cooling.

Sulfate formation due to the oxidation of SO_2 to sulfate in the liquid or solid phase is a chemical process. Its rate depends on oxidation mechanisms and kinetics and therefore, it is specific for given conditions such as amount and type of metallic catalysts present, temperature, and pH, etc. The near-stack formation of sulfate aerosol due to reaction with condensed water drops which may have a high pH has been extensively studied by others, so it was not studied in this research.

EXPERIMENTAL APPARATUS

Figure 3 shows the experimental design. The basic design for all experiments was the same and consisted of a flue gas simulator for supplying acid and particle laden gas to the cooling apparatus. Cooling apparatus are:

1. Double-pipe heat exchanger (for slow cooling).
2. Packed bed (for rapid quenching).
3. Parallel stream dilution chamber (for dilution cooling).

Descriptions on the experimental design are presented in the following sections.

Flue Gas Simulator

Simulated flue gas was used in all experiments. Figure 4 shows the process flow diagram of the flue gas simulator. Major components of the simulator include an acid vapor generator, a steam generator, a fly ash particle generator, and a SO_2 gas cylinder. Room air was used as the carrier gas because the

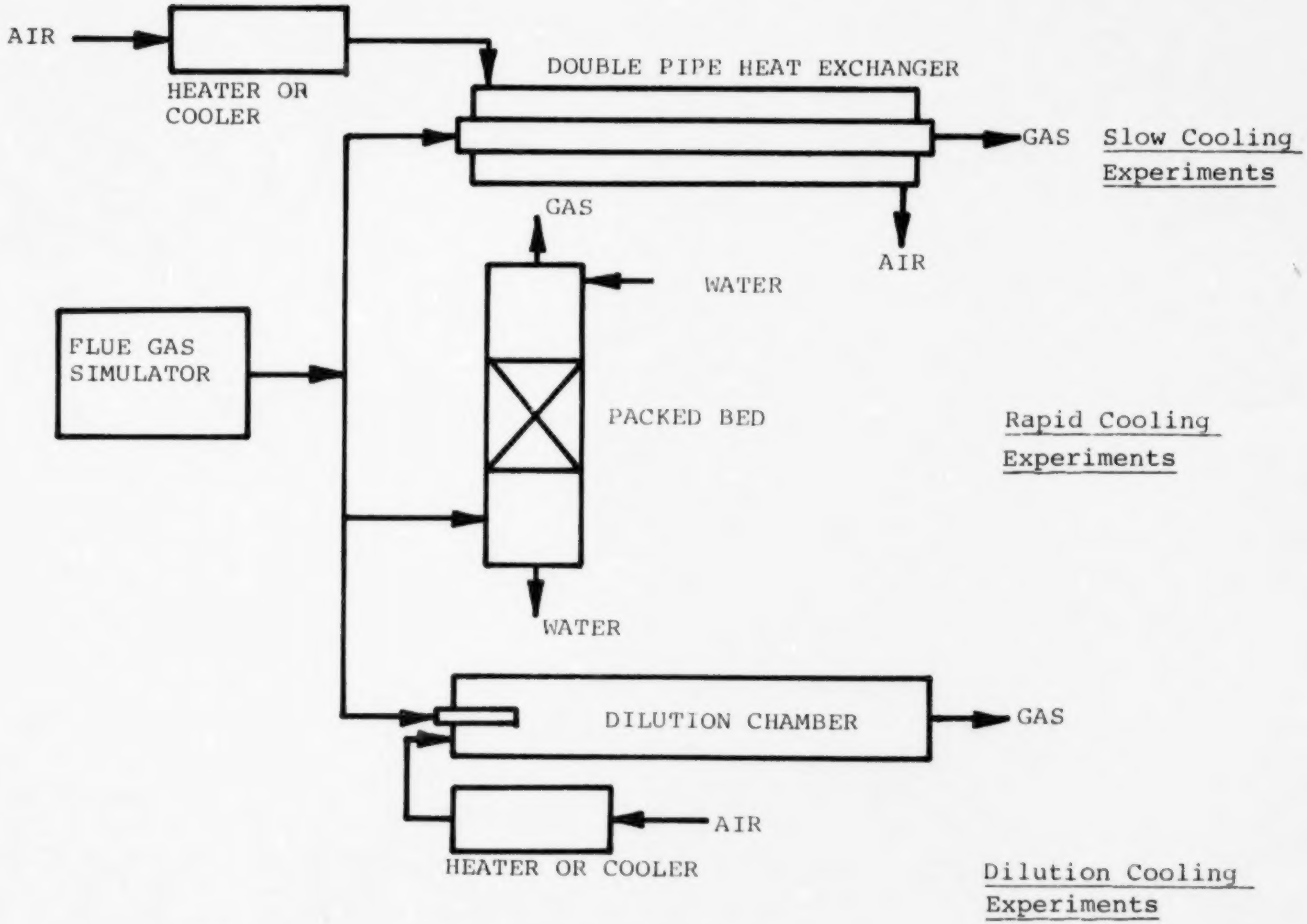

Figure 3. Experimental system design.

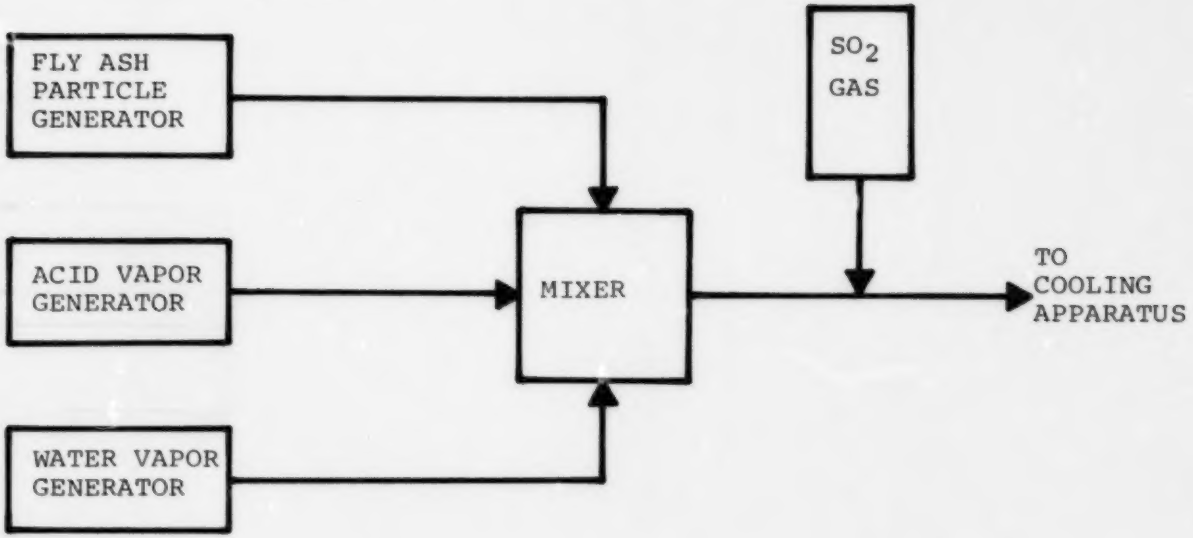

Figure 4. Process flow diagram of flue gas simulator.

amount of oxygen in the flue gas and the presence of carbon dioxide and nitrogen oxides have no effect on acid vapor condensation in the stack.

The nominal gas flow rate and composition at the simulator outlet were:

1. Gas flow rate = 28 l/min.
2. Gas temperature = 200°C.
3. Water vapor = 8% by volume nominal (range = 5-15% by volume).
4. Acid vapor = 20 ppm monimal (range = 10-100 ppm).
5. SO_2 concentration = 1,000 ppm.
6. Fly ash particle concentration = 1.3 g/m^3.

Acid Vapor Generator

Since SO_3 is not available in a gas cylinder, a sulfuric acid vapor generator was required for the experiments. Most of the literature is on sulfuric acid particle generation but some of the methods adaptable to acid vapor generation are:

1. Bubbling dry nitrogen carrier gas through liquid SO_3, which is maintained at 35°C to prevent crystallization.
2. Bubbling dry nitrogen carrier gas through fuming sulfuric acid (120%) which is maintained at a constant temperature of 31°C.
3. Vaporizing dilute sulfuric acid solution at a controlled rate, such as by passing sulfuric acid in aerosol or liquid form through a heated tube.

Methods (1) and (2) are hazardous. Liquid SO_3 and fuming sulfuric acid must be handled with extreme care. The carrier gas must be absolutely free of moisture to avoid chemical reactions. Method (3) is simple and was adopted in the present laboratory experiments.

Preliminary experiments were performed to study the vapor generator's operational characteristics. In the first design (Figure 5), dilute sulfuric acid solution is fed into a heated, sloping tube by means of a peristaltic pump. The solution is

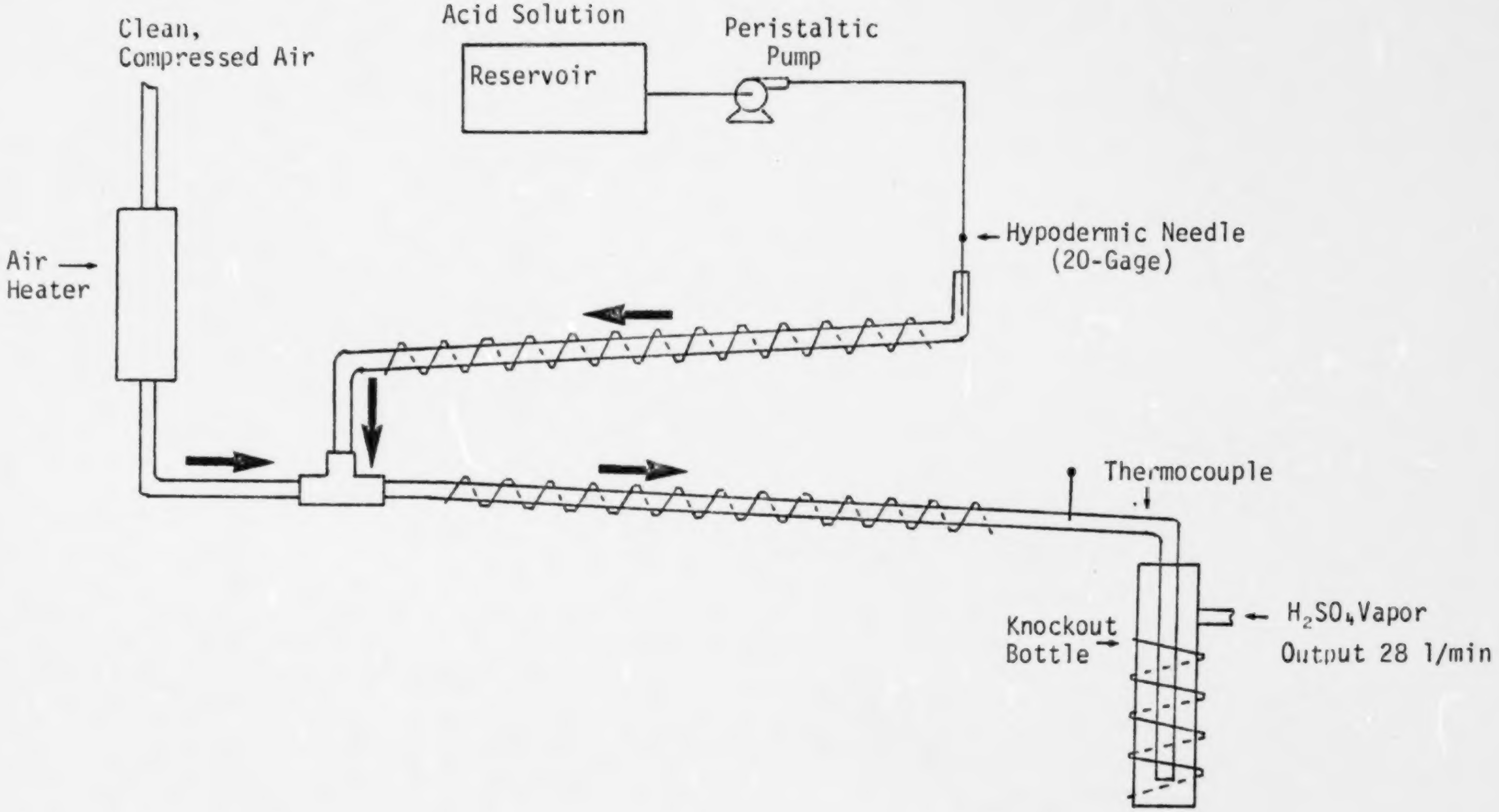

Figure 5. Schematic diagram of the acid vapor generator

forced through a 20-gauge hypodermic needle to maintain a steady stream of solution feed. The solution is heated and partially vaporized in the sloped tube. The partially vaporized solution flows into a second heated tube where a combination of hot air (650°C) and contact with the heated tube completely vaporizes the solution. The hot air also acts as the vapor carrier.

A few experiments were done to determine the operational characteristics of this vapor generator. It was found that this vapor generator had unsteady vapor output because of the low acid solution feed rate (about 1.8 ml/min). The hypodermic needle cannot maintain a steady continuous liquid stream. Dropwise feed was observed and resulted in vapor pulsation, i.e. a pulse of vapor was observed when a drop of acid was fed and was in contact with the hot tube.

The hypodermic needle was subsequently replaced with a nebulizer (Bird Model 4144). The solution in the nebulizer reservoir was maintained at a constant level by continuously feeding solution into it with a peristaltic pump. The modified acid vapor generator was found to give a steady and reproducible output of acid vapor.

Water Vapor Generator

The acid vapor generator could produce about 2% by vol. of water vapor which was lower than the required 5 to 15% vol. for the experiments. A packed column water evaporator, shown in Figure 6, was added to increase the water evaporation capacity. The column was 3.8 cm in diameter, 20 cm in length, and was packed with 2.5 cm ceramic Berl saddles. Water and hot air (648°C, 1,200°F) were metered co-currently into the evaporator, which was also externally heated with electrical tapes.

Sulfur Dioxide and Vapor Mixer

Anhydrous sulfur dioxide gas was supplied from a cylinder. The gas was metered through a rotameter and was mixed with acid and water vapors in an externally heated, 10 cm diameter, 30 cm long column packed with 2.5 cm ceramic Berl saddles in a 5 cm

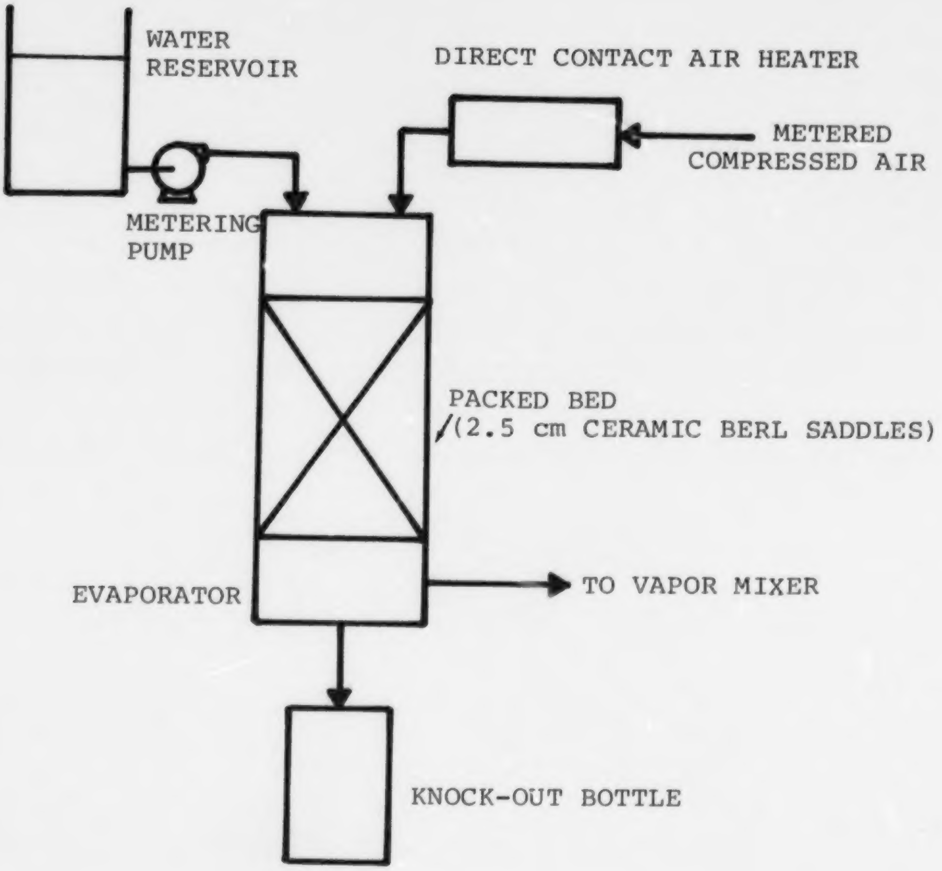

Figure 6. Water vapor generator.

deep bed. The mixer was maintained at a temperature above 371°C (700°F).

Fly Ash Particle Generator

Several small fly ash particle generators, including a fluidized bed and an ejector type generator, were evaluated for providing a steady stream of fly ash particles to the gas streams. The final choice was the ejector system shown in Figure 7.

The major parts of the particle generator included a 30 cm diameter turntable, a Venturi ejector, a dust hopper, a drive motor, and a surge tank. The turntable was made of PVC and a groove was cut into the surface at 25 cm diameter. The turntable was powered by the drive motor through a friction disk and its angular velocity was controlled by a variable transformer power supply to the motor.

A vibrating dust hopper was placed on top of the groove on the turntable. As the turntable rotates, the fly ash filled the groove. A radial arm scraper was used to pack the ash into the groove and to remove excess ash particles. The ash particles in the groove were loosened with a needle downstream from the scraper arm and were then sucked up and dispersed with an air jet ejector. The dispersed particles were passed through a baffled surge tank to remove large particles and minimize the fluctuations of the gas flow.

SAMPLING AND ANALYSIS METHODS

Sulfuric Acid Particle Size Distribution

Since the acid particles are very fine and temperature-sensitive, they can easily deposit, evaporate, grow by condensation, or agglomerate. Therefore, the major requirement for the measuring method is that it either should not change the aerosol size distribution, or should do so in an accountable manner. An instrument that can measure the particles in situ would be ideal.

To evaluate the suitability of various measurement methods and instruments, acid particle diameters, were estimated by

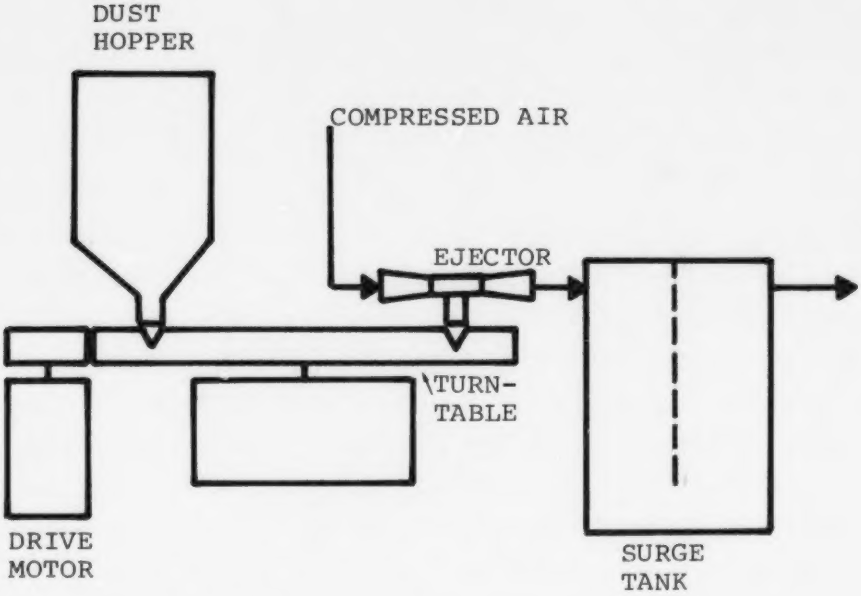

Figure 7. Fly ash particle generator.

assuming that the particles are of uniform size and are formed by hetermolecular nucleation of sulfuric acid and water vapors. Calculations were made for final acid particle number concentrations of 1x10^7, 1x10^8, and 1x10^9/cm. Figure 8 shows the predicted acid particle diameter as a function of initial acid vapor concentration in gas phase. The nucleated particles are smaller than 0.5 μm diameter.

The nucleation temperature was predicted to be in the range of 90°C to 120°C and the acid concentration in the drop was 70 to 80% by weight. From these calculations, the measurement method chosen must, ideally, satisfy the following criteria:

1. Can detect particles as small as 0.001 to 0.005 μm diameter
2. Can sample particles with number concentration $\geq 10^7/cm^3$
3. Can be operated at gas temperatures from 90° to 120°C, and
4. Can resist concentrated sulfuric acid.

Table 7 shows a list of available instruments and their capabilities. The particles are outside the detection capability of optical counters such as the Climet and Royco counters, which have a lower detection limit of 0.3 μm diameter. They are also too small to be measured with regular cascade impactors such as the University of Washington Mark III impactor, the Lundgren impactor, and the Marple impactor. There are some impactors, such as Sierra's ambient impactor and U.W. low pressure impactor, which claim to be able to measure particle diameter down to 0.05 μmA. However, these impactors have high pressure drop which could cause drop evaporation and changes in the particle diameter. There are also impactors which use piezo-electric crystal sensors. This type of impactor will not work in the present study because of gas temperature and humidity effects on the natural frequency of vibration of the crystal.

The particle diameter is within the detection capability of an electrical mobility analyzer (EMA) which detects particles

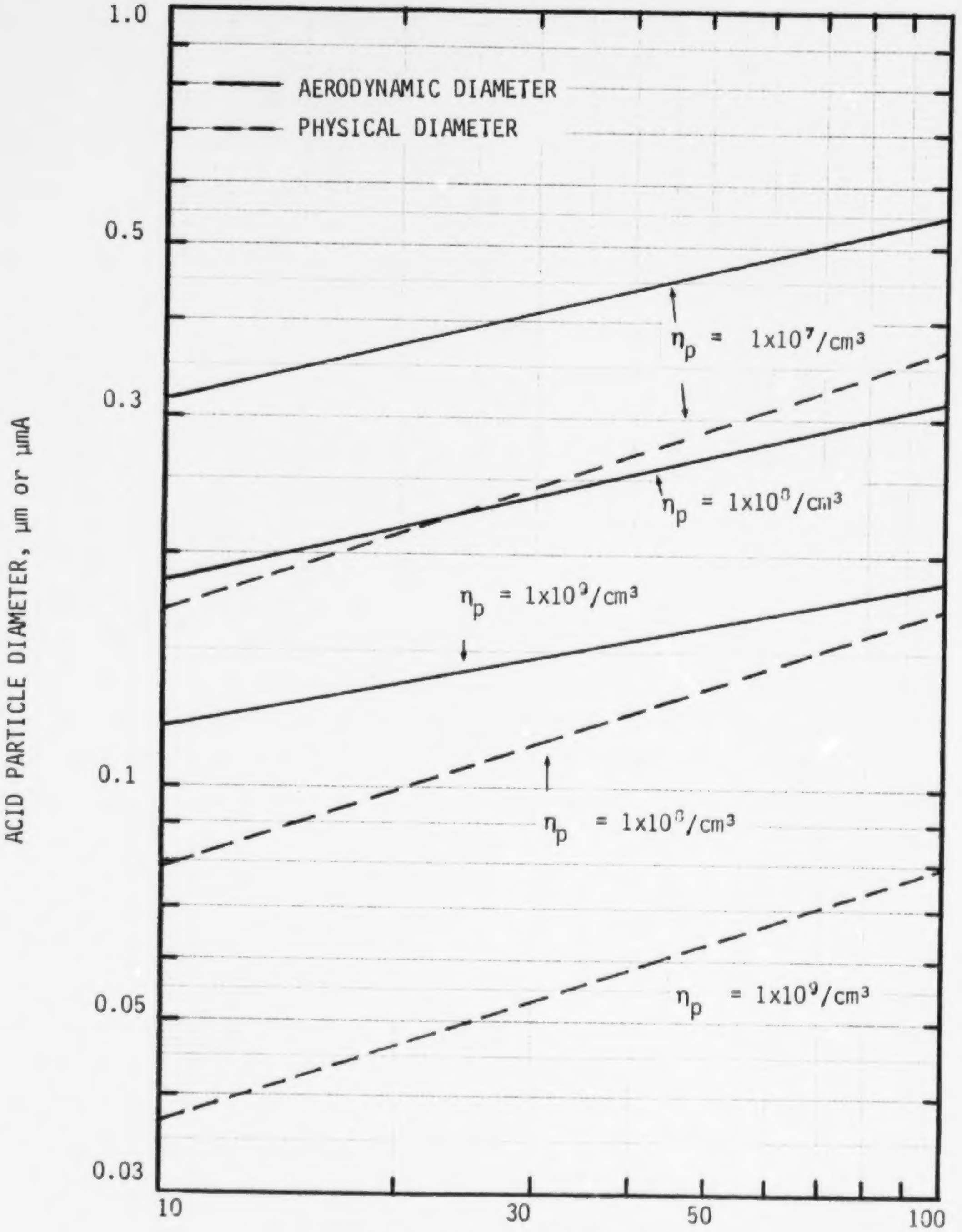

Figure 8. Predicted Acid Particle Diameter.

TABLE 7. SOME CHARACTERISTICS OF AEROSOL MEASUREMENT DEVICES

Instrument	Minimum detectable particle diameter (μm)	Maximum number conc. (#/cm^3)	Maximum operating temperature (°C)	In situ
Climet 208	0.3	4×10^4	50	No
Royco LAS 226	0.1	2×10^3	90	No
General Electric CNC-2	0.001	10^6	-	No
Gardner CNC	0.001	10^6	-	No
Thermo Systems CNC Model 3020	0.02	10^7	30	No
Thermo Systems EAA Model 3030	0.003	10^6	50	No
Diffusion Battery	0.001		260	No
Standard Impactor	0.3	~50mg/m	260	No
Low Pressure Impactor	0.01	-	260	No
Quartz Crystal Microbalance	0.01	~10mg/m	40	No
Classical Scattering Spectrometer (Laser)	0.5	10^4	260	Yes

from 0.01 to 1.0 μm. However, the particle number concentration may be too high for the EMA so a dilution system is needed. Unless the dilution air stream perfectly matches the humidity and temperature of the sample stream, it could change the particle size distribution (Sem, 1977). Even though dilution has this problem, it could still be used if the rate of particle diameter change is slow.

Besides the number concentration limitation, the EMA has temperature and material problems. The acid particle could damage the internal parts of the EMA, which is made of stainless steel. The EMA is usually operated at near-ambient temperatures. The gas could have a temperature near its dew point temperature of about 135°C (275°F). Therefore, cooling is necessary and it will cause changes in the particle size distribution because of condensation and evaporation.

A laser aerosol spectrometer is capable of measuring particle size distributions in situ. An in situ measuring device would be desirable in the present study because it could alleviate acid drop evaporation, deposition, condensation, and agglomeration problems encountered in extractive sampling and sizing techniques. Unfortunately, these instruments can only detect particles larger than 0.5 μm and also have number concentration detection limits (approx. $10^4/cm^3$).

Diffusion battery can meet the particle detection and material requirements. However, it needs careful temperature control to avoid evaporation and condensation of acid particles and its data reduction procedure is tedious.

A diffusion battery has been used successfully by Ikebe and Yamada (1976) for sulfate particle size distribution measurements. This method was finally chosen and an A.P.T. screen diffusion battery was used downstream of an impactor (with final filter removed) for size distribution measurements. The impactor segregates the large particles according to size. The fine particles passing through the impactor are fractionated by the diffusion battery. The size distributions measured with the cascade impactor and the diffusion battery are combined to give the total mass size distribution of the acid drops. The impactor and the diffusion battery were heated to and maintained at gas temperature to minimize drop condensation and evaporation problems.

Sampling Trains

Figure 9 shows the sampling systems. Train "A" was used at the inlet of the cooling apparatus. It consists of a cascade impactor and/ or a quartz filter followed by a condensation coil, quartz filter, three impingers, and gas metering and moving instruments. The sampling probe and the cascade impactor (or the quart filter were heated to above acid dew point to prevent condensation. The condensation coil was water cooled and its tempertaure was maintained between 60°C to 90°C when SO_2 was present. The temperature was not controlled when SO_2 was not injected.

Train "B" was used at the outlet of cooling apparatus. It consisted of an impactor (with final filter removed), connected in series with a screen diffusion battery, a quartz filter, a condensation coil, another quartz filter, 3 impingers, and the gas metering and moving instruments. The impactor, diffusion battery, and the first quartz filter were heated to and maintained at gas temperature. The condensation coil was water cooled and its temperature was controlled at 60°C to 90°C when SO_2 was injected.

With the diffusion battery, it is necessary to measure the particle number concentration penetrating the battery. A condensation nuclei counter (CNC) can be used for this purpose. To prevent acid particle growth, alcohol such as butyl alcohol should be used in the CNC as the condensing vapor rather than water.

There are several commercially available CNC's, such as G.E., Pollack, Gardner, and Thermo-Systems. The Thermo-Systems CNC uses alcohol as the condensing vapor and the other three use water. The G.E., Pollack, and Gardner CNC's are available in A.P.T. laboratory and were evaluated for possible usage. All

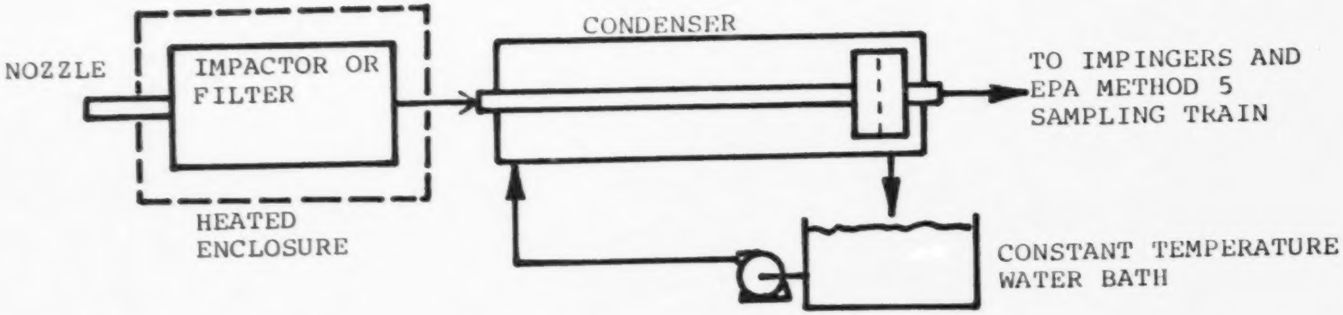
NOZZLE
IMPACTOR OR FILTER
HEATED ENCLOSURE
CONDENSER
TO IMPINGERS AND EPA METHOD 5 SAMPLING TRAIN
CONSTANT TEMPERATURE WATER BATH

TRAIN "A"

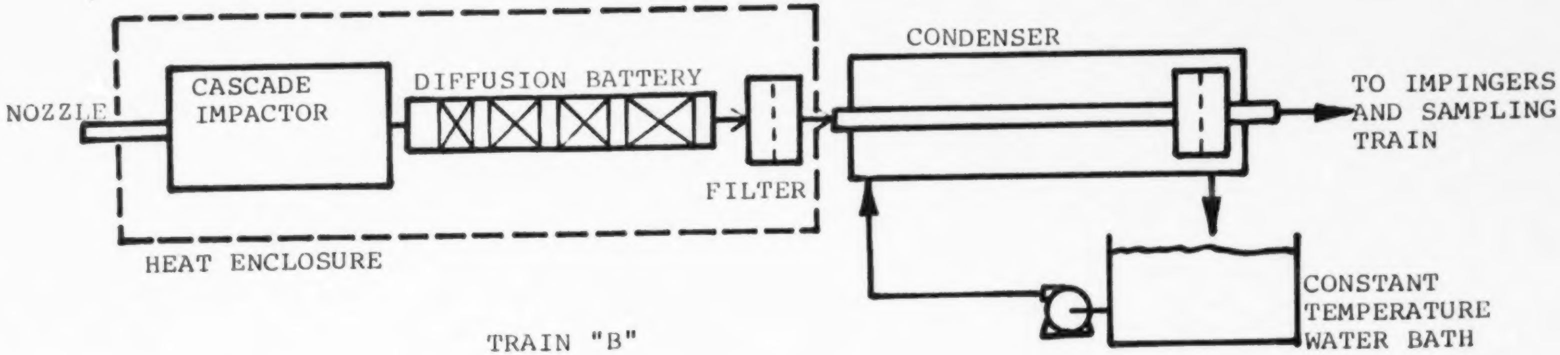

TRAIN "B"

Figure 9. Acid concentration and particle size distribution sampling system.

three CNC's gave erratic, non-reproducible results. It was finally decided to determine the amount of acid collected in each stage of the diffusion battery instead of determining the particle number concentration penetrating the battery. The acid was analyzed by washing the screens from each stage and titrating the washing solution for acid.

The acid collected on impactor substrates was analyzed by extraction and titration. Several filters, including glass fiber filter, quartz filter, and Teflon filter, were evaluated for use as impactor substrates. Quartz filters were finally chosen because they contain no leachable acids, give high percentage of acid recovery, and have the same texture as the filters used in impactor calibrations.

Sulfuric Acid Condensed on Particles

As the sulfuric acid laden gas cools, the acid vapor can either condense on pre-existing particles or nucleate to form new particles. The nucleated acid particles are usually very small and in high number concentration. These small acid particles can be scavenged by the pre-existing particles. Therefore, a major portion of acid vapor will be condensed on the pre-existing particles. Whitby et al. (1978) determined the nuclei formation rates in a coal-fired power plant plume and found that 95% of acid vapor was condensed on pre-existing particles.

Fly ash particles were injected into the gas stream in some experiments. The amount of acid vapor condensed on the fly ash particles needed to be determined for those experiments.

Literature on analyzing the acid content of an aerosol was reviewed. Available methods are:

1. extraction method
2. low temperature volatilization

Extraction Method

Particles are collected on inert filters such as Teflon and quartz filters. After drying and weighing the filter, it is immersed in a selective solvent to extract the sulfates. Water and some organic solvents such as isopropanol and benzaldehyde have been used as the extracting solvent.

The type of solvents to be used depends on the sulfate species to be extracted. Water is generally used for soluble sulfates. Isopropanol is used for extracting sulfuric acid and ammonium bisulfate. Benzaldehyde is used for extracting sulfuric acid.

Benzaldehyde extraction method has been used by Leahy et al. (1975) and Barrett et al. (1977). Leahy et al. (1975) observed that benzaldehyde would extract sulfuric acid from a filter with high efficiency; but would not extract significant amounts of ammonium bisulfate or other sulfates. However, Barrett et al. (1977) reported that reagent grade benzaldehyde will extract ammonium bisulfate as well as other sulfates. Barrett et al. (1977) also found that this interference can be eliminated by distillation of the benzaldehyde.

In a study of Eatough et al. (1978), they found that benzaldehyde is useful as a selective solvent for H_2SO_4 only if the levels of benzoic acid in the solvent are kept low. If the benzaldehyde contains benzoic acid, significant quantities of bivalent metal sulfate salts are also extracted.

The accuracy of banzaldehyde extraction method is limited by the recovery of sulfuric from the filter. Typically, 10μg of sulfuric acid must be present on the filter to be determined by this method (Newman, 1978; Tanner, et al. 1977), and the recoveries found at this level are about 70%. Recovery of 95% is obtained when the filter has 100 μg of sulfuric acid.

After the sulfuric acid has been extracted with benzaldehyde, the acid in benzaldehyde is transferred to water by liquid-liquid extraction and then the acid concentration in aqueous phase is determined by analytical methods. Suitable analytical methods are (Appel et al. 1979; Richard, 1978):

1. Titration with strong base
2. Titration with barium perchlorate
3. Ion chromatograph
4. Flash volatilization - flame photometric detection

5. Turbidimetric determination

Low Temperature Volatilization

The low temperature volatilization (LTV) method for sulfuric acid was developed at the Cabot Corporation (Richards, 1973) under an EPA contract.

The LTV method uses a two-step procedure for separating sulfuric acid from other sulfur-containing compounds. In the first step. particles are collected on a Teflon filter. In the second step, the sulfuric acid is selectively volatilized by a stream of warm, dry, methanolated air. The air is maintained at a temperature between 60°C to 130°C to minimize the volatilization of other sulfate compounds such as ammonium bisulfate. The concentration in the air is determined continuously with a flame photometer. The total mass of sulfuric acid on the filter is determined by integrating the area under the photometer response curve.

Richards et al. (1978) estimated that 55% to 60% of the sulfuric acid is volatilized from the filter and detected. Treatment of the filter with a silicone compound increased the sulfuric acid recovery by a factor of about 1.5.

Selected Method

Due to its higher recovery of sulfuric acid from the filter and simplicity in operation. the extraction method was used in the present experiments. Since interference from ammonium bisulfate was not expected to exist in the laboratory experiments, water was used as the extracting solvent. The acid concentration in the water was determined by titration with barium perchlorate.

Total Sulfate Concentration Measurement

SO_2 and acid vapor concentrations were determined at the inlet and outlet of the experimental apparatus to determine the SO_2 conversion to sulfate and the acid vapor condensation as particles. Methods available for determining the acid vapor concentration are:

1. Absorption of acid vapor in aqueous solutions followed by titration
2. Controlled condensation
3. Dew-point method

Absorption Method

A number of aqueous solutions such as 80% isopropanol (IPA), boiling water, and sodium hydroxide solution can absorb SO_3/H_2SO_4 vapor. The acid vapor laden gas is bubbled through these aqueous solutions to remove the acid vapor which is, then, determined by titration or measured with a sulfur specific ion electrode.

This method has the disadvantage that SO_2 is also absorbed by the aqueous solution. Even though inhibitors can be added to the solution, absorption of SO_2 cannot be completely eliminated. The absorbed SO_2 could be oxidized to sulfates in the solution to give a higher acid concentration.

Controlled Condensation Method

This method has been used to measure the SO_3/H_2SO_4 concentration in power plant flue gas and plumes (Cheney and Homolya, 1978; Patterson et al., 1979; Maddelone and Garner, 1979). The apparatus consists of a heated filter followed by a controlled condensation coil and three impingers. The filter, which is maintained at temperatures above the acid dew-point temperature, is used for removing ash particles. Following the heated filter is a water cooled condensation coil which has a fritted disc at the outlet. The coil and the disc are maintained at a temperature between 60° and 90°C which is below the dew-point of SO_3 but above that of water. The acid vapor condenses on condenser walls or nucleates to form particles which are deposited on walls or collected by the fritted disc. The SO_3 concentration is determined by washing the coil and the fritted disc with isopropanol and titration.

Three impingers filled with hydrogen peroxide follow the condensation coil for collecting the gaseous SO_2 and oxidizing it to sulfates. The solution is titrated for sulfates afterward.

Dew Point Method

The dew-point method determines the dew-point temperature of the gas and then back calculates the acid vapor concentration based on the dew-point temperature. This method has limited applicability because of poor accuracy

Selected Method

The controlled condensation method has been used successfully by A.P.T. in a previous study (Patterson et al., 1979) and was selected for this study with minor modifications. The sampling system consists of a heated quartz filter followed by a condensation coil, another quartz filter, three impingers, and gas moving and metering devices. The front quartz filter was maintained at gas temperature instead of above acid dew point. The front filter was used to remove particulate sulfates. The acid vapor, which passed through the filter condensed and nucleated in the condensation coil. The nucleated acid particles were collected by the filter downstream. When SO_2 was injected into the gas stream, the cooling water temperature was controlled at 60°C to 90°C and the impingers were filled with H_2O_2 solution. The cooling water temperature was not controlled when SO_2 was not injected.

Other Measurements

Water vapor concentration, gas temperature, gas flow rate, SO_2, and acid vapor condensation on wall were also measured for each experiment. Water vapor concentration, gas temperature, gas flow rate, and SO_2 were measured with EPA Method 4, type "K" thermocouples, and rotameters, and a DuPont SO_2 analyzer respectively. The amount of acid vapor condensed on wall was determined by washing with isopropanol or distilled water and titrating the wash liquor with barium perchlorate.

INSTRUMENT CALIBRATION

Cascade Impactors

Cascade impactors were calibrated according to the EPA guidelines developed by A.P.T. (Calvert et al., 1976).

SO_2 Analyzer

The DuPont SO_2 analyzer was calibrated with certified SO_2 and air mixtures.

Diffusion Battery

The A.P.T. screen diffusion battery consists of a number of stages in series, each stage consisting of different numbers of identical screen elements for differential particle size fractionation. The particle collection efficiency of each stage depends on the number of screens, the screen mesh size and the gas flow rate.

Experiments were done with 325 and 400 mesh screens for:

1. Determining the optimum mesh size, and;
2. Determining the best available model which could be used to predict screen performance.

The experimental setup is shown in Figure 10. A 4-jet Collison atomizer was used to generate sodium chloride aerosols from a 1% solution. The aerosol was dried, diluted and neutralized before passing through the diffusion battery. An electrical aerosol analyzer (E.A.A.) was used as a particle size-concentration monitor for the inlet and outlet gas streams. Ten to 140 screens, both 325 and 400 mesh, were tested. The E.A.A. data were reduced into particle penetrations by a laborious iterative procedure discussed by Liu et al. (1979).

Results are presented in Tables 8 and 9 and also in Figures 11 and 12. A fairly good straight line correlation is observed between particle diameter 'd_p' and penetration 'Pt_d'.

Published screen diffusion battery models relate penetration to screen solidarity factor and single cylinder efficiency:

$$Pt_d = \exp(-a\,n\,S\,\eta) \qquad (53)$$

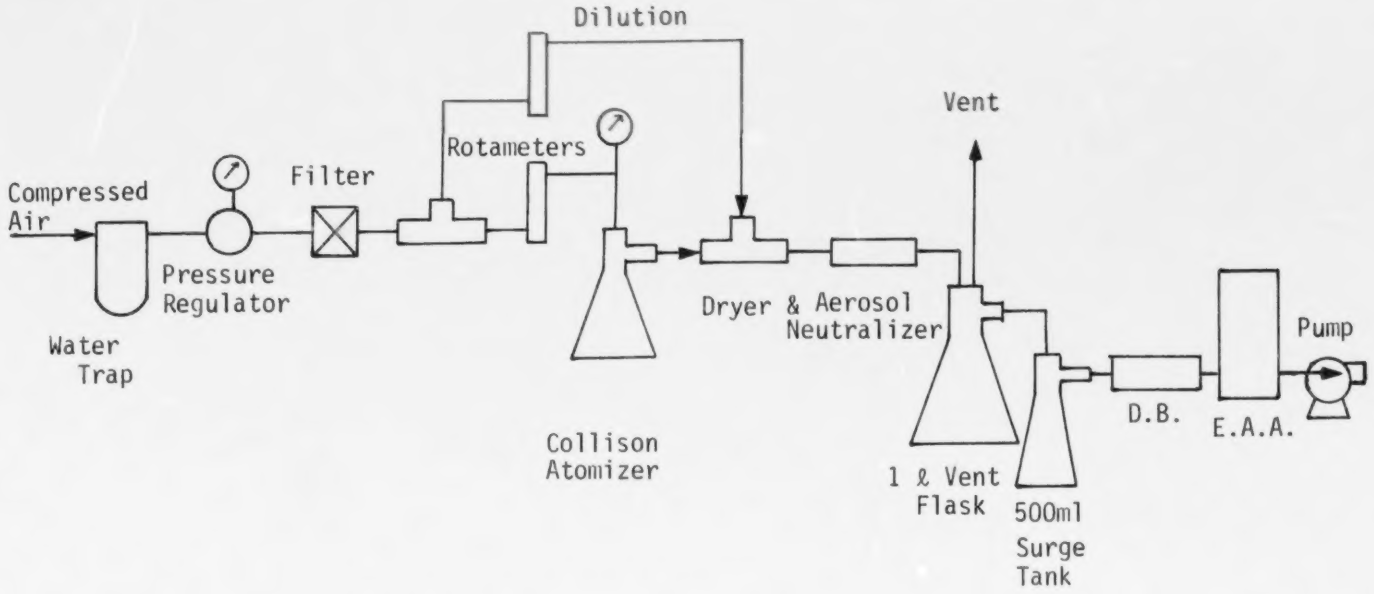

Figure 10. Diffusion Battery (D.B.) calibration set-up.

TABLE 8. MEASURED PENETRATION OF 325 MESH SCREENS.

d_p, µm	10 Screens	20 Screens	45 Screens	95 Screens	145 Screens
0.0042	-	-	-	-	-
0.0075	-	-	-	-	-
0.0133	22.9*	4.0	-	-	-
0.0237	40.1	18.3	3.4	0.4	0.4
0.0422	63.7	48.6	13.3	5.2	2.6
0.075	87.7	62.0	33.3	13.3	7.7
0.133	99.0	89.9	69.7	37.2	26.9
0.237	100.0	100.0	86.3	57.3	44.9
0.422	-	-	-	77.5	80.6
0.75	-	-	-	-	-

*Numbers represent penetration 'Pt_d' in %

TABLE 9. MEASURED PENETRATION OF 400 MESH SCREENS.

d_p(μm)	10 Screens	25 Screens	50 Screens	100 Screens	140 Screens
0.0042	-	-	-	-	-
0.0075	-	-	-	-	-
0.0133	17.08*	10.69	3.48	3.03	1.9
0.0237	51.19	16.34	1.49	0.66	0.29
0.0422	69.75	38.15	8.99	2.29	1.22
0.075	89.60	59.36	22.33	7.86	3.37
0.133	96.42	76.74	46.37	20.88	12.77
0.237	95.37	78.00	54.69	30.49	22.38
0.422	81.44	64.57	54.12	26.38	22.83
0.75	50.00	46.17	53.06	9.68	12.95

*Numbers represent penetration 'Pt_d' in %

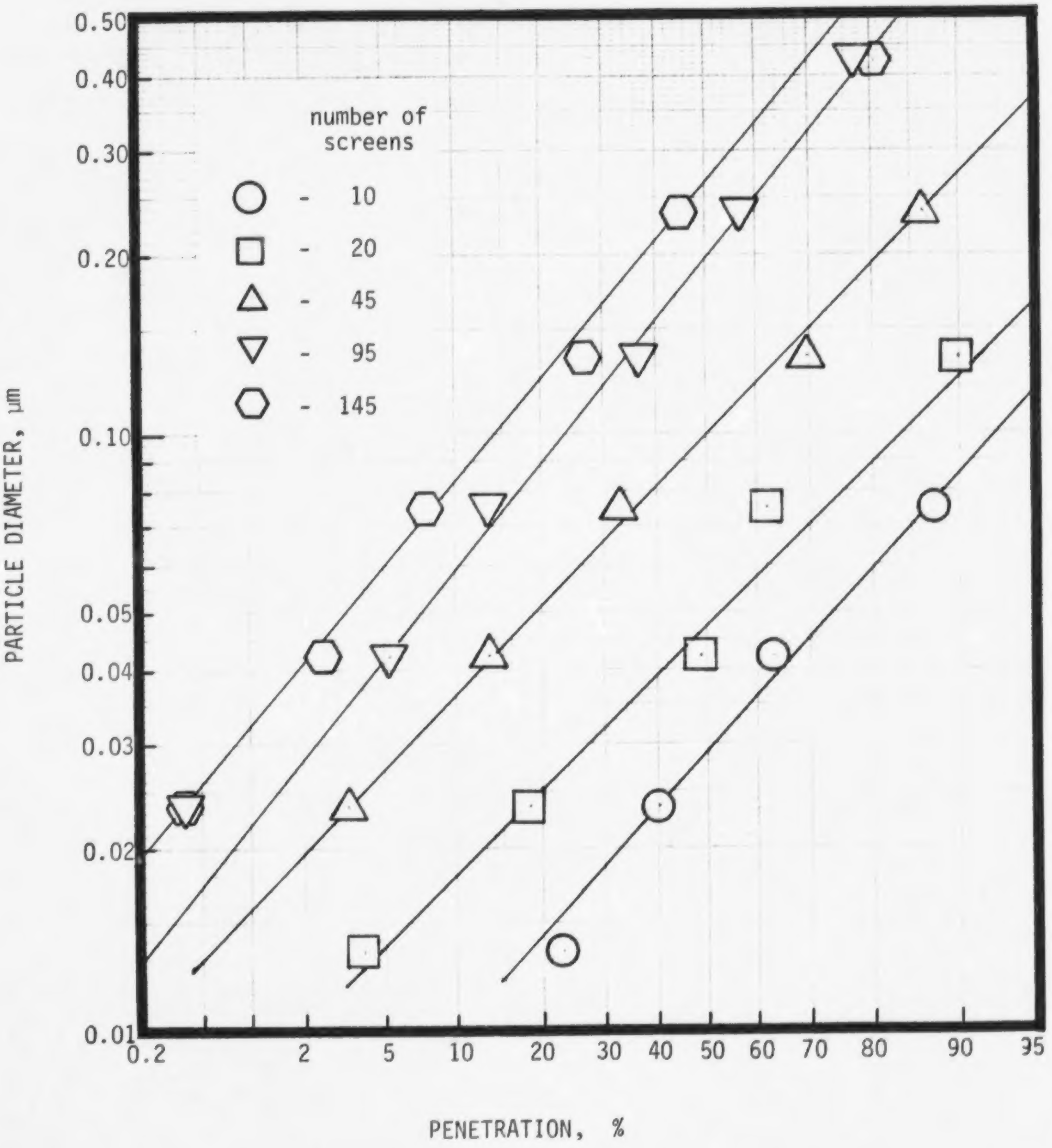

Figure 11. Calibration of D.B. made up of 325 mesh screens.

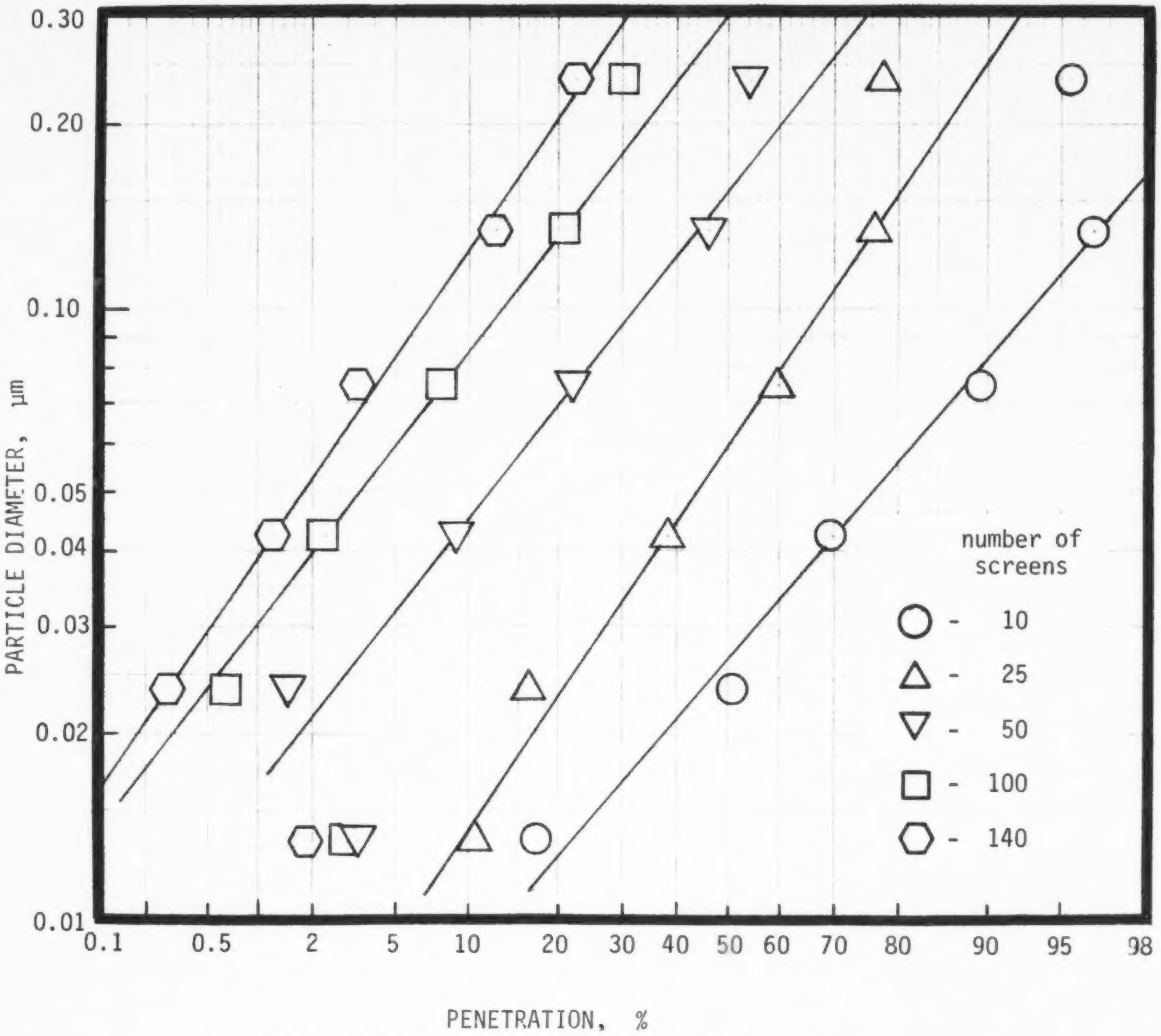

Figure 12. Calibration of D.B. made up of 400 mesh screens.

where Pt_d = penetration, fraction
a = constants, dimensionless
n = number of screens, number
S = solidity factor of screens, dimensionless
η = single cyliner collection efficiency, dimensionless

The single cylinder efficiency is related to Peclet number according to the following equation:

$$\eta = N_{Pe}^{-b} = \left(\frac{u_s d_c}{D_p}\right)^{-b} \tag{54}$$

where N_{Pe} = Peclet number, dimensionless
b = constant, dimensionless
u_s = superficial gas velocity, cm/s
d_c = wire diameter, cm
D_p = particle diffusivity, cm²/s

The empirical models developed by Patterson and Calvert (1978) and Rangaraj (1980) were considered for use as data reduction basis.

Patterson and Calvert (1978):

$$Pt_d = \exp\ (-6\ n\ S\ N_{Pe}{}^{-2/3}) \tag{55}$$

and Rangaraj (1980):

$$Pt_d = \exp\ (-4.3\ n\ S\ N_{Pe}{}^{-.59}) \tag{56}$$

From Figures 11 and 12, the cut diameters for the various sets of screens for both 325 and 400 mesh, were determined. The penetrations for measured "d_{pc}" was back calculated from equations (55) and (56) to determine which equation agrees with measurements. The results of this calculation are shown in Table

TABLE 10. COMPARISON BETWEEN DIFFUSION BATTERY MODEL PREDICTIONS AND DATA

(a) 325 Mesh Screens

NO. OF SCREENS	MEASURED d_{p50}, μm	CALCULATED Pt_d FOR MEASURED d_{pc}, %		CALCULATED d_{pc}, μm	
		Eqn.(55)	Eqn.(56)	Eqn.(55)	Eqn.(56)
10	0.0295	54.1	48.8	0.027	0.030
20	0.044	47.4	39.8	0.046	0.056
45	0.097	53.0	41.6	0.091	0.12
95	0.18	46.3	41.6	0.19	0.22
145	0.27	48.3	32.2	0.28	0.41

(b) 400 Mesh Screens

NO. OF SCREENS	MEASURED d_{p50}, μm	CALCULATED Pt_d FOR MEASURED d_{pc}, %		CALCULATED d_{pc}, μm	
		Eqn.(55)	Eqn.(56)	Eqn.(55)	Eqn.(56)
10	0.0265	40.1	36.6	0.033	0.036
25	0.059	45.8	37.8	0.065	0.079
50	0.155	54.3	42.8	0.14	0.18
100	0.3	58.7	44.3	0.25	0.34

10. Equation (55) fits the 325 mesh screen data well; but neither equation (55) nor (56) fits the 400 mesh data closely. By comparison, equation (55) fits data better than equation (56); therefore equation (55) was chosen for diffusion battery data reduction.

DATA REDUCTION

The acid particle size distributions were calculated from the cascade impactor and diffusion battery weight gains which were determined by titration with barium perchlorate. The particle diameter measured by an impactor is called "aerodynamic diameters" and it has the units of "aerodynamic micrometer, µmA". This is the effective diameter for particle separation by inertial impaction and it takes into account the effects of particle density and particle slip between gas molecules. Aerodynamic diameter is related to geometric diameter (actual size) by the following relationship (Calvert, 1970).

$$d_{pa} = d_p \, (C' \, \rho_p)^{0.5} \qquad (57)$$

where d_{pa} = aerodynamic diameter, µmA = µm $(g/cm^3)^{0.5}$

d_p = actual diameter, µm

C' = Cunningham slip factor, dimensionless

ρ_p = particle density, g/cm^3

The Cunningham slip factor is a complex function of the mean free path of the gas and the particle diameter. It increases as temperature increases and as pressure decreases. It is an empirical factor generally based on the data of Millikan (1923 a,b), and is given by Davies (1945) as:

$$C' = 1 + N_{Kn} \, [1.257 + 0.400 \exp(-1.10/N_{Kn})] \qquad (58)$$

where "N_{Kn}" is the Knudsen number, defined by:

$$N_{Kn} = \frac{2l_m}{d_p} \tag{59}$$

and where "l_m" is the mean free path of the gas molecules.

The cut diameter of each diffusion battery stage was calculated from equation (55). The diameter is physical diameter of the mist and it is converted to aerodynamic microns according to equation (58) with an assumed particle density of 1.64 for the acid drops.

The distributions measured by the impactor and diffusion battery are reported in terms of frequency curve and are plotted on log-log paper with $\Delta C_p/C_{pt}\Delta$ (log d_{pa}) as the ordinate and geometric mean of Δ (log d_{pa}) as the abscissa. The mass concentration on stage "n" is designed by "C_p" and is, in approximation, the particle mass concentration with diameters between $(d_{pc})_n$ and $(d_{pc})_{n+1}$. The Δ (log d_{pa}) associated with ΔC_p is log $(d_{pc})_{n+1}$ - log $(d_{pc})_n$. With this approximation, the derivatives term (ordinate) associated with stage "n" is:

$$\left.\frac{\Delta C_p}{C_{pt}\,\Delta\,(\log d_{pa})}\right|_n = \left.\frac{\Delta\, C_{pn}}{\Delta\,(\log d_{pc})}\right|_n$$

$$= \frac{\text{mass concentration on stage "n"}}{(\text{Total Particle Concentration})\,[\log (d_{pc})_{n+1} - \log (d_{pc})_n]} \tag{60}$$

The abscissa is:

$$[(d_{pc})_{n+1} \times (d_{pc})_{n+1}]^{0.5} \tag{61}$$

Table 11 shows an example of the data reduction calculations and Figure 13 shows the plot. An impactor stage collects particles larger than the stage cut diameter and passes particles

TABLE 11. SAMPLE DATA REDUCTION CALCULATIONS.

STAGE NO.	d_{pc}, μmA	log d_{pc}	Δlog d_{pc}	$(d_{pa})_g$	ACID MASS, mg	ΔCp, mg/Nm^3	$\frac{\Delta Cp}{C_{pt}\Delta(\log d_{pa})}$
C.I. 1	36.1	1.6	0.36	23.5	0	-	-
2	15.8	1.2	0.41	9.8	0	-	-
3	6.1	0.79	0.29	4.3	24.5	5.5	0.27
4	3.1	0.49	0.24	2.4	4.9	11.0	0.65
5	1.8	0.26	0.21	1.4	5.88	13.2	0.89
6	1.1	0.04	0.22	0.85	6.87	15.4	1.0
7	0.66	-0.18	0.33	0.45	2.45	5.5	0.24
D.B. 4	0.31	-0.51	0.21	0.24	1.96	4.4	0.30
3	0.19	-0.72	0.32	0.13	2.94	6.6	0.29
2	0.092	-1.04	0.43	0.056	2.45	5.5	0.18
1	0.034	-1.47	0.30	0.024	1.47	3.3	0.16

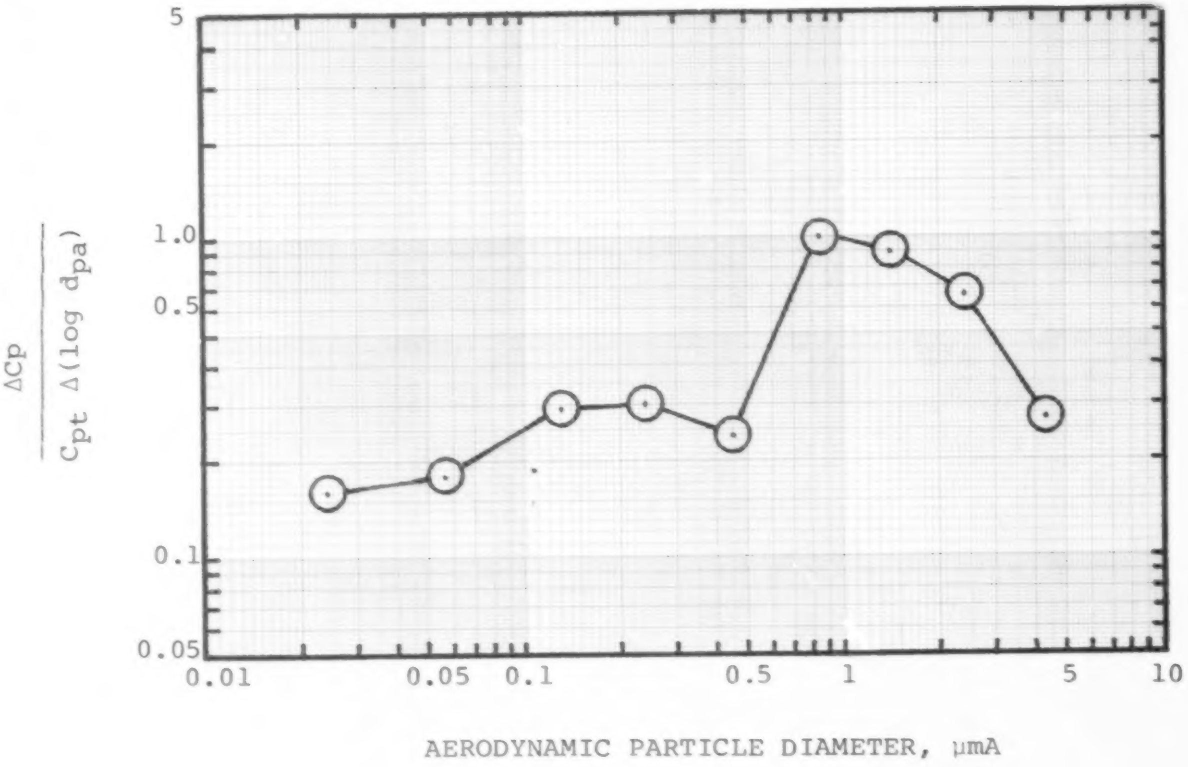

Figure 13. Acid particle size distribution.

smaller than the cut diameter. The diffusion battery classifies particles in a manner opposite to the impactor. Its stage collects particles smaller than the cut diameter and passes particles larger than the cut diameter. Therefore, the particles collected by the filter after the diffusion battery have diameters smaller than the impactor stage 7 cut diameter and larger than the cut diameter of the diffusion battery stage 4.

The tabulation in Table 11 for diffusion battery is in reversed order so that the calculations can be carried out correctly.

SECTION 5

EXPERIMENTAL RESULTS

RAPID QUENCHING EXPERIMENTS

Apparatus

Figure 14 shows a schematic diagram of the apparatus. The quencher is a randomly packed bed of 2.5 cm ceramic Berl saddles. The bed is about 5.1 cm in diameter and the depth is about 10 cm. The simulated flue gas, at a temperature over 246°C (475°F) and a flow rate of 42 l/min, enters the quencher below the bed, flows upward through the bed, contacts with quench water countercurrently in the bed, and then exhausts into the atmosphere.

Gas samples are taken at the bed and the quencher exits simultaneously. The average gas residence time from bed exit to quencher exit is about 9 seconds. A gas sample is also taken at the quencher inlet; but it is not taken simultaneously with that at the exit.

Experimental Procedure

The experimental procedure for rapid quenching experiments is as follows:

1. Set the flue gas simulator conditions to produce the required acid vapor and water vapor concentrations.
2. Since the output from the flue gas simulator may vary at the same operating conditions, a gas sample is taken with a condenser train (3 cold impingers). Acid vapor concentration is determined by chemical analysis and water vapor concentration is calculated from the impinger water volume gain and the weight gain of the silica gel.
3. Connect the flue gas simulator to the quencher inlet and set the required cooling water rate.
4. When steady state is reached, draw a gas sample at the bed exit and the quencher exit simultaneously.

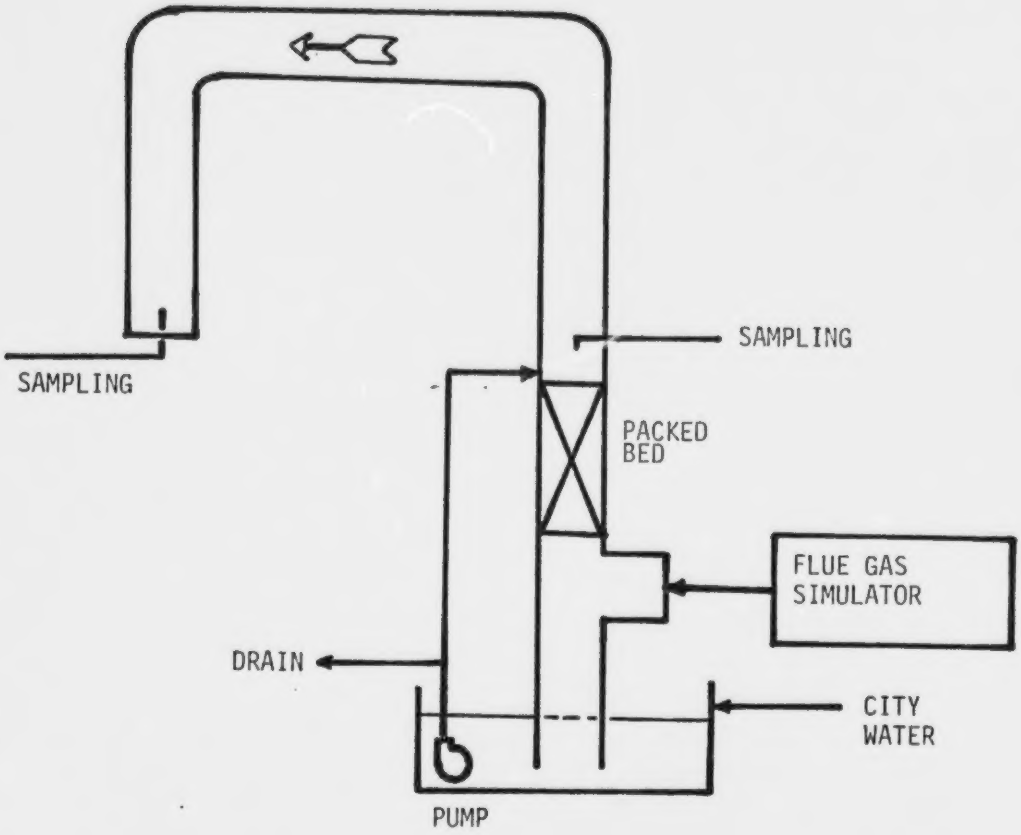

Figure 14. Rapid quenching experimental setup.

5. At the completion of an experiment, the sampling probe, impactor substrates, diffusion battery screens, the quartz filter, the condensation coil, and the impingers are either washed with or soaked in de-ionized distilled water. The acid in the solution is determined by titration with sodium hydroxide with bromophenol blue as an indicator or with barium perchlorate and thorin indicator.
6. For some runs, the glass tube between the two sampling points is also washed and analyzed for acid.

Results

Table 12 shows a summary of the rapid cooling experiments. Tables 13 and 14 present the acid particle size distributions measured at the bed exit and the quencher exit. The particle diameter is the geometric mean of the two neighboring particle diameters. The smallest particles removed by the diffusion battery were assumed to have a diameter of 10 A (0.0165 μmA assuming a particle density of 1.64).

No acid was detected in the condensation coil and impingers downstream of the quartz filter of the outlet sampling train. This implies that all acid vapor was nucleated into acid drops. More than 50% of the acid vapor was removed by the packed bed. Wall losses of nucleated particles between the bed and stack exits were small.

Figures 15 and 16 show typical acid particle size distribution measured at the bed and quencher exits. The average gas residence time between the two points was 9 seconds. Since all acid vapor was transformed into particles in the quencher and the change in temperature between the two locations was small, the acid particle size distribution measured at the two locations is about the same, i.e. particle growth due to agglomeration and additional condensation is negligible.

The effect of acid vapor concentration on the nucleated acid particle size distribution is shown in Figure 17. A larger portion of the acid vapor was nucleated into sub-micron particles when the vapor concentration was lowered.

TABLE 12. SUMMARY OF RAPID QUENCHING EXPERIMENTAL CONDITIONS

RUN NO.	INLET GAS FLOWRATE, N l/min	GAS TEMPERATURE, °C			WATER VAPOR Vol %	ACID CONCENTRATION, mg/Nm			QUENCH WATER		FLY ASH g/m³	SO_2 ppm
		INLET	BED EXIT	QUENCHER EXIT		INLET	BED EXIT	QUENCHER EXIT	FLOW RATE, l/min	TEMP. °C		
70	42	230	28	27	7.1	380.6	111.6	107.7	0.20	26	0	0
71	42	230	29	27	8.4	366.5	167.0	157.5	0.22	26	0	0
72	42	255	29	24	7.7	400.8	221.0	100.6	0.22	26	0	0
73	42	251	31	27	10.4	339.7	148.3	137.4	0.42	26	0	0
74	42	250	35	31	10.8	379.6	152.5	145.5	0.42	26	0	0
75	42	252	32	29	10.9	99.9	47.7	45.9	0.42	26	0	0
76	42	269	32	29	10.7	153.2	48.6	44.0	0.42	26	0	0
77	42	258	27	27	11.0	178.8	82.2	85.3	0.42	26	0	0
78	42	263	29	29	11.5	146.6	69.9	65.9	0.42	26	0	0
79	42	274	29	28	10.4	92.9	28.9	24.3	0.42	26	0	0
80	42	260	30	29	10.2	81.7	31.7	33.9	0.42	26	0	0
81	42	263	30	30	9.2	82.0	41.1	36.4	0.42	26	0	0
82	42	268	31	28	10.0	34.4	21.4	17.8	0.60	26	0	0

TABLE 12. SUMMARY OF RAPID QUENCHING EXPERIMENTAL CONDITIONS (continued)

RUN NO.	INLET GAS FLOWRATE, N l/min	GAS TEMPERATURE, °C			WATER VAPOR Vol %	ACID CONCENTRATION, mg/Nm			QUENCH WATER		FLY ASH g/m³	SO_2, ppm
		INLET	BED EXIT	QUENCHER EXIT		INLET	BED EXIT	QUENCHER EXIT	FLOW RATE, l/min	TEMP. °C		
83	42	274	29	29	9.6	29.6	11.1	9.4	0.60	26	0	0
84	42	268	31	31	10.8	51.8	14.2	10.1	0.60	26	0	0
85	42	275	48	45	9.6	105.5	79.6	84.1	0.60	51	0	0
86	42	285	47	42	9.0	124.0	60.8	44.5	0.60	51	0	0
87	42	290	21	21	8.0	131.3	45.9	61.4	0.60	19	0	0
88	42	304	47	41	7.0	116.7	49.4	44.7	0.60	50	0	0
89	42	302	22	21	6.7	84.1	38.9	44.7	0.50	19	0	0
90	42	302	48	42	4.2	68.1	24.8	20.8	0.60	50	0	0
91	42	307	22	22	3.7	46.1	6.7	6.8	0.60	19	0	0
92	42	305	22	22	5.0	31.0	3.4	3.6	0.60	19	0	0
94	52	281	23	23	9.2	54.1	21.8	—	0.60	23	1.103	0
95	52	274	49	46	10.5	29.4	8.5	—	0.60	52	0.21	0
96A	62	290	57	53	10.2	27.0	3.6	—	0.60	60	0	01
96B	62	278	57	57	12.64	20.8	5.4	—	0.60	60	0.78	0
98A	62	279	57	53	6.0	61.1	14.5	—	0.60	60	0	0
98B	62	284	57	53	6.0	37.7	17.5	—	0.60	60	0.74	0
100A	62	282	54	49	10.74	47.1	12.6	—	0.50	60	0	0
100B	62	289	56	51	10.74	32.1	15.9	—	0.50	60	0.63	900-1000
105A	52	290	57	49	8.0	64.0	25.3	—	0.50	63	0	0
105B	52	289	55	51	8.0	79.0	69.1	—	0.50	63	0	900-1000

TABLE 13. ACID PARTICLE SIZE FREQUENCY DISTRIBUTION

Run No.	$\Delta C_p/\Delta(\log d_{pa})$, mg/Nm³, at d_{pa} = 0.023 umA	0.045	0.075	0.10	0.29	0.85	1.40	2.40	4.40	9.7	23.4
70Q	14.4	24.8	47.0	53.5	20.2	88.2	71.2	71.2	47.6	0	6.2
70S	18.1	20.6	40.2	49.1	19.5	115.3	45.1	77.4	27.7	0	0
71Q	10.8	16.4	33.2	52.9	20.7	138.7	130.0	173.4	101.9	1.3	4.6
71S	9.1	16.2	29.6	35.0	18.3	129.5	83.4	182.8	100.6	0	0
72Q	24.1	39.1	81.5	90.4	45.6	402.0	139.2	15.5	0	1.8	2.1
72S	19.3	44.8	90.7	120.6	52.8	421.0	128.5	12.8	2.7	0	0
73Q	9.2	18.8	33.8	35.9	19.6	155.0	131.5	110.3	65.8	1.4	1.6
73S	10.8	22.2	49.1	47.9	24.4	152.2	111.0	124.4	36.6	0	0
74Q	9.2	16.6	30.3	44.8	19.5	145.6	143.6	123.3	67.5	1.4	1.6
74S	9.2	18.9	30.7	36.2	18.2	132.4	142.0	158.6	58.3	0	0
75Q	5.5	8.3	16.8	13.4	20.6	42.0	26.3	20.6	3.8	0	0
75S	3.6	6.3	13.5	18.0	21.3	40.1	33.0	19.2	5.6	0	0
76Q	9.0	13.2	11.9	6.3	12.3	50.6	42.4	31.9	13.1	0	0
76S	3.1	2.4	3.2	3.1	0.7	57.3	56.9	37.6	15.2	0	0

Note: Q = sampled at bed outlet
S = sampled at quench outlet

TABLE 14. ACID PARTICLE SIZE FREQUENCY DISTRIBUTION

Run No.	$\Delta C_p/\Delta(\log d_{pa})$, mg/Nm³, at d_{pa} =										
	0.023 µmA	0.05	0.13	0.24	0.43	0.82	1.40	2.40	4.40	9.7	23.5
77Q	10.9	10.3	21.3	13.2	18.3	82.1	76.2	57.6	27.2	0	0
77S	10.9	15.4	28.3	20.9	16.7	68.8	69.3	66.7	27.8	0	0
78Q	10.9	12.7	21.0	20.7	15.6	68.6	56.9	51.2	18.9	0	0
78S	10.8	11.0	18.7	20.1	18.5	69.4	47.0	45.7	17.6	0	0
79Q	7.4	10.7	17.1	14.5	10.5	19.6	13.4	6.7	3.9	0	0
79S	4.8	7.6	7.0	6.9	8.3	24.4	15.8	13.6	3.8	0	0
80Q	7.3	5.2	16.8	14.2	10.1	27.1	20.5	13.0	7.0	0	0
80S	4.8	4.9	13.7	10.1	9.0	33.2	26.1	24.9	7.3	0	0
81Q	9.0	11.3	20.4	17.7	12.4	36.7	29.8	9.8	7.5	0	0
81S	7.3	5.1	10.6	12.2	9.5	36.2	30.3	24.2	9.0	0	0
82Q	6.0	9.6	13.2	10.1	8.6	12.8	3.5	5.0	2.4	1.2	0
82S	5.0	7.0	8.3	4.5	4.7	16.4	8.8	7.6	2.8	0	0
83Q	4.1	4.7	7.3	5.4	3.4	4.9	3.5	2.5	1.4	0.9	0
83S	4.5	2.4	5.0	4.3	6.4	3.4	3.7	3.7	1.8	0.3	0
84Q	4.6	3.3	4.1	5.4	5.6	12.2	9.1	4.7	3.6	0	0
84S	3.2	4.8	8.7	4.3	5.5	13.7	6.0	4.4	2.3	0	0
85Q	31.0	31.9	46.4	43.3	13.2	94.5	10.4	3.1	5.6	0	0
85S	28.0	36.1	56.4	59.7	29.8	96.8	8.3	3.1	0.6	0	0
86Q	26.8	29.9	47.4	41.5	28.7	14.9	3.8	1.9	4.7	0	0

TABLE 14. ACID PARTICLE SIZE FREQUENCY DISTRIBUTION (continued)

Run No.	$\Delta C^p/\Delta(\log d^{pa})$, mg/Nm^3, at d_{pa} =										
	0.023 μmA	0.05	0.13	0.24	0.43	0.82	1.40	2.40	4.40	9.7	23.5
86S	24.6	28.6	27.1	23.4	21.7	13.7	3.5	1.5	0.6	0	0
87Q	15.7	12.4	27.9	16.1	20.3	63.4	6.6	1.8	1.6	0	0
87S	11.8	16.5	17.1	25.3	15.0	137.3	9.7	2.3	0.58	0	0
88Q	25.3	19.5	38.1	48.0	19.8	11.3	3.4	1.9	1.7	0	0
88S	20.4	25.1	33.1	30.9	17.1	16.1	5.3	2.4	0	0	0
89Q	8.5	8.1	14.8	16.4	15.0	76.7	7.6	1.9	0.7	0	0
89S	9.4	10.6	14.6	13.3	14.5	95.7	10.4	2.3	0	0	0
90Q	13.5	15.0	8.5	10.8	13.8	11.9	4.1	4.3	0	0	0
90S	11.1	9.8	12.0	12.7	13.6	8.9	1.3	0	0	0	0
91Q	2.4	1.8	2.4	0.9	6.8	5.2	3.3	0	0	0	0
91S	1.2	3.3	1.2	0.8	8.4	6.0	1.8	0	0	0	0
92Q	0.6	1.6	0.6	0.3	3.2	6.0	0	0	0	0	0
92S	1.8	0.4	2.4	1.8	2.2	3.4	0	0	0	0	0

Note: Q = sampled at bed outlet
S = sampled at quencher outlet

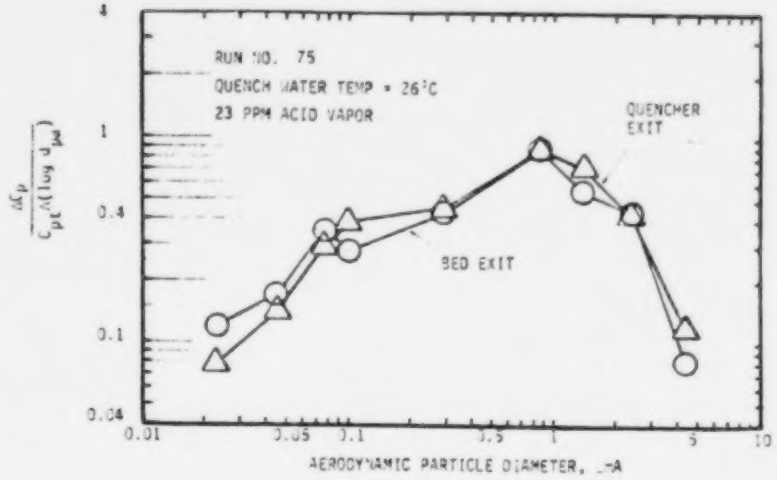

Figure 15. Measured acid particle size distribution.

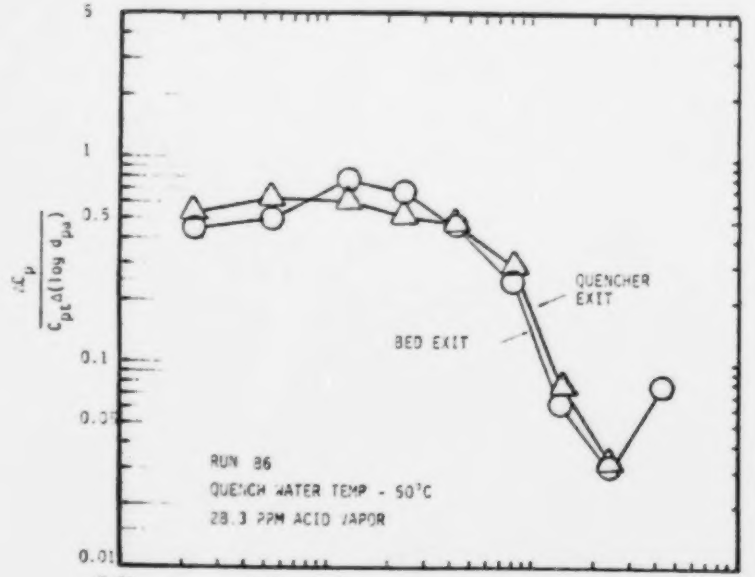

Figure 16. Measured acid particle size distribution

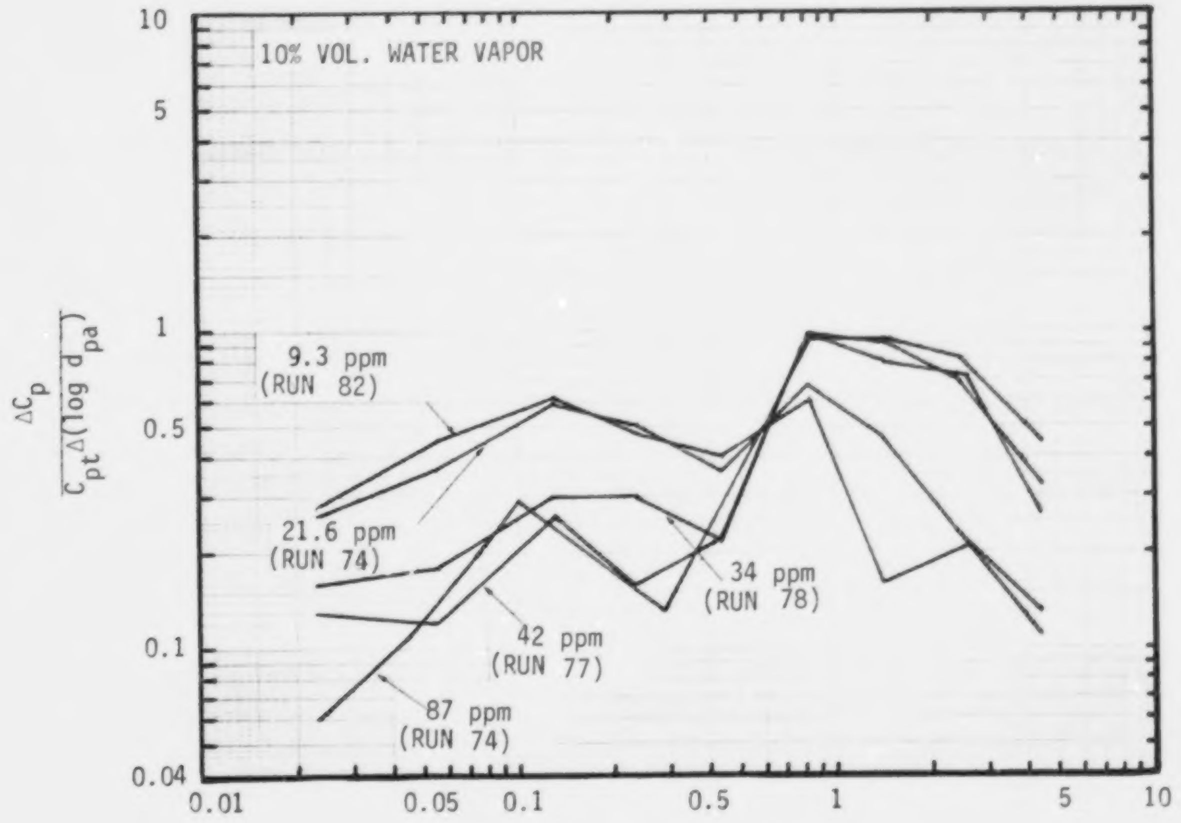

Figure 17. Effect of acid vapor concentration on acid particle size distribution.

Figures 18 and 19 show the effect of quench water temperature on acid particle size distribution. Higher water temperature resulted in finer particles. Low water temperature decreased the gas temperature and caused additional water vapor condensation on the nucleated particles.

Figures 20 and 21 show the effect of water vapor concentration on size distribution. Because more water can condense, a higher water vapor concentration in the inlet gas stream resulted in larger acid particles.

Figures 22 through 24 show the effect of injected SO_2 and fly ash on nucleated acid particle size distribution. Sulfur dioxide has no effect on acid nucleation. When fly ash is present the acid particles appear larger because of condensation on the ash particles. Even in the presence of fly ash particles some self nucleation of acid particles occurred.

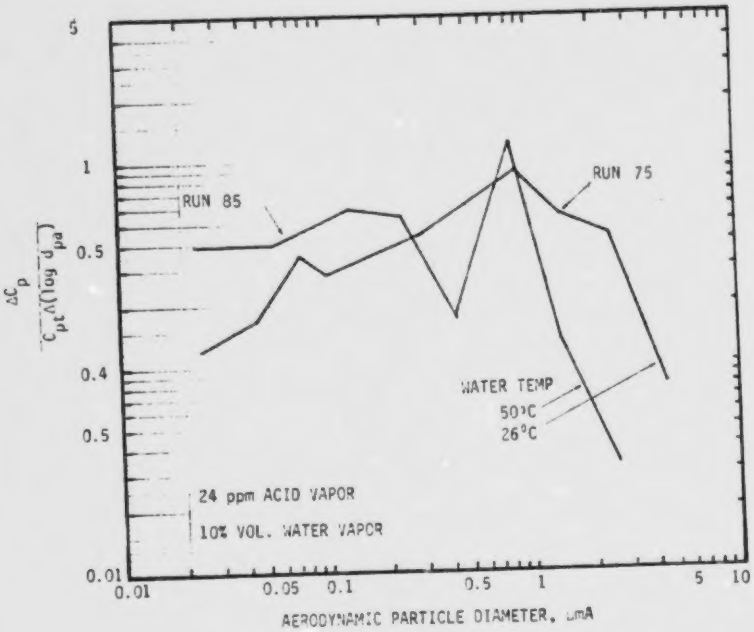

Figure 18. Effect of quench water temperature on nucleated acid particle size distribution.

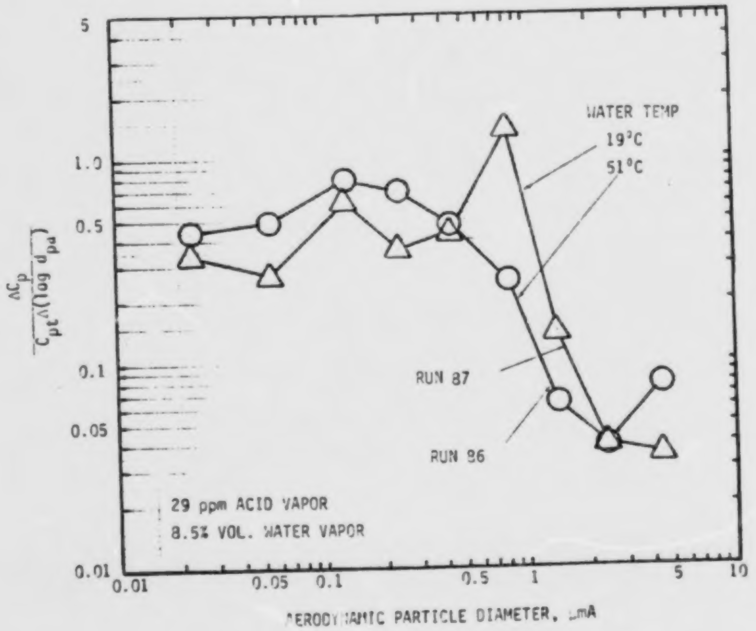

Figure 19. Effect of quench water temperature on nucleated acid particle size distribution.

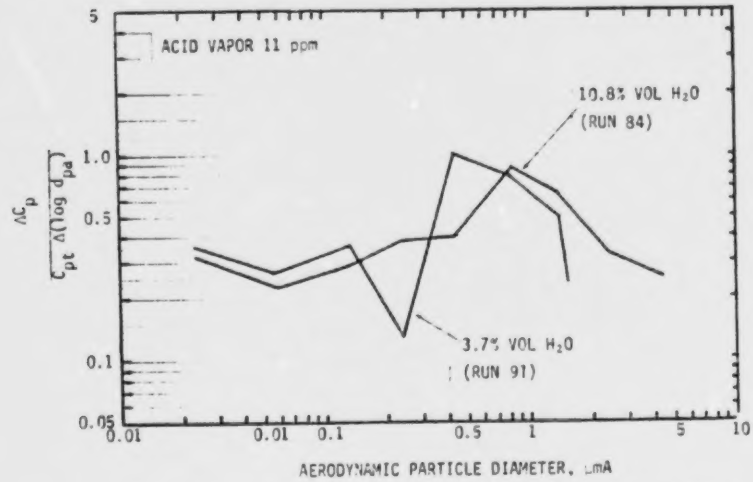

Figure 20. Effect of water vapor concentration on nucleated acid particle size distribution.

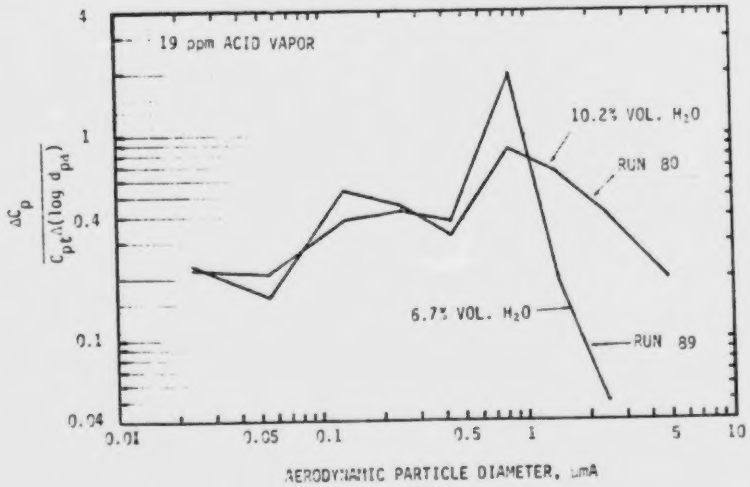

Figure 21. Effect of water vapor concentration on nucleated acid particle size distribution.

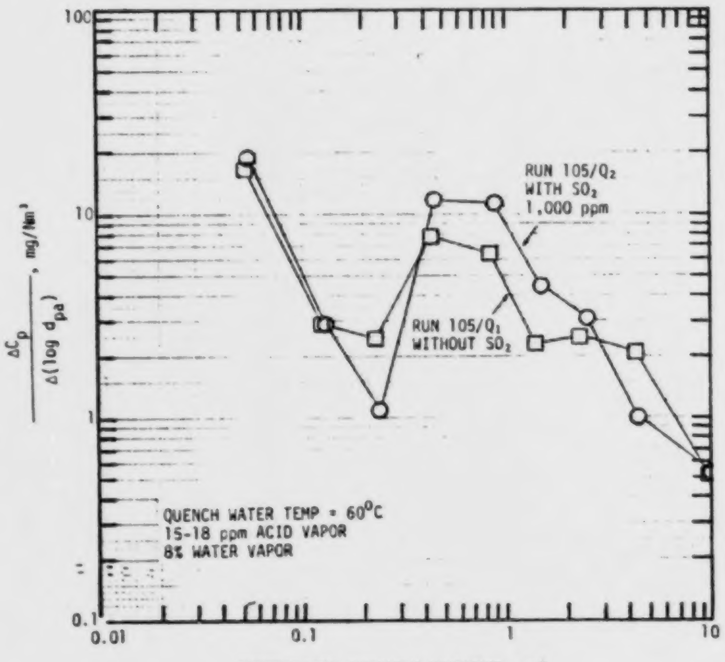

Figure 22. Effect of sulfur dioxide on nucleated acid particle size distribution.

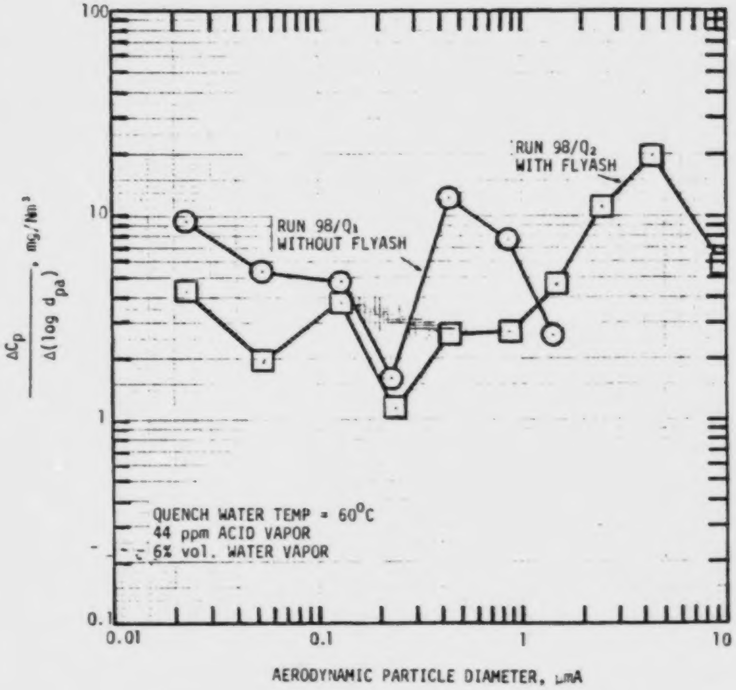

Figure 23. Effect of flyash on nucleated acid particle size distribution.

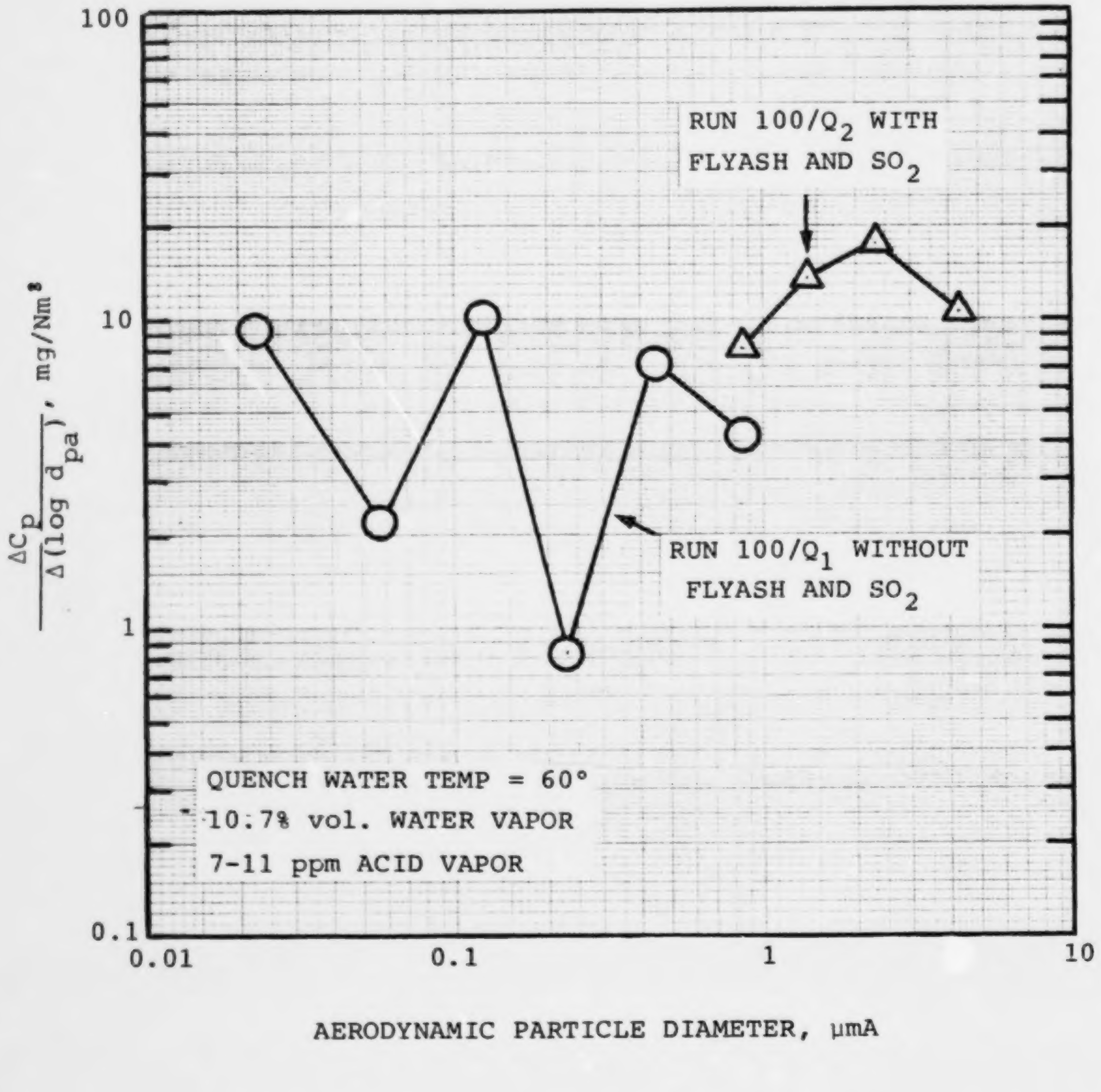

Figure 24. Effect of flyash and SO_2 on nucleated acid particle size distribution.

DILUTION COOLING EXPERIMENTS

Experimental Apparatus

The sulfate formation due to dilution cooling was studied in a parallel flow dilution chamber shown in Figure 25. The central tube (1.25 cm I.D.) had a alumina tube sleeve to prevent cooling before mixing. The outside was a 5.1 cm I.D. glass pipe.

The simulated flue gas, at a temperture over 246°C (475°F) and a flow rate of 55 Nl/min, entered the dilution chamber through the insulated central tube. The dilution air, which could be either pre-heated or pre-cooled to simulate various ambient air temperatures, formed a sheath around the flue gas. The velocities of the sheath air and flue gas streams were closely matched so that mixing was slow and gradual.

Experimental Procedure

The experimental procedure for dilution cooling experiments is as follows:

1. Set the flue gas simulator conditions to produce the required acid vapor and water vapor concentrations.
2. Connect the flue gas and dilution air supplies to the dilution cooler and allow the system to stabilize by running it for about half an hour before sampling. Heat or cool the dilution air as required.
3. Set up one sample train for measuring total mass of acid at inlet. This consists of a condenser followed by 4 impingers and a dryer. Also, set up another sample train consisting of the University of Washington cascade impactor followed by a 4-stage screen diffusion battery, a quartz filter a condensation coil, impinger train and dryer. This is used for size distribution measurement.
4. When the system has reached steady state operation, draw samples simultaneously for a period of 1 hour at points before and after sample dilution.
5. At the completion of an experiment the sample trains are washed with deionized, distilled water. The acid

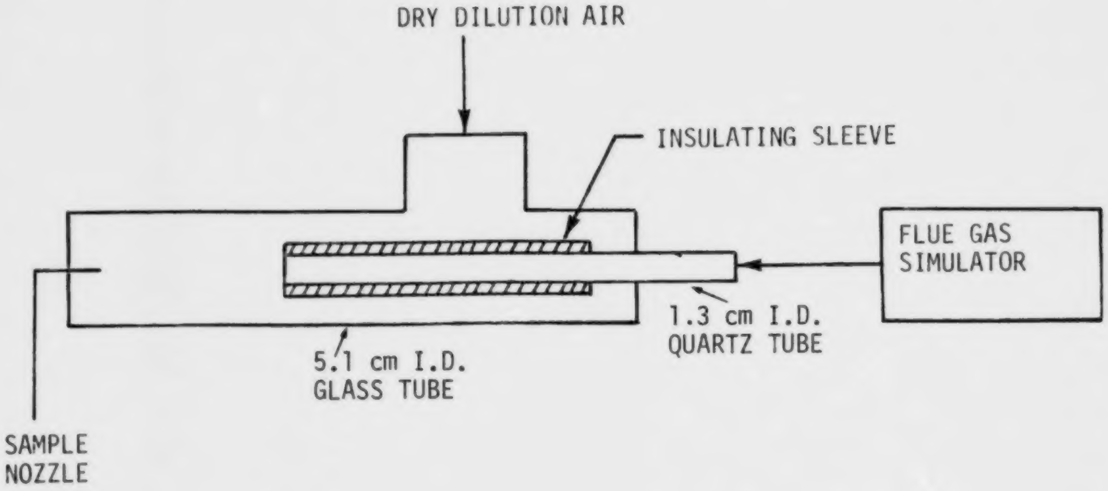

Figure 25. Dilution cooling experimental apparatus.

in the washing solutions is determined by titration with sodium hydroxide with bromophenol blue as an indicator.

Results

Table 15 shows a summary of the dilution cooling experiments. Table 16 presents the frequency distribution of the acid particle size.

Table 17 shows a typical temperature profile of the gas stream in the diluter. The gas was well mixed at 15 cm downstream from the flue gas entrance. The wall loss of acid vapor was negligible between the flue gas entrance point and 15 cm downstream from the entrance. A few samples were taken at 15 cm and 60 cm downstream from the flue gas entrance and the acid particle size distributions measured at these two locations were the same. Therefore, the acid particle size did not change much and all samples were taken at a point 15 cm downstream of the flue gas feed tube.

Figures 26 and 27 show that the injection of SO_2 into the flue gas has no significant effect on acid nucleation and particle size distribution.

Figures 28 and 29 show the effect of fly ash on nucleated acid particle size distribution. The concentration of small particles decrease and that of large particles increase with the addition of fly ash because of condensation on fly ash particles and the scavenging of nucleated acid particles by the fly ash.

Figure 30 shows the effect of fly ash in the presence of sulfur dioxide. Sulfur dioxide has no influence on the acid particle size distribution whether fly ash is simultaneously present or not. Figure 31 leads us to this same conclusion.

Figure 32 shows the effects of water vapor concentration on acid particle size distribution. A higher water vapor concentration makes more water available for condensation and leads to a decrease in the concentration of fine acid particles and an increase in the concentration of larger acid particles.

TABLE 15. SUMMARY OF DILUTION COOLING EXPERIMENTAL CONDITIONS

Run #	Acid Conc. (ppm)		Water Vapor (vol.%)		Sample Temp. (°C)		Dilution Air Temp (°C)	Total Flue Gas Flow (Nl/min)	Dilution Air Flow (Nl/min)	SO_2 Conc. (ppm)	Flyash Conc. (g/m^3)
	Inlet	Outlet	Inlet	Outlet	Inlet	Outlet					
103/02	33.8	4.24	11.6	2.9	266	99	38	55	139	--	--
104/02	37.0	5.5	11.7	3.1	271	94	38	55	139	--	--
107/01	23.7	3.1	12.1	2.6	266	69	10	55	153	--	--
107/02	37.7	3.2	11.5	2.1	268	83	21	55	146	--	--
108/01	26.1	3.1	11.7	2.9	271	97	38	55	139	--	--
108/02	44.6	4.96	10.4	2.2	266	74	10	55	153	--	--
109/01	31.0	2.9	11.0	2.43	260	74	21	55	146	--	--
109/02	32.3	3.1	12.1	---	263	66	10	55	153	--	--
110/01	38.1	3.5	8.35	2.0	268	79	21	55	146	100-200	--
110/02	36.9	3.6	8.0	2.1	266	79	21	55	146	--	--
111/01	36.7	3.4	8.0	1.52	266	82	22	55	146	100-200	--
111/02	37.6	5.8	6.4	1.7	266	84	22	55	146	100-200	0.79
112/01	30.3	5.1	7.4	2.0	266	84	22	55	146	--	0.61
112/02	30.4	4.9	8.4	1.9	266	83	22	55	146	--	0.71
113/01	13.8	2.0	10.6	2.3	266	82	23	55	146	--	--
113/02	17.9	2.5	7.5	1.4	266	82	24	55	146	--	--
114/01	20.0	2.5	11.0	2.2	266	74	23	55	146	--	--
115/01	22.6	3.6	7.4	1.7	271	79	22	55	146	--	--
115/02	34.5	4.0	10.2	1.8	268	79	22	55	146	--	--

TABLE 16. ACID PARTICLE SIZE DISTRIBUTION

	$\Delta C_p/\Delta(\log d_{pa})$, mg/Nm^3 at d_{pa} =									
Run No.	0.0195 umA	0.0372	0.0836	0.144	0.29	0.616	1.02	1.68	3.09	7.00	17.01
103/02	13.7	0.67	0.98	0.50	4.6	2.7	4.2	7.0	6.1	6.0	6.0
104/02	17.8	1.9	0.90	2.1	7.3	3.7	7.8	10.0	8.7	6.6	6.2
107/01	17.2	8.0	2.9	0.96	1.8	6.4	4.0	2.0	1.4	0.73	0.76
107/02	25.9	10.7	3.2	1.8	4.4	9.2	9.2	8.8	6.2	4.6	4.3
108/01	9.2	2.9	0.42	0.49	3.4	3.0	6.5	6.2	4.9	5.0	3.5
108/02	30.3	10.4	3.8	3.0	3.7	16.7	6.3	5.9	4.2	2.5	1.7
109/01	5.6	6.0	1.8	0.46	2.9	5.6	4.5	5.3	3.4	1.3	1.7
109/02	18.0	3.3	1.2	0.64	0.82	6.5	5.4	4.6	2.9	3.7	2.4
110/01	10.9	3.5	2.0	1.3	0.22	6.5	8.1	6.8	5.4	4.9	3.6
110/02	17.6	2.5	0.95	0.49	0.28	9.4	8.0	7.7	5.6	3.0	2.7
111/01	11.5	1.2	1.2	0.65	0.58	5.8	8.4	6.8	5.3	3.8	3.1
111/02	13.4	2.5	0.87	0.38	1.1	10.2	12.7	15.2	13.0	8.0	4.6
112/01	10.0	2.3	1.9	0.65	0.19	8.5	12.5	12.5	11.0	5.6	3.9
112/02	8.1	1.0	1.0	0.43	0.19	6.5	9.9	15.2	12.1	7.7	4.8
113/01	6.6	0.47	0.26	0.17	0.70	2.6	3.7	3.4	3.3	2.2	2.0
113/02	6.6	0.074	0.11	0.17	0.53	2.4	4.1	5.3	4.1	4.1	3.5
114/01	1.1	0.18	0.10	0.058	0.20	0.44	0.53	0.50	0.40	0.29	0.22
115/01	1.2	0.052	0.034	0.026	0.16	0.48	0.56	0.62	0.43	0.33	0.26
115/02	1.5	0.54	0.25	0.032	0.090	0.56	0.40	0.31	0.23	0.12	0.096

TABLE 17. TYPICAL TEMPERATURE PROFILE

Distance (cm)	Temp, °C 1.25 cm below axis	Temp, °C At Axis	Temp, °C 1.25 cm above axis
0	28	216	29
5	52	136	52
7.5	57	114	58
10.0	72	100	73
12.5	77	88	79
15.0	78	85	82
17.5	79	81	79

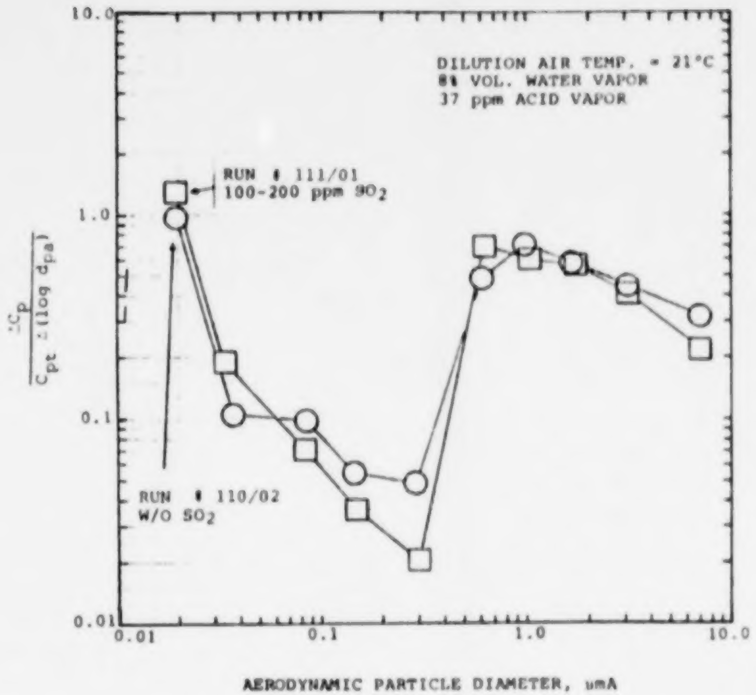

Figure 26. Effect of SO_2 on nucleated acid particle size distribution.

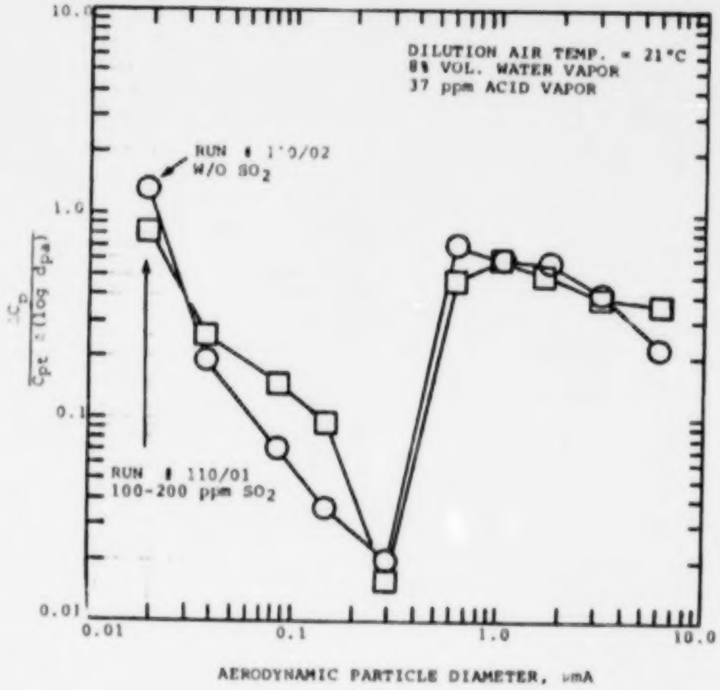

Figure 27. Effect of SO_2 on nucleated acid particle size distribution.

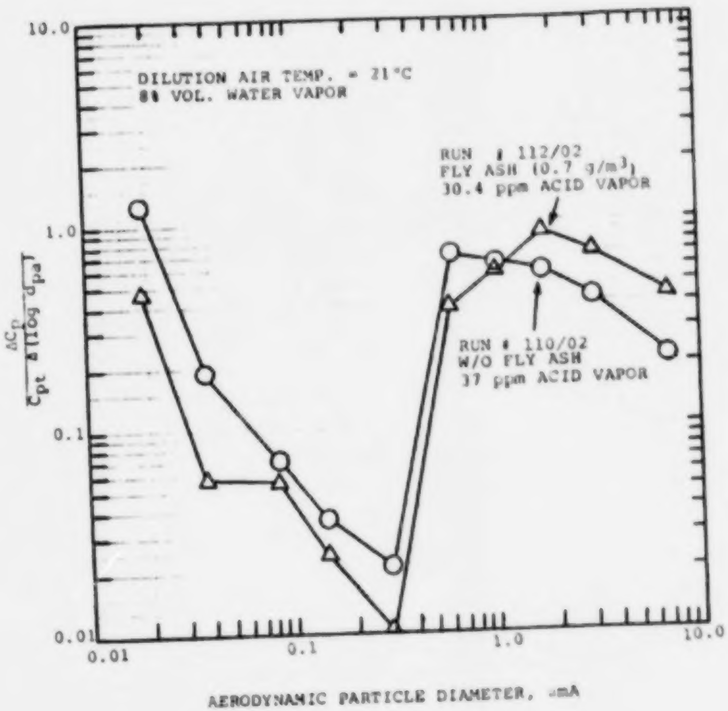

Figure 28. Effect of fly ash on nucleated acid particle size distribution.

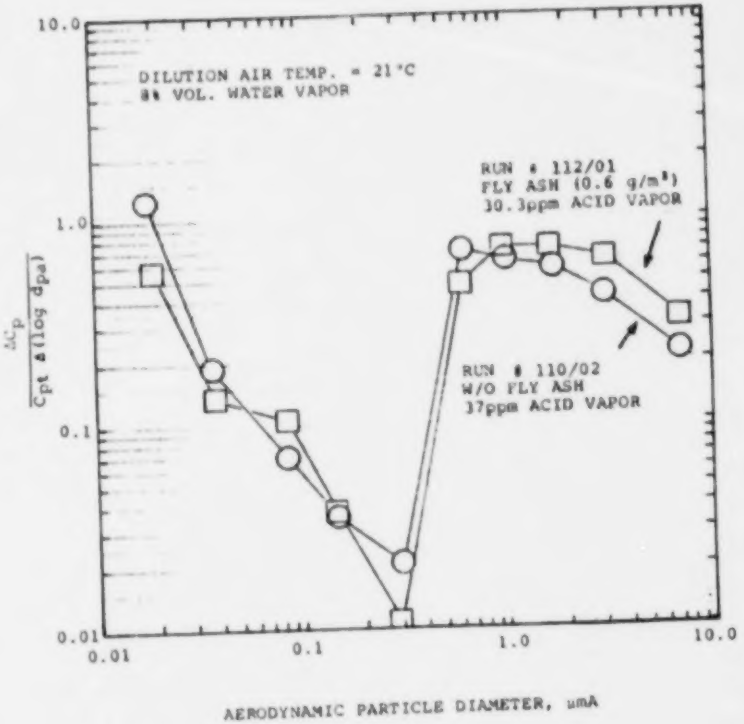

Figure 29. Effect of fly ash on nucleated acid particle size distribution.

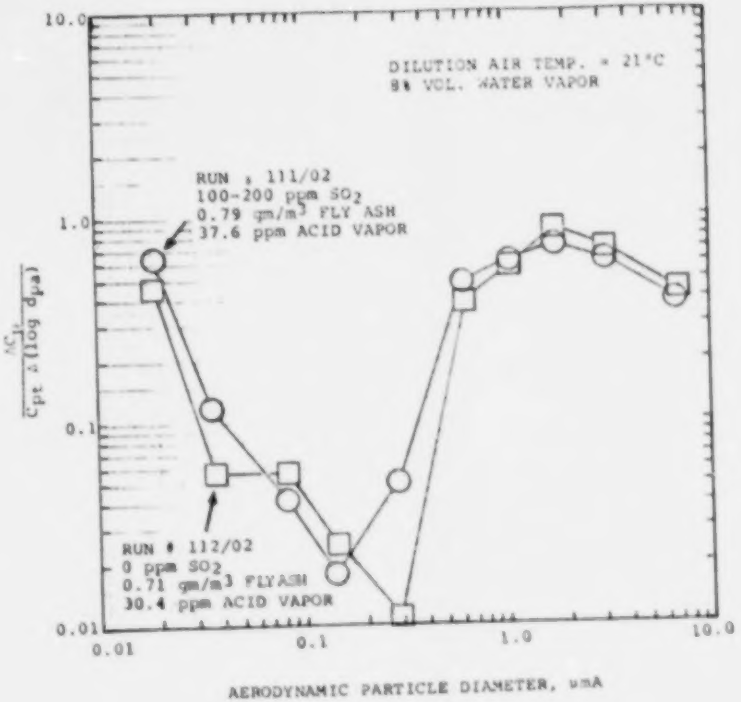

Figure 30. Effect of fly ash and SO_2 on nucleated acid particle size distribution.

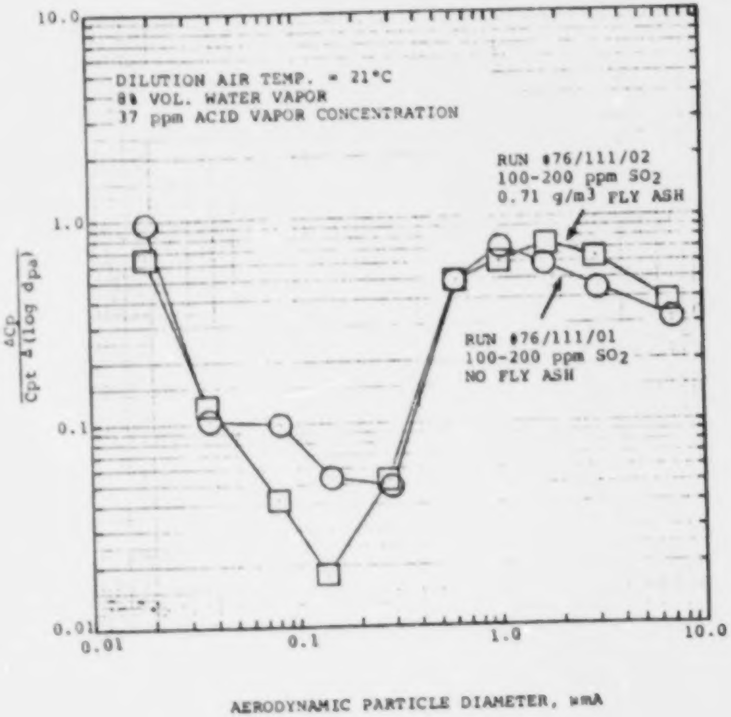

Figure 31. Effect of fly ash and SO_2 on nucleated acid particle size distribution.

Reproduced from
best available copy.

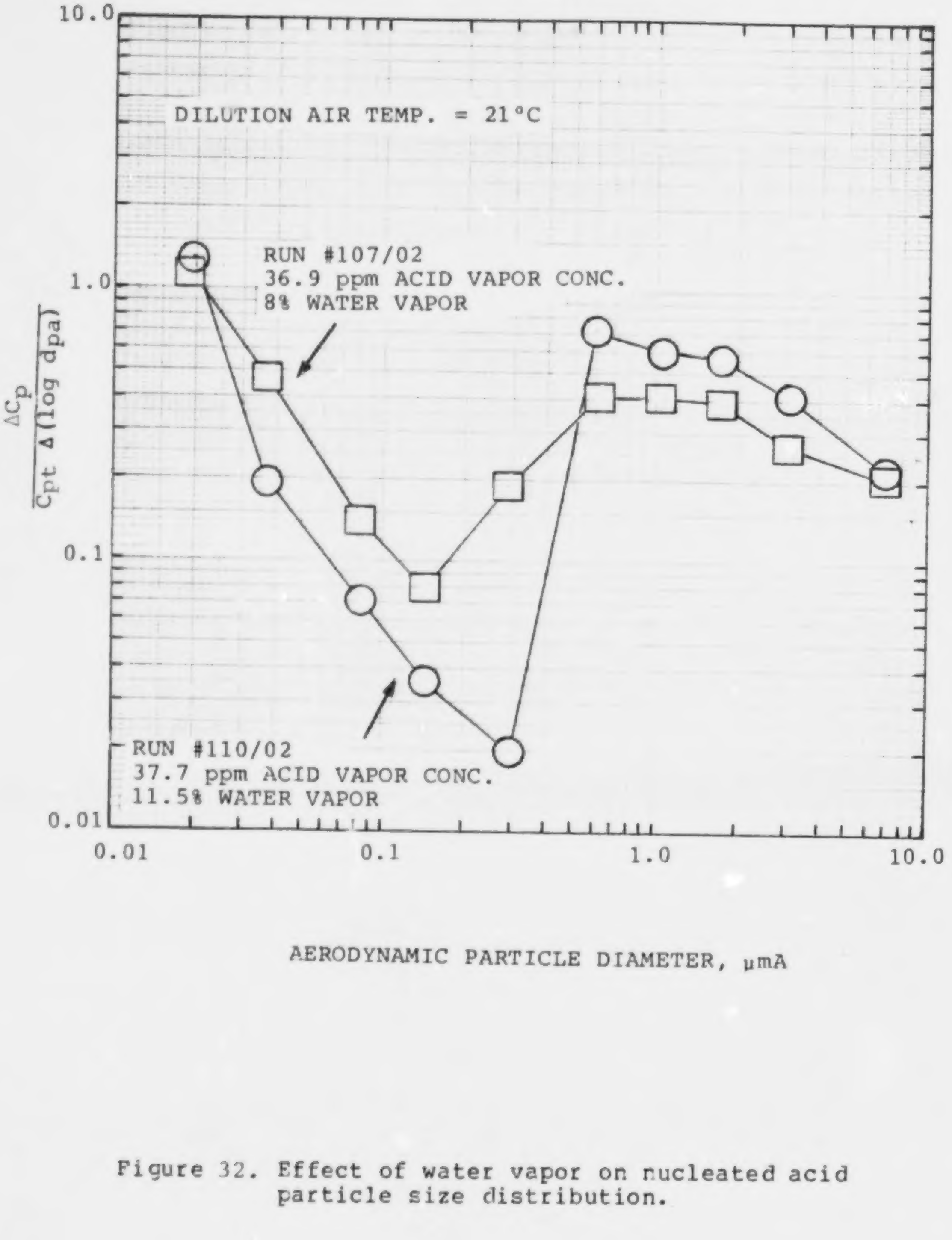

Figure 32. Effect of water vapor on nucleated acid particle size distribution.

Figure 33 shows the effect of acid concentration on acid particle size distribution. With decreasing acid vapor concentration, the concentration of fine acid particles decreases and that of the larger particles increases.

Figure 34 shows the effect of dilution air temperature on nucleated acid particle size distribution. The concentration of fine acid particles decreases sharply with increasing dilution air temperature. This decrease is matched by a corresponding increase in the concentration of the larger acid particles.

It seems that lower acid vapor concentration and higher dilution air temperature minimize the occurrance of localized supersaturation and lower the acid particle nucleation rate and number concentrations.

SLOW COOLING EXPERIMENTS

Experimental Apparatus

Figure 35 shows a schematic diagram of the slow cooling experimental apparatus. The cooling apparatius was a cocurrent, double pipe heat exchanger. The inner pipe was 1.35 cm I.D. glass tube and the outer pipe was 3.8 cm I.D. clear PVC tube. Both tubes were built in sections so as to permit variation in the length of the heat exchanger.

The flue gas flowed in the inner pipe of the heat exchanger. The volumetric flow rate of the gas was about 15 Nl/min and the gas temperature was about 246°C (475°F) at the exchanger inlet.

Cooling fluid was room air. The cooling rate was controlled by regulating the air flow rate and air temperature.

Experimental Procedure

The experimental procedure for determining the nucleation temperature is as follows:

1. Start up the flue gas simulator and set the conditions to produce the required acid and water vapor concentrations.
2. Connect the heat exchanger and adjust cooling air flow rate and temperature.

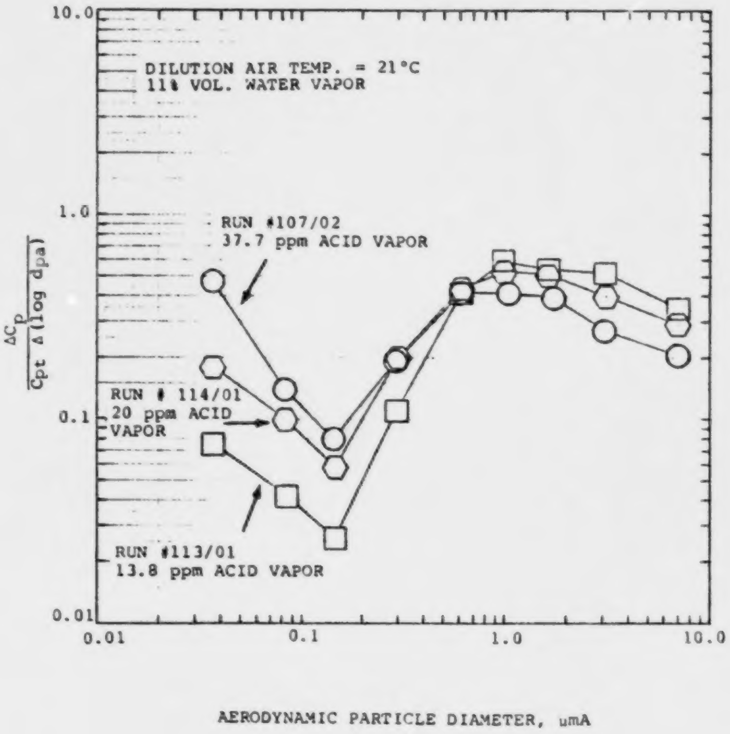

Figure 33. Effect of acid concentration on nucleated acid particle size distribution.

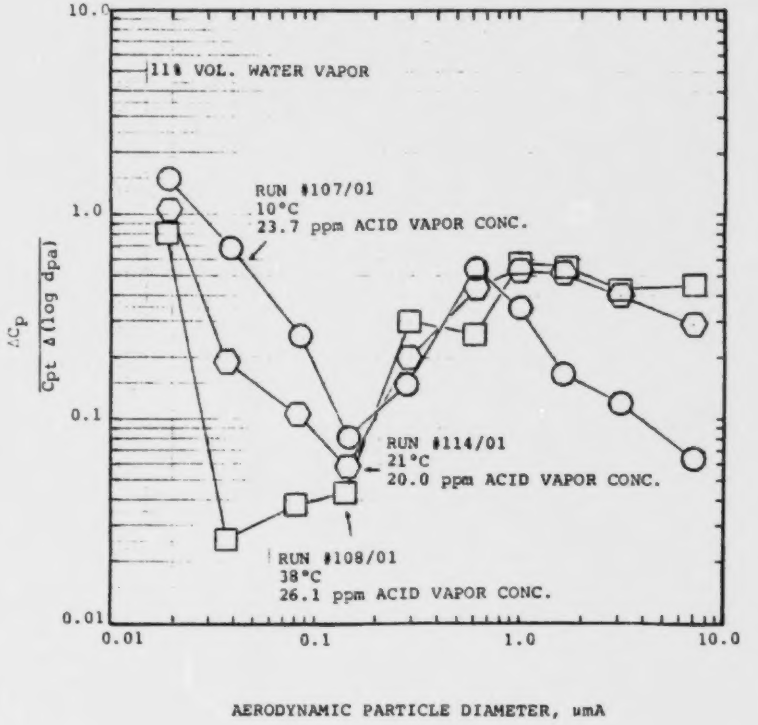

Figure 34. Effect of dilution air temperature on nucleated acid particle size distribution.

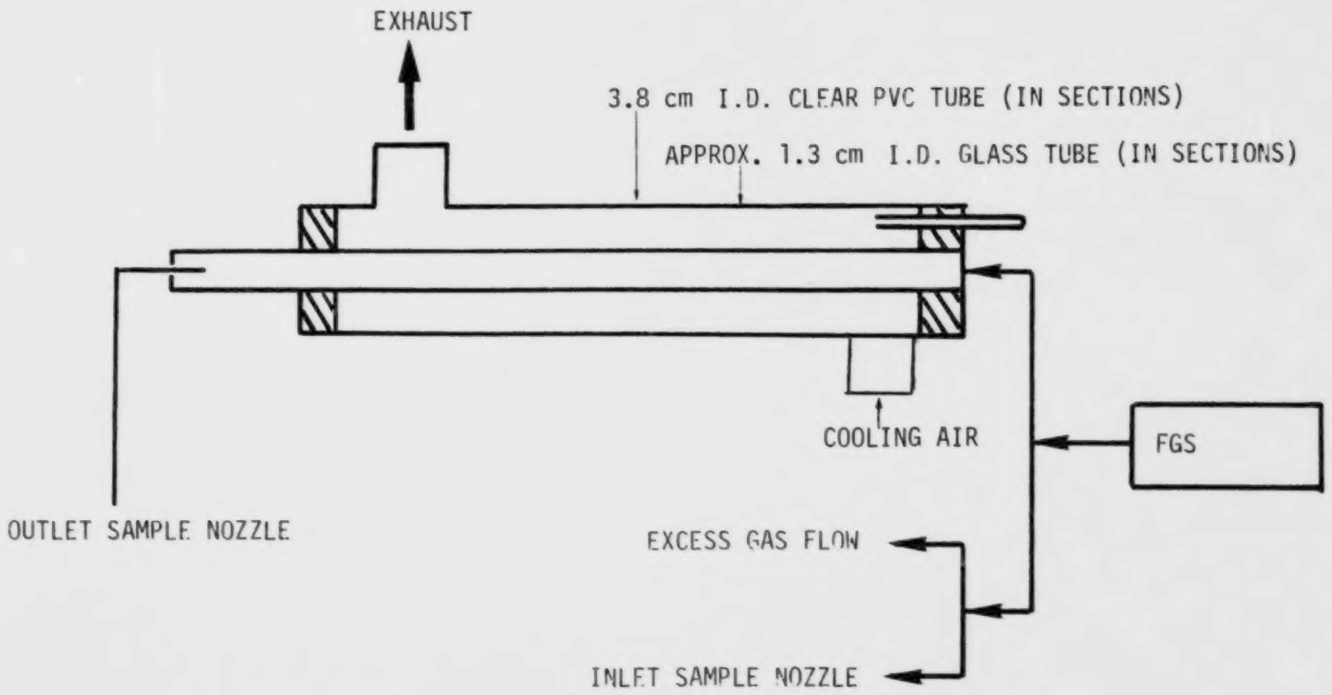
EXHAUST
3.8 cm I.D. CLEAR PVC TUBE (IN SECTIONS)
APPROX. 1.3 cm I.D. GLASS TUBE (IN SECTIONS)
COOLING AIR
FGS
OUTLET SAMPLE NOZZLE
EXCESS GAS FLOW
INLET SAMPLE NOZZLE

Figure 35. Slow cooling experimental setup.

3. Use a laser beam to detect (by light scattering) the acid particle nucleation location in the heat exchanger. When there are no particles in the gas stream, the laser beam is invisible. The beam is visible as a solid red line when there are particles. the nucleation location in the heat exchanger is defined as the location where the laser beam is just visible as a flickering red line. The gas temperature at this location is measured with thermocouples.
4. Sample the gas at the heat exchanger inlet and at the nucleation point simultaneously. The inlet sampling train consists of a water cooled condenser, 4 impingers (3 with water), and a final filter. The other train consists of a heated filter (heated to gas temperature), 4 impingers (3 with water), and a final filter.

Results

Nucleation Temperature

Acid particle nucleation temperature was measured with the above method for several acid vapor and water vapor concentrations. The results are shown in Table 18. The acid nucleation temperature was verified in three experiments with the same acid and water vapor concentrations, flow rate, and gas temperature. In experiment No. 1, a gas sample was taken at the nucleation point. The sampling system consisted of a quartz filter, which was heated to, and maintained at gas temperature, followed by three impingers and another quartz filter.

In Experiment No. 2, sampling was done at the same location as in Experiment No. 1. However, the cooling rate was adjusted so that the gas temperature at the sampling point was higher and the laser beam was not visible. In Experiment No. 3, the gas temperature at the sampling location was lowered and the laser beam was visible upstream of the sampling nozzle.

Experimental results are shown in Table 19. Since little acid was collected by the front filter in Experiment No. 2 and almost all acid was collected by the front filter in Experiment

TABLE 18. NUCLEATION TEMPERATURE MEASUREMENT

Run No.	Inlet Acid Vapor Conc., ppm	Inlet Water Vapor Conc., Vol.%	Nucleation Point Acid Vapor Conc., ppm	Nucleation Point Water Vapor Conc., Vol.%	Nucleation Point Gas Temperature °C
116/01	83.4	10	65.2	10	106
116/02	49.9	5.5	39.6	2.8	96
116/04	52.1	4.7	46	2.9	99
116/05	61.9	14.5	60.4	14.5	109
117/01	29.0	10.1	11.6	4.9	104
117/02	40.2	5.0	19.9	2.5	86
117/03	35.5	13.8	26.1	12.2	103
118/01	22.1	10.1	19.3	9.6	96
118/02	27.6	14.0	17.3	11.6	103
119/01	22.0	10.1	4.6	10.6	91
119/02	31.4	4.8	17.7	3.1	101

TABLE 19. EFFECT OF GAS TEMPERATURE ON ACID NUCLEATION

	RUN #		
	1	2	3
Temperature, °C (°F)	110 (230)	135 (275)	96 (205)
Probe Wash, mg		5.19	4.08
Front Filter, mg	10.05*	0.98	13.73
Hose, mg	0.75	1.05	0.50
Impinger #1, mg	1.00	2.0	0.21
Impinger #2, mg	0.0	0.98	0.0
Impinger #3 + #4, mg	0.0	0.0	0.0
Back Filter, mg	1.23	3.68	0.0
Total Acid Conc., ppm	27.2	28.8	40.5
Total Water Conc., % Vol.	6.5	6.8	7.5

---

*Includes probe wash.

No. 3, the acid nucleation temperature should be higher than the gas temperature of Experiment No. 3 and lower than that of Experiment No. 2. The nucleation temperature should be close to the gas temperature of Experiment No. 1 because both the front and back filters collected appreciable amounts of acid.

Condensation on Walls

A few experiments were performed to determine the amount of acid vapor condensed on walls before the acid nucleation point. Figure 35 shows the apparatus. The double pipe heat exchanger was built in sections. The dimensions of the inner pipe were shown in Figure 35. The heat exchanger was connected to the FGS outlet and the cooling air flow rate was adjusted so that nucleation was observed to start at the exit of Section 6.

Acid vapor concentration was determined at the inlet of the heat exchanger and at the exit of Section 6 with the sampling train shown in Figure 9. The amount of acid vapor condensed on walls was determined by washing each section of the heat exchanger with distilled water followed by titrating the solution with sodium hydroxide. Gas temperature in the heat exchanger was measured with thermocouples at the exit of each section.

The experimental results are shown in Table 20. The data were used to perform mass balance calculations. The results are as follow:

Run No.	Acid vapor conc., ppm		Amount of vapor condensed on wall, ppm	
	Inlet	Outlet	from wall washings	Calc. from vapor measurements
76/134	32.9	20.1	21.3	12.8
76/136	60.5	40.5	38.8	20.0
76/138	78.2	30.5	40.6	47.7

The amount of acid vapor condensed on wall determined from wall washing is higher than that calculated from inlet and outlet vapor concentration measurements. The higher amount from wall washing could be due to initial condensation when the cold heat exchanger was connected to the flue gas simulator.

Particle Size Distribution

Table 21 shows a summary of slow cooling experiments and Table 22 presents the frequency distribution of the acid particle size. All samples, except Run No. 76/140, were taken at the nucleation starting point. Run No. 76/140 was a simultaneous run with Run No. 76/139 and was sampled at 30 cm downstream from the nucleation point.

Figures 36 and 37 show the effects of SO_2 and fly ash particles injection on acid nucleation. While SO_2 injection has no effect on acid nucleation, fly ash particles have great effect. When there were no ash particles, all acid particles passed through the cascade impactor and were caught by the diffusion battery. When there were ash particles, over 80% (wall condensation excluded) of the acid vapor was condensed on ash particles and collected by the impactor. The balance of the acid vapor was nucleated to form ultra-fine particles which were collected by stage 1 of the diffusion battery. This result is consistent with the sampling data of Whitby et al. (1978) on power plane plumes.

Figure 38 shows the effect of sampling location on acid particle size distribution. Run No.s 76/139 and 76/140 were simultaneous runs. Run No. 76/139 was sampled at nucleation starting point and Run No. 76/140 was sampled 30 cm downstream. Due to agglomeration or additional water vapor condensation, acid particles had grown at the downstream location.

Higher acid vapor and lower water vapor concentrations lead to the formation of large quantity of ultra-fine acid particles as shown in Figures 39 and 40.

TABLE 20. WALL LOSS EXPERIMENTAL RESULTS

RUN NO.	ACID CONC.. INLET	VAPOR ppm OUTLET	INLET WATER VAPOR CONC., % Vol.	INLET GAS FLOW RATE N/min	GAS TEMPERATURE, °C							MASS OF ACID CONDENSED, mg						SAMPLING DURATION min.	COOLING AIR FLOW-RATE 1/min	COOLING AIR TEMP, °C
					T_{in}	T_1	T_2	T_3	T_4	T_5	T_6	M_1	M_2	M_3	M_4	M_5	M_6			
76/138	78.2	30.5		42	246	223	209	189	178	166	118	184.4	158.9	131.4	137.3	117.7	278.6	146	41.6	20
76/136	60.5	40.5		42	246	225	209	196	185	176	130	131.4	70.6	68.7	121.6	105.	278.6	117	15.6	21
76/134	32.9	20.1		42	246	222	199	184	179	169	102	120.6	103.	84.	78.5	66.	239.3	190	37.1	20

TABLE 21. SUMMARY OF SLOW COOLING EXPERIMENTAL CONDITIONS

RUN NO.	INLET GAS FLOW RATE, Nl/min.	WATER VAPOR Vol. %	ACID CONCENTRATION ppm		SO_2, ppm		FLYASH, g/Nm^3	GAS TEMPERATURE AT SAMPLING POINT, °C
			INLET	SAMPLING POINT	INLET	SAMPLING POINT		
76/126	42	10	--	19.9	--	--	--	105
76/127	42	10.1	--	16.3	--	--	--	105
76/128	42	9.9	--	15.2	--	--	--	105
76/129	42	9.3	--	21.3	--	--	--	106
76/133	42	5.0	32.9	20.1	--	--	--	99
76/135	42	10.8	60.5	40.5	--	--	--	102
76/137	42	4.9	78.2	30.5	--	--	--	92
76/139	42	10.4	--	27.8	--	--	--	99
76/140	42	10.4	--	27.8	--	--	--	99
76/141	42	5.2	--	38.1	--	100	--	96
76/142	55	4.9	--	44.4	--	--	0.39	96
76/143	42	4.6	--	43.3	--	--	--	96

TABLE 22. ACID PARTICLE SIZE FREQUENCY DISTRIBUTION

RUN NO.	$\Delta C_p/C_{pt}\Delta(\log d_{pa})$, mg/Nm³, at d_{pa} = 0.022	0.049	0.11	0.20	0.40	0.82	1.35	2.22	4.09	9.29	22.6 µm
76/126	0.22	0.32	0.68	0.34	1.39	---	---	---	---	---	---
76/127	0.49	0.48	0.80	0.76	0.31	---	---	---	---	---	---
76/128	1.70	0.076	0.11	0.039	0.89	0.034	0.16	0.14	0.11	0.040	0.090
76/129	0.23	0.14	0.42	0.79	1.55						
76/133	0.51	0.31	0.60	0.96	0.94						
76/135	1.12	0.31	0.57	0.64	0.72						
76/137	0.81	0.44	0.62	0.61	0.75						
76/139	0.78	0.31	0.64	0.47	0.97						
76/140	0.22	0.16	0.51	0.84	1.43						
76/141	1.28	0.44	0.74	1.20	0.043						
76/142	0.53	1.6×10^{4}	2.2×10^{4}	3.3×10^{4}	1.2	0.22	0.42	0.48	0.26	0.042	0.17
76/143	0.84	0.46	0.63	0.87	0.57						

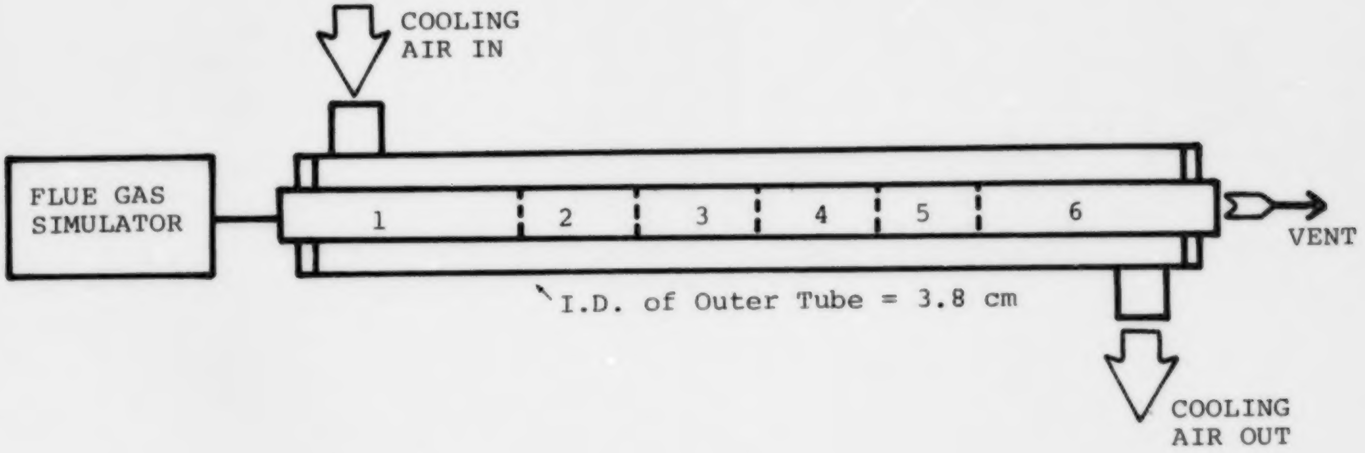

SECTION	I.D., cm	LENGTH, cm	AREA, cm^2
1	1.54	30.5	147
2	1.54	14.0	67.4
3	1.54	14.0	67.4
4	1.54	14.0	67.4
5	1.54	14.0	67.4
6	1.54	31.0	151

Figure 35. Wall loss experimental set-up.

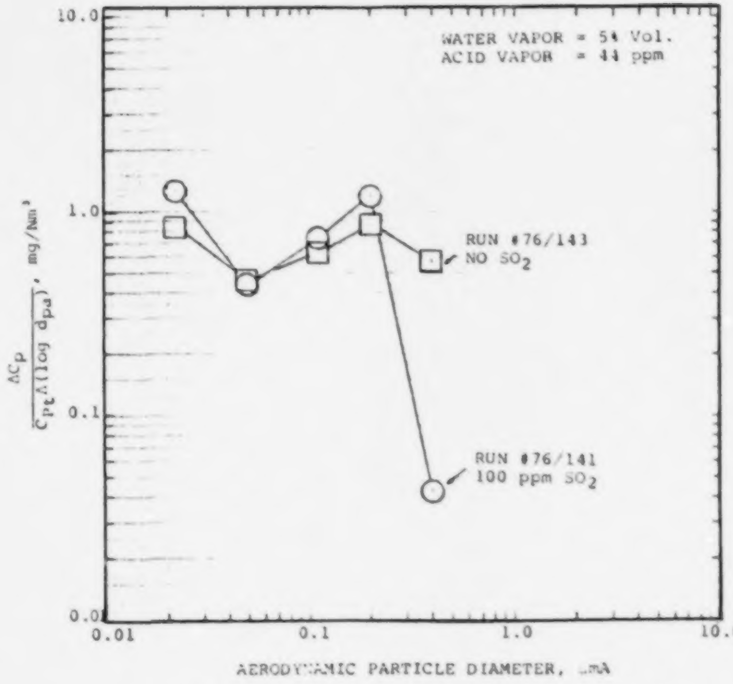

Figure 36. Effect of SO_2 on nucleated acid particle size distribution.

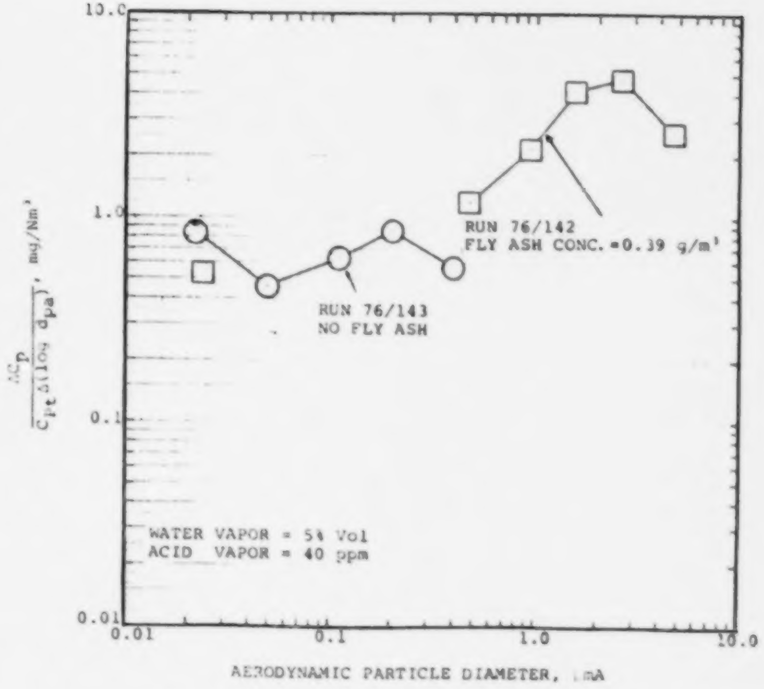

Figure 37. Effect of injected fly ash on nucleated acid particle size distribution.

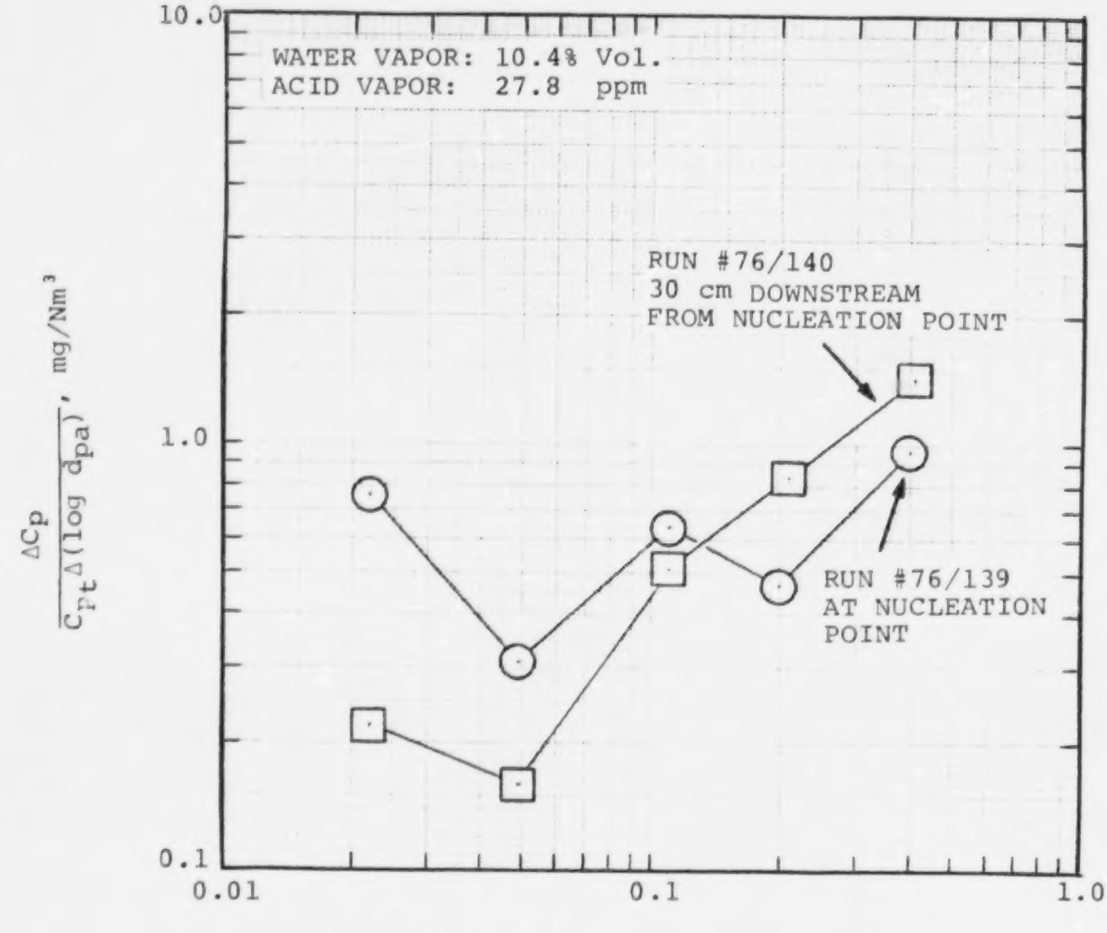

Figure 38. Effect of sampling location on acid particle size distribution.

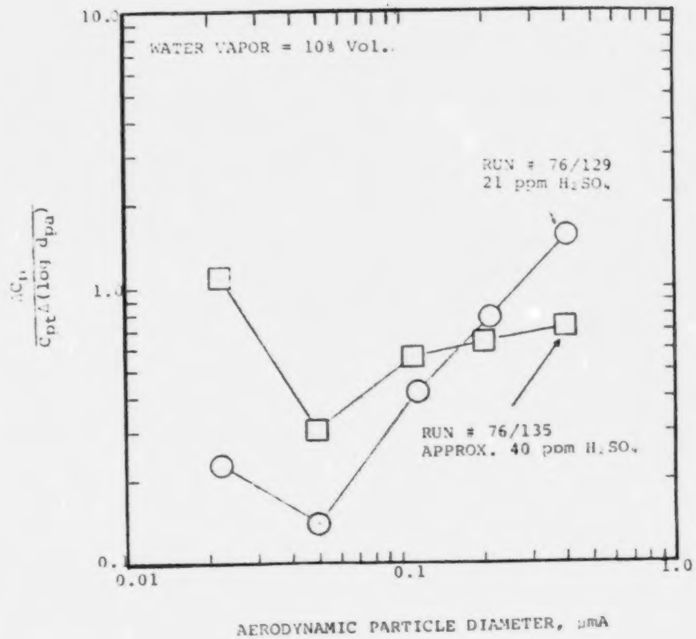

Figure 39. Effect of acid vapor concentration on particle size distribution.

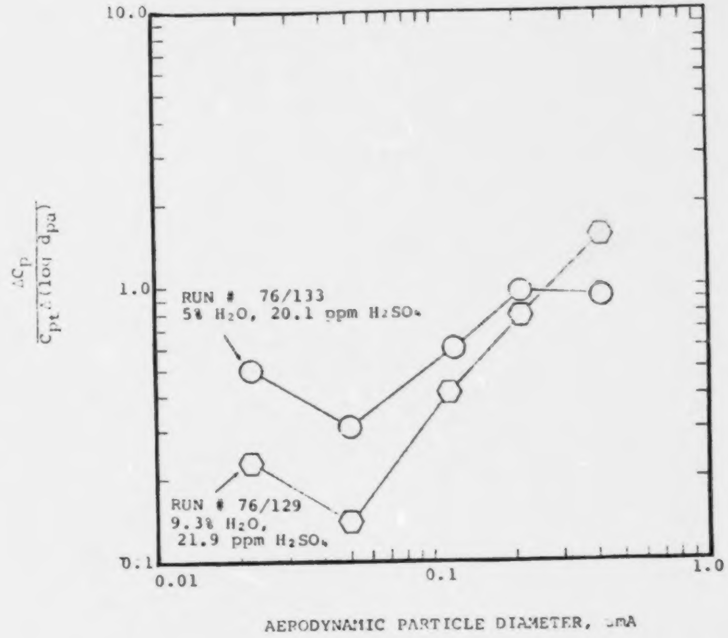

Figure 40. Effect of water vapor concentration on nucleated particle size distribution.

SECTION 6
COMPARISON BETWEEN THEORY AND RESULTS

NUCLEATION TEMPERATURE

The nucleation of sulfuric acid particles involves two condensible species - water and sulfuric acid vapors. The nucleation rate can be calculated from the classical kinetic theory presented in Section 3. The rate of critical nucleus formation is given as the product of the critical nucleus concentration, the collision cross-sections of the sulfuric acid molecule and the nucleus, and the molecular flux of sulfuric acid molecules (Kiang and Stauffer, 1973):

$$I^* = A_C\ B_A\ n^*$$

$$= n_A \left[\frac{kT}{2\pi\ m_A}\right]^{0.5} (4\pi\ r^{*2})\ n_W \exp\left(-\frac{\Delta G^*}{kT}\right) \qquad (62)$$

where: I^* = rate of critical nucleus formation, $m^{-3}\ s^{-1}$

B_A = molecular flux of H_2SO_4 molecules on to a given surface, $m^{-2}\ s^{-1}$

A_C = cross-sectional area of target critical nuclei, m^2

n^* = concentration of target critical nuclei, m^{-3}

n_A = concentration of acid molecules, m^{-3}

k = Boltzmann constant, J/K

m_A = mass weight of an acid molecule, kg

r^* = radius of a critical condensation nucleus, m

n_W = concentration of water molecules, m^{-3}

ΔG^* = Gibbs free energy of formation of critical nuclei, J

T = Temperature, K

The terms "critical" in "critical nucleus" and "critical radius" refer to the condition at which the Gibbs free energy of formation of a nucleus is maximized with respect to the addition of any more water or sulfuric acid molecules. The Gibbs free energy of formation of a nucleus from "n_A" molecules of acid and "n_W" molecules of water is given by equation (14) and the free energy of formation of a critical nucleus is given by equation 24.

For a given water and acid vapor concentration combination, the temperature at which nucleation of sulfuric acid particles starts can be predicted by solving equations (14), (24), and (62) simultaneously. Most authors take $I^* = 10^6\ m^{-3}\ s^{-1}$ as the minimum easily observable nucleation rate (Friedlander, 1977; Green and Lane, 1964; Fletcher, 1962). Therefore, the nucleation temperture in the present study was defined as the temperature which gives a nucleation rate of $10^6/m^3$-s ($1/cm^3$-s) for the given acid and water concentration.

Equations (62), (14), and (24) were solved by means of a computer with the following procedure:

1. Guess a temperature.
2. Calculate the critical nucleus composition.
3. Calculate the critical radius.
4. Calculate the critical nucleation current.
5. If the current is not $10^6\ m^{-3}$-s^{-1} then go back to step 1, otherwise exit.

With a given temperature, water concentration and vapor-phase acid concentration, the critical nucleus composition was calculated by the method of Yue (1979). Yue wrote the following relation for the relative acidity.

$$S_A = a_A \exp \frac{M_A}{M_W V} \ln \frac{S_W}{a_W} \tag{63}$$

$$\text{with } h = \frac{1 - \frac{1-x_A}{\rho} \frac{d\rho}{dx_A} + \frac{3}{2} \frac{(1-x_A)}{\sigma} \frac{d\sigma}{dx_A}}{1 + \frac{x_A}{\rho} \frac{d\rho}{dx_A} - \frac{3}{2} \frac{x_A}{\sigma} \frac{d\sigma}{dx_A}} \tag{64}$$

and: S_A = relative acidity of vapor phase (prevailing partial pressure of H_2SO_4 divided by the vapor pressure of pure H_2SO_4 at the same temperature), dimensionless

a_A = liquid phase acid activity (ratio of the vapor pressure of H_2SO_4 above sulfuric acid solution to the pure component sulfuric acid vapor pressure), dimensionless

M_A = molecular weight of sulfuric acid, kg/mol.

M_W = molecular weight of water, kg/mol.

S_W = relative humidity of the vapor phase, dimensionless

V = molar volume of solution, m^3/mol

a_A = activity of water in solution in the drop, dimensionless

x_A = weight fraction H_2SO_4 in the drop, fraction

ϱ = density of the sulfuric acid solution drop, kg/m^3

σ = surface tension, N/m

For a given condition (T, S_A, and S_W known), equation (63) was solved for "x_A". Since a_A, a_W, ϱ, and σ are implicit functions of "x_A", analytic solutions could not be obtained. These equations were solved by numerical methods. Yue (1979) noticed that for a given "x_A", equation (63) is a straight line when "S_A" is plotted against "S_W" on log-log paper. Therefore, the following steps were used in solving equation (63).

1. Guess two initial compositions which bracket the actual composition.
2. Calculate "S_A" using equation (63) and (64) at the guessed composition.
3. Interpolate between the two calculated "S_A" to find the "x_A" corresponding to the known "S_A".
4. Repeat steps 2 and 3 using the calculated "x_A" until the calculated "S_A" is close to the known "S_A".

Knowing the critical composition, the critical radius was calculated from the following equation.

$$r^* = \frac{2M_A}{RT}\,\frac{\sigma}{\rho}\left[1 + \frac{x_A}{\rho}\,\frac{d\rho}{dx_A} - \frac{3}{2}\,\frac{x_A}{\sigma}\,\frac{d\sigma}{dx_A}\right]\ell n^{-1}\,\frac{S_A}{a_A} \qquad (65)$$

Where σ, ϱ, $d\varrho/dx_A$, and $d\sigma/dx_A$ were evaluated at the critical composition found above and "R" is the universal gas constant. The nucleation current was then calculated from equations (62) and (74). The computer proram written in Mircrosoft Fortran-80 is given in Appendix "A".

Physical Properties

The following physical properties of sulfuric acid are needed as a function of composition and temperature: ϱ; $d\varrho/dx_A$; σ; $d\sigma/dx_A$; p_A, the vapor pressure of acid above acid solution. The data for the various physical properties were found in the literature in tabular form. The source and range of the reported properties are listed in Table 23. The reported data were fitted with a curve as functions of temperature for each composition. Vapor pressure data were linearly fitted as log vs. reciprocal absolute temperature. Surface tension and density were linearly fitted with temperature. The data for surface tension were extrapolated for temperatures from 50°C to 100°C. To find the property for a given composition, Aitken-Lagrange Interpolation was used between the constant-composition curves. To find the slopes of the density and surface tension versus composition curves as functions of composition, the constant-composition curves were evaluated as the specified temperature; the resulting array was fitted with a parabola and differentiated.

Calculation Results

Figure 41 shows a family of curves of nucleation temperature versus vapor phase acid concentration with water vapor concentration as a parameter. As can be seen, the nucleation temperature increases with increasing water vapor and acid vapor concentrations. This means less cooling of flue gas is needed for the formation of acid particles if the acid vapor and water vapor concentrations are high.

Based on the calculations, nucleation, once it starts, goes to completion quickly. Acid vapor is depleted in a very short time interval. Therefore, the criteria ($I_p = 10^6/m^3$-s) for determining the nucleation temperature will not cause serious error.

TABLE 23. SOURCE OF PHYSICAL PROPERTY DATA FOR SULFURIC ACID-WATER SOLUTION

Physical Property	Source	Range
Density	Chemical Engineers' Handbook Perry & Chilton (1972)	0-100°C 0-100% (wt) H_2SO_4
Surface Tension	Sabinina and Terpugov (1935)	10-50°C 0-100% (wt) H_2SO_4
Vapor Pressure of Sulfuric Acid And Water	Gmitro and Vermeulen (1964a,b) Keenan et al. (1969)	20-200°C 0-100% (wt) H_2SO_4

Reproduced from
best available copy.

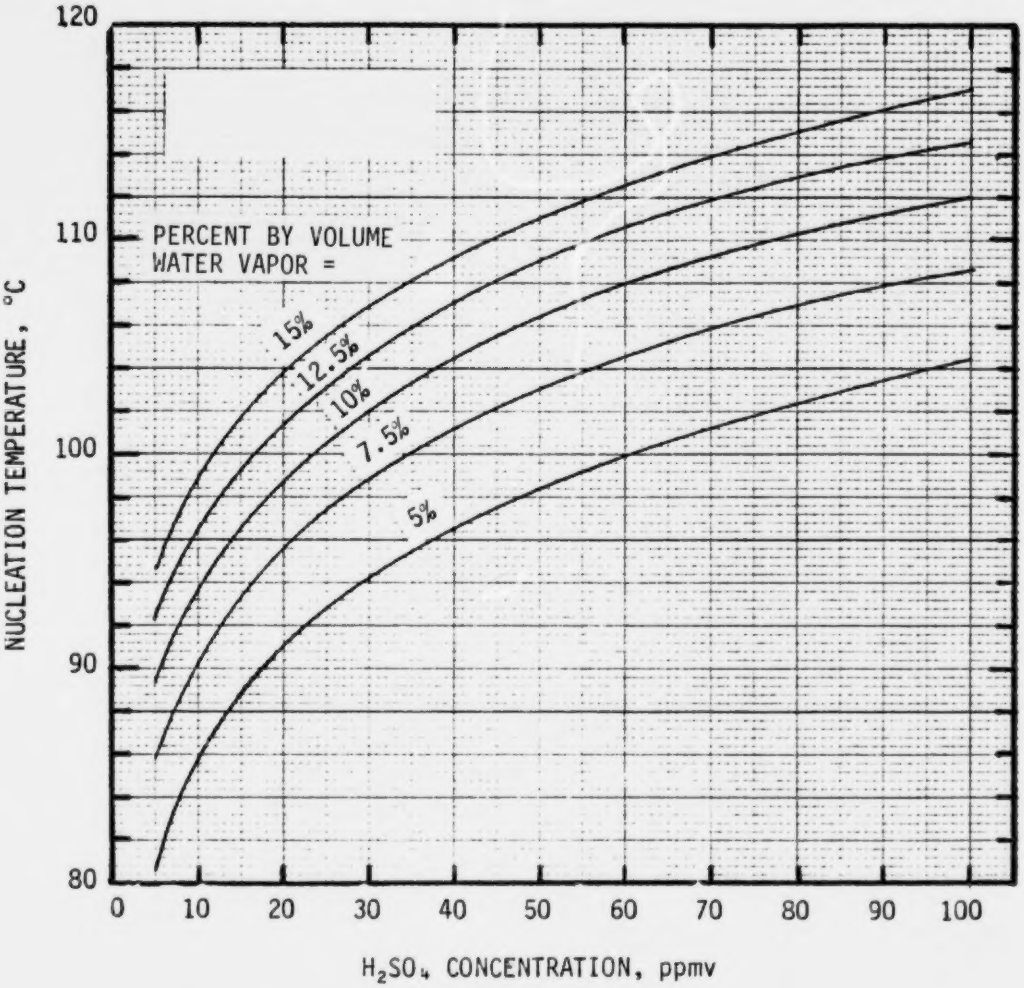

Figure 41. Predicted nucleation temperature.

Comparison with Experiments

Table 24 shows a comparison between the predicted and measured acid particle self-nucleation temperatures. There are discrepancies between theory and experiment for some of the runs. However, by considering the uncertainties in vapor pressure and surface tension data, the agreement between theory and experiment is considered to be good.

SLOW COOLING THEORY

A mathematical model, which characterizes the nucleation, condensation, and growth of sulfuric acid particles in a flow system, such as in a length of pipe, was developed. The model accounts for gas cooling, vapor loss to the wall, homogeneous binary nucleation, heterogeneous condensation on existing particles, diffusional loss of nucleated particles and coagulation. A computer program was written for applying the model to slow cooling experiments. The program uses a quasi-steady state approach, and follows a small element of fluid through the pipe, and computes changes in temperature, vapor concentration, and particle concentration due to the above mentioned mechanisms in successive increments of distance along the pipe.

A particle size distribution evolves by treating the particles formed in each increment as a separate group of particles. The initial number and size of the particles in each group are determined by the nucleation equations presented in Section 3. However, the number and size in each group change due to particle growth and coagulation as the flow element proceeds down the flow path. The final particle concentration and size distribution are given by these quantities at the end of the pipe.

A discussion of the model is presented in the following sections.

TABLE 24. NUCLEATION TEMPERATURE MEASUREMENT

	Inlet		Nucleation Point			
Run No.	Acid Vapor Conc., ppm	Water Vapor Conc., Vol.%	Acid Vapor Conc., ppm	Water Vapor Conc., Vol.%	Gas Temperature °C	Predicted Nucleation Temperature, °C
116/01	83.4	10	65.2	10	106	105
116/02	49.9	5.5	39.6	2.8	96	97
116/04	52.1	4.7	46	2.9	99	98
116/05	61.9	14.5	60.4	14.5	109	113
117/01	29.0	10.1	11.6	4.9	104	95
117/02	40.2	5.0	19.9	2.5	86	91
117/03	35.5	13.8	26.1	12.2	103	105
118/01	22.1	10.1	19.3	9.6	96	98
118/02	27.6	14.0	17.3	11.6	103	102
119/01	22.0	10.1	4.6	10.6	91	99
119/02	31.4	4.8	17.7	3.1	101	90

Gas Cooling

In a quasi-steady state model, the gas is assumed to cool at a constant rate for a short period of time. The cooling rate over this perid is a balance between the following processes:

a. Sensible heat of the vapor.

b. Latent heat liberated from water condensing on the wall.

c. Heat transferred through the wall to the cooling air.

By rearranging the heat balance equation featuring these three mechanisms, the gas temperature at the end of each time period is:

$$T_{i+1} = \frac{\dot{N}_G M_G C_{PG} T_i + J_{ws} A_i M_w L + U\ A_i (T_{oi} - \tfrac{1}{2} T_i)}{\dot{N}_G M_G C_{PG} + \tfrac{1}{2} U\ A_i} \qquad (66)$$

Where: T_{i+1} = vapor temperature at the end of time interval i, °C

N_G = flue gas flow rate, mol/s

M_G = flue gas molecular weight, kg/mol

C_{PG} = flue gas specific heat capacity, J/kg-K

J_{ws} = flux of condensing water vapor on the wall, mol/(m²-s)

A_i = wall area tranversed by flue gas during time interval i, m²

M_w = molecular weight of water, kg/mol

L = latent heat of vaporization of water, J/kg

U = overall heat transfer coefficient for heat transfer through the wall, W/(m²-K)

T_{oi} = outside cooling gas temperature on interval i, °C or K

T_i = vapor temperature at the inlet of time interval i, °C or K

Likewise, a heat balance on the cooling air yields the following equation for finding the outside cooling gas temperature at each time step.

$$T_{oi+1} = T_{oi} + \frac{U\ A_i \left[\frac{T_i + T_{i+1}}{2}\right] - T_{oi}}{\dot{N}_{Go} M_G C_{PGo}} \qquad (67)$$

Where: T_{oi+1} = cooling gas temperature at the end of time interval i, °C or K

N_{Go} = flow rate of cooling gas, mol/s

M_G = molecular weight of cooling gas, kg/mol

C_{pGO} = specific heat capacity of cooling gas, J/(kg-K)

When excess cooling air is used, cooling air temperature can be assumed to be a constant, i.e. $T_{oi+1} = T_{oi}$. The heat transfer area is based on the inside tube diameter and is calculated from the following equation:

$$A_i = \frac{4}{d_i} \frac{RT_i}{p} \dot{N}_G \Delta t \qquad (68)$$

Where: d_i = inside tube diameter, m

R = universal gas constant, J/(mol-K)

p = total pressure of the flue gas being cooled, Pa

Δt = time interval, s

The temperature in equation (68) must be expressed in absolute units (Kelvins).

Vapor Condensation

As the gas cools, sulfuric acid and water vapors can condense on the system boundaries, nucleate to form acid drops and condense on pre-existing particles.

Homogeneous Nucleation of Sulfuric Acid

The nucleus formation rate is calculated from equation (62).

Condensation on the System Boundaries

Water and sulfuric acid vapor condensations on wall are calculated from mass transfer.

$$J_{ws} = k_w(n_{wi} - \frac{P_{ws}}{RT_i}) \qquad (69)$$

$$J_{As} = k_A(n_{Ai} - \frac{P_{As}}{RT_i}) \qquad (70)$$

Where: k_w = mass transfer coefficient for water vapor, m/s

p_{ws} = equilibrium vapor pressure of water over the acid solution at the wall, Pa

J_{As} = mass transfer flux of the sulfuric acid onto the wall, mol/(m²-s)

J_{ws} = mass transfer flux of water vapor onto the wall, mol/(m²-s)

k_A = mass transfer coefficient for sulfuric acid vapor, m/s

p_{As} = equilibrium vapor pressure of H_2SO_4 over the acid solution at the wall, Pa

n_{Ai} = acid vapor concentration at inlet of time interval i, mol/m³

n_{wi} = Water vapor concentration at the inlet of time interval i, mol/m³

Condensate Composition

The vapor pressures "p_{As}" and "p_{ws}" depend on the wall temperature and the composition of the acid solution on the wall (if any). The composition of the acid on the wall is calculated by assuming it to be at its bubble point at the wall temperature. The bubble point composition is that composition which satisfies the following equation (McCabe and Smith, 1976; Treybal, 1968):

$$x_A K_A + (1-x_A)K_w = 1 \tag{71}$$

Where: $$K_A = \frac{p_A(x_A, T_s)}{xp} \tag{72}$$

$$K_w = \frac{p_w(x_A, T_s)}{(1-x_A)p} \tag{73}$$

x_A = mole fraction H_2SO_4 in liquid condensate, fraction

T_s = wall temperature, °C, or K

K_A = vapor-equilibrium partition coefficient for H_2SO_4, dimensionless
K_w = vapor-equilibrium partition coefficient for H_2O, dimensionless
p_A = equilibrium vapor pressure of H_2SO_4 above sulfuric acid solution, Pa
p_w = equilibrium vapor pressure of H_2O above sulfuric acid solution, Pa

Wall Temperature

The temperature of the inside wall may be found by proportioning the temperature drops and heat transfer resistances across the wall (McCabe and Smith, 1976):

$$T_s = T_i - \frac{U}{h_i} (T_i - T_{oi}) \left(1 + \frac{2x_w}{d_i}\right) \tag{74}$$

Where: h_i = inside tube heat transfer coefficient, W/m²-K)
x_w = thickness of the tube wall, m

Heterogeneous Condensation

Acid and water vapors will condense on pre-existing particle (or newly nucleated particles) so long as the vapor pressure at their surface, as determined by the Kelvin equation (equation 39), is less than the particle pressure of the vapor in the gas stream. The condensation rate depends on the exchange of mass and heat between a particle and the gas phase and can be predicted from equations (34) through (37).

The equilibrium vapor pressure, "p_d°", in equations (34) through (37) is a function of particle diameter and particle temperature. When vapor condenses on the surface of the particle, the latent heat of condensation is released and the temperature of the particle becomes higher than the temperature of the gas. The temperature of the particle can be predicted by performing an energy balance around the particle. The resulting equation is:

$$\frac{1}{6} \pi d_p \rho_p C_{pp} \frac{dT_p}{dt} = \frac{dq}{dt} L - 2\pi d_p h \left(T_p - T\right) \tag{75}$$

where T_p = temperature of the particle, K

C_{pp} = heat capacity of the particle, J/kg

h = heat transfer coefficient, $W/(m^2\text{-}k)$

ϱ_p = particle density, kg/m^3

Equation (75) neglects the effect of heat of solution. Azarniouch et al (1973) performed simultaneous heat and mass balances on sulfuric acid drops growing by condensation of water vapor. They determined that heat of solution effects are important for high acid concentrations.

To simplify the calculations and yet include as many of the important effects as possible, the temperature of the drop is calculated as the multicomponent wet bulb temperature including heat of solution effects.

$$T_{pi} = \frac{L/N_{Av}}{h/k_w}\left[n_{wi} - \frac{p^o_{dw}}{kT}\right] + \frac{\Delta h_{soln}/N_{Av}}{h/k_A}\left[n_{A\,i} - \frac{P_{SA}}{kT}\right] + T_i \tag{76}$$

where
$$\frac{h}{k_w} = \frac{k_G}{D_w}\,\frac{\left[1 + \dfrac{1.333 + 0.71\,\dfrac{d_p}{2l_w}}{\dfrac{d_p}{2l_w}}\right]\dfrac{2l_w}{d_p}}{\left[\dfrac{1}{1 + \dfrac{2l_m}{d_p}} + \dfrac{3.17}{a_T}\,\dfrac{2l_m}{d_p}\right]} \tag{77}$$

and
$$l_w = \frac{3\,D_w}{\left(\dfrac{8}{\pi}\,\dfrac{RT}{M_w}\right)^{\frac{1}{2}}} \tag{78}$$

where T_{pi} = particle temperature in interval "i" °C

h = Newton law coefficient for conduction to particle, $W/(m^2\text{-}K)$

k_w = mass transfer coefficient of water vapor transpiration from particle, m^2/s

P_{dw} = equilibrium water vapor pressure above particle, Pa

Δh_{soln} = heat of solution of sulfuric acid, J/mol

k_A = mass transfer coefficient for sulfuric acid vapor to particle, $m^2\text{-}s^{-1}$

p_{SA} = equilibrium sulfuric acid vapor presure above acid, Pa

L = latent heat of evaporation, J/kg

l_w= mean free path for collisions of water vapor molecules with themselves, m

l_m = mean free path of air molecules, m

a_T = thermal accommodation coefficient = 0.92 (Hidy and Brock, 1970, Table 5.3)

N_{av} = Avogadri's number

Vapor Concentration

The acid and water vapor concentrations at the end of a given time interval are determined from a material balance:

$$n_{wi+1} = n_{wi} - \frac{4}{d_i} J_{ws}\Delta t - \frac{4\pi}{3} \frac{\rho^*(1-x^*)r^*}{M_w} I^*\Delta t - \left(\frac{dn_w}{dt}\right)\Delta t \qquad (79)$$

$$n_{Ai+1} = n_{Ai} - \frac{4}{d_i} J_{As}\Delta t - \frac{4\pi}{3} \frac{\rho^* x^* r^*}{M_A} I^*\Delta t - \left(\frac{dn_\Delta}{d_k}\right)\Delta t \qquad (80)$$

Where: n_{wi+1} = water vapor concentraiton at the end of the time interval, mol/m³

n_{wi} = water vapor concentration at the beginning of the time interval, mol/m³

ρ^* = density of a critical condensation nucleus of sulfuric acid, kg/m³

x^* = weight fraction H_2SO_4 in critical size acid drop, fraction

r^* = rate of critical size acid drop, m

I^* = rate of formation of critical size acid drop, m^{-3} $-s^{-1}$

n_{Ai+1} = H_2SO_4 vapor concentration at the end of the time interval, mol/m³

n_{Ai} = H_2SO_4 vapor concentration at the beginning of the time interval, mol/m³

J_{As} = mass transfer flux of sulfuric acid on the wall, mol/m²-s

J_{ws} = mass transfer flux of water vapor on the wall, mol/m²-s

M_A = molecular weight of sulfuric acid, kg/mol

d_i = pipe inside diameter, m

Transfer Coefficients

In Equations 62, 66, 69, 70 and 76, heat or mass transfer coefficients have been employed. The methods of calculating the transfer coefficients are presented together here because of their similarity.

The inside tube heat transfer coefficient depends on the flow regime (Knudsen, 1972). In the laminar regime (N_{Re} = < 2,000), the relationship due to Sieder and Tate (1936) is:

$$h_i = 1.86\, N_{Re}^{1/3}\; N_{Pr}^{1/3}\; \left(\frac{d_i}{L_t}\right)^{1/3} \left(\frac{k_G}{d_i}\right) \tag{81}$$

$$= 0.51\, N_{Re}^{1/3}\; N_{Pr}^{1/3}\; \left(\frac{k_G}{d_i}\right) \tag{82}$$

Where: N_{Re} = Reynolds number inside the tube, dimensionless

N_{Pr} = Prandtl number inside the tube, dimensionless

L_t = total tube length, m

k_G = thermal conductivity of the gas inside the tube, W/(m-K)

d_i = tube inside diameter, m

Equation (82) results from estimating "d_i/L_t" to be approx. 0.02.

For 2,000 < N_{Re} < 10,000, the transition regime equation of Hausen (1934) is used.

$$h_i = 0.116\left(N_{Re}^{2/3} - 125\right) N_{Pr}^{1/3} \left(\frac{k_G}{d_i}\right) \tag{83}$$

Viscosity and entrance effects were neglected in equation (83).

For the outside (shell-side) cooling air heat transfer coefficient, the turbulent flow regime correlation is used.

$$h_o = 0.020\ N_{Reo}^{0.8}\ N_{Pro}^{0.33}\ (\frac{d_s}{d_i})^{0.53}\ (\frac{k_{Go}}{d_s - d_i - 2x_w}) \qquad (84)$$

Where: h_o = the outside (shell-side) heat transfer coefficient, W/(m²-K)
N_{Reo} = Reynolds number for shell-side, dimensionless
N_{Pro} = Prandtl number for shell-side, dimensionless
d_s = inside diameter of heat exchanger shell, m
k_{Go} = shell-side gas thermal conductivity, W/(m-K)

Knowing the inside and outside resistances to heat transfer, the overall heat transfer coefficient, U, can be calculated according to the following equation:

$$\frac{1}{U} = \frac{1}{h_i}\left(1 + \frac{2x_w}{d_i}\right) + \frac{2x_w}{k_s}\left(\frac{d_i + 2x_w}{d_{1m}}\right) + \frac{1}{h_o} \qquad (85)$$

Where: $$d_{1m} = \frac{2x_w}{\ln(1 + \frac{2x_w}{d_i})} \qquad (86)$$

and k_s = thermal conductivity of the wall material, W/(m-K)
d_{1m} = logarithmic-mean diameter of the tubewall, m

The mass transfer coefficients are calculated from the relations of Gilliland and Sherwood (1934).

$$k_w = 0.023\ N_{Re}^{0.83}\ N_{Scw}^{0.44}\ \frac{D_w}{d} \qquad (87)$$

$$k_A = 0.023\ N_{Re}^{0.83}\ N_{Re}^{0.44}\ \frac{D_A}{d} \qquad (88)$$

Where: N_{Scw} = Schmidt number for water vapor, dimensionless
D_w = diffusivity of water vapor in air, m²/s
N_{ScA} = Schmidt number for H_2SO_4 vapor, dimensionless
D_A = diffusivity of H_2SO_4 vapor, m²/s

Transport Properties

The dimensionless groups such as the Reynolds number, Prandtl number, and Schmidt number are calculated from the transport properties of diffusivity, viscosity and thermal conductivity. These transport properties are functions of temperature, and, in the case of diffusivity, pressure also. Transport properties were predicted by the following relations.

$$D_w = D_w^o\left(\frac{p^o}{p}\right)\left(\frac{T_i}{T^o}\right)^{1.5} \tag{89}$$

$$D_A = D_A^o\left(\frac{p^o}{p}\right)\left(\frac{T_i}{T^o}\right)^{1.5} \tag{90}$$

$$\mu_G = \mu_G^o\left(\frac{T_i}{T^o}\right)^{0.5} \tag{91}$$

$$k_G = k_G^o\left(\frac{T_i}{T^o}\right)^{0.5} \tag{92}$$

Where: D_w^o = a given value of diffusivity of steam in air, m^2/s

p^o =pressure at which the standard property is known, Pa

T^o = absolute temperature at which the property is known, K

D_A^o = given value of the diffusivity of H_2SO_4 in air, m^2/s

μ_G^o = viscosity of flue gas at one given condition, Pa-s

k_G^o = thermal conductivity of the flue gas at the given conditions, W/(m-K)

Relations (89) through (92) are based on the kinetic theory expressions for the transport properties (Fuchs and Sutugin, 1971; Bird et al., 1960). Variations of the collision integral and the heat capacity with temperature are neglected (Sherwood et al., 1975).

The dimensionless groups are defined as:

$$N_{ScA} = \frac{\mu_G}{\rho_G D_A} \tag{93}$$

$$N_{Scw} = \frac{\mu_G}{\rho_G D_W} \tag{94}$$

$$N_{Pr} = \frac{C_{PG}\mu_G}{k_G} \tag{95}$$

$$N_{Re} = \frac{4}{\pi}\frac{\dot{N}_G M_G}{d_i \mu_G} \tag{96}$$

$$N_{Reo} = \frac{16}{\pi}\frac{\dot{N}_{Go} M_G}{(d_s - d_i - 2x_w)\mu_G} \tag{97}$$

Where: ϱ_G = flue gas density, kg/m³

The Reynolds number for the outside or shellside gas is calculated with the appropriate hydraulic radius (Bird et al., 1960), which appears in the denominator of equation (97).

Changes in Particle Size Distribution

Downstream from the acid particle nucleation point, the partice size distribution may change due to additional condensation, particle deposition on walls, and coagulation. Theory for particle growth due to additional condensation is the same as heterogeneous condensation. Theory for particle wall losses and coagulation are presented in the following sections.

Particle Wall Losses

As with vapor losses, particles migrate toward the wall. The particle population balance equation is:

$$n_{i,n-1} - n_{i,n} = \frac{4\ k_{pw}\ \Delta t}{d}\ n_{i,n-1} \tag{98}$$

The mass transfer coefficient for smooth walls can be calculated from (Friedlander, 1977):

$$N_{Sh,p} = \frac{k_{pw} d}{Dp} = 0.079\ N_{Re}\ f^{1/2}\ N_{Sc,p}^{1/4} \qquad (99)$$

$$= 0.0222\ N_{Re}^{7/8}\ N_{Sc,p}^{1/4}$$

where f = Fanning friction factor, dimensionless

$N_{Sh,p}$ = Sherwood number for particles, dimensionless

$N_{Sc,p}$ = Schmidt number for particles, dimensionless

The particle diffusivity in the Schmidt and Sherwood numbers can be calculated from the Stokes-Einstein expression as corrected by the Cunningham slip factor.

$$D_p = \frac{kT}{3\pi\mu d_p}\left[1 + \frac{2l_m}{d_p}(1.257) + 0.40\ \frac{2l_m}{d_p}\exp\left(-0.55\ \frac{d_p}{l_m}\right)\right] \qquad (100)$$

where

$$l_m = \frac{1}{\sqrt{2}}\left(\frac{1}{4\pi\sigma_G^2}\right)\left(\frac{kT}{p}\right)\frac{1}{O\mu\left(\frac{kt}{e_d}\right)} \qquad (101)$$

where k_{ps} = mass transfer coefficient for particles to the inside tube surface, m/s

D_p = diffusivity of particle, m²/s

σ_G = Lennard-Jones zero potential diameter, m

O_μ = collision integral (see Bird et al, 1960, Table B-1)

e_d = well depth of Lennard-Jones potential, J

Coagulation

The rate of coagulation of particles of different sizes was given by Davies (1966, 1979).

$$\frac{d\,n_i}{dt} = \frac{d\,n_j}{dt} = -\ K_{ij}\ b_{Dij}\ n_i n_j \qquad (102)$$

$$K_{ij} = 2\pi(d_{pi} + d_{pj})\ (D_i + D_j) \qquad (103)$$

$$b_{Dij} = \left[1 + \frac{2^{5/2}}{N_{Peij}} \exp(-9.03\, N_{Peij})\right]^{-1} \qquad (104)$$

$$N_{Peij} = \frac{\frac{1}{2}(d_{pi} + d_{pj})(\overline{V}_i^2 + \overline{V}_j^2)^{1/2}}{(D_i + D_j)} \qquad (105)$$

$$\overline{V}_i = \left(\frac{48}{\pi^2} \frac{kT}{\rho_i\, d_{pi}^3}\right)^{1/2} \qquad (106)$$

where n_i = number concentration of particles of size d_{pi}, m^{-3}

K_{ij} = heteromolecular coagulation constant, m^3/s

b_D = correction for size regime dependence (Davies, 1979)

d_{pi} = diameter of particle "i", m

D_i = diffusivity of particle "i", m^2/s

N_{Pe} = Peclet number, dimensionless

V_i = average thermal velocity of particle "i", m/s

For identical particles, the collision rate in equation (102) must be divided by two to avoid counting each collision twice. The diffusivities of the particles are calculated by equations (100) and (101) above.

Calculations

A computer program was written for applying the above equations to slow cooling experiments. The output of a sample calculation is shown in Table 25. The calculation stopped at the nucleation point. The initial conditions were that of Run No. 76/138.

The predicted flue gas cooling rate and wall deposition of acid vapor are less than that determined experimentally. The discrepancy could be due to the omission of entrance effect in the mathematical models.

TABLE 25. SLOW COOLING SAMPLING CALCULATION.

```
                                 APT PROJECT 76
                                 EPA CONTRACT 68-02-3650
                                 FLUE GAS SLOW COOLING
                                 HEAT EXCHANGER DESIGN
TUBE INSIDE DIAMETER:                         1.470E+01 mm
SHELL INSIDE DIAMETER:                        3.810E+01 mm
TUBEWALL THICKNESS:                           9.500E-01 mm
TUBESIDE VOLUME FLOWRATE:                     4.600E+01 Nl/min
SHELLSIDE VOLUME FLOWRATE:                    1.000E+03 Nl/min
TUBESIDE REYNOLDS NUMBER, INLET:              3.216E+03
TUBESIDE REYNOLDS NUMBER, OUTLET:             3.790E+03
SHELLSIDE REYNOLDS NUMBER:                    2.490E+04
OVERALL HEAT TRANSFER COEFFICIENT, INLET:     1.738E+01 W/(sq m-K)
OVERALL HEAT TRANSFER COEFFICIENT, OUTLET:    1.852E+01 W/(sq m-K)
TOTAL HEAT EXCHANGER DUTY:                    2.548E+02 W
WATER CONDENSATION RATE:                      3.155E-08 kg/s
ACID CONDENSATION RATE:                       5.484E-06 kg/s

   SECTION    DISTANCE    TEMPERATURE      WATER         H2SO4      NUCLEATION
   NUMBER        m          DEG.. C    MOL FRACTION  MOL FRACTION     RATE
                                                                     m-3*s-1
      1       8.004E-01    2.460E+02    1.000E-01     4.000E-05     0.000E+00
      1       1.601E+00    2.460E+02    1.000E-01     4.000E-05     0.000E+00
      2       2.217E+00    1.268E+02    1.000E-01     3.653E-05     0.000E+00
      3       2.833E+00    1.258E+02    9.570E-02     3.414E-05     0.000E+00
      4       3.424E+00    1.101E+02    9.295E-02     3.191E-05     0.000E+00
      5       4.000E+00    1.008E+02    9.045E-02     2.991E-05     9.121E+06
```

Section 7

DISCUSSION AND RECOMMENDATIONS

CONTROL STRATEGY IMPLICATIONS

The prediction of the flue gas dew point, which increases with sulfur trioxide concentration, is vital for the proper design and operation of power plant and air pollution control equipment.

Several methods were used to determine the dew point of flue gas. In one method, a cooled electrical conductivity probe was used to determine the temperature at which condensation occurs from a gas containing sulfuric acid and water. By measuring the temperature of the probe tip as cooling occurs, the dew point is noted by the sudden increase in the conductivity between two electrodes on the surface of the probe as caused by the liquid sulfuric acid solution formed thereon. Kiyoura et al. (1972) and Francis (1952) employed this method. Their data were correlated by an equation proposed by Verhoff and Banchero (1974):

$$\frac{10^4}{T_{Dp}} = 22.76 - 0.2943 \ln p_w - 0.855 \ln p_a + 0.0620 \ln p_w \ln p_a \tag{107}$$

where T_{Dp} = dew point temperture, K
P_w = partial pressure of water, mmHg
P_A = partial pressure of sulfuric acid vapor, mmHg

Another commonly used dew point determination method is the condensation sampling method. A flue gas stream with known acid vapor concentration is cooled by passing it through a condenser to a known temperature between the acid dew point and water dew point. At the end of the sampling period, the condensed acid is determined by washing the condenser with a 5% solution of isopropyl alcohol in water and titrating the acid with NaOH. Then the exit equilibrium acid concentration is computed. The gas temperature in the condenser is acid dew point for the calculated exit vapor concentration. Figures 42 and 43 show the experimental results of Lisle and Sensenbaugh (1965) and Martin et al. (1974), respectively.

Dew points also can be predicted from equilibrium theromdynamic data. Figure 44 shows dew point predictions by Muller (1969) based upon the partial pressures calculated by Abel (1946).

Figure 45 shows the predicted flue gas dew point temperature and sulfuric acid self-nucleation temperature. Although there are differences in dew point temperature between different investigators, they are all higher than the predicted nucleation temperature. Thus, if one can cool the gas slowly to between the dew point and nucleation temperatures, it is possible to force the sulfuric acid to condense on surfaces rather than forming mist.

The experimental results shown in Figure 37 show the above control method is feasible. Both Runs 76/142 and 76/143 were done at the same conditions and sampled at the same location - the nucleation starting point. Run 76/142 was done with ash particle injection and Run 76/143 without. Since in Run 76/142, most of the acid vapor was found in the impactor, heterogeneous condensation on particles occurred at a gas temperature above the nucleation temperature.

Rapid cooling of the flue gas caused localized high degree of supersaturation which promotes the formation of ultra-fine acid particles by nucleation and therefore, should be avoided. In cases where the flue gas must be quenched, present results indicate that to reduce the amount of fine particles the quench water should be as cold as possible and the water vapor concentration should be as high as possible. Cold water cools the gas and induces water condensation on nucleated acid particles. The acid particles will grow and be easily collected by pollution control devices. This control method is termed flux-force/condensation (F/C) scrubbing and has been studied in detail by Calvert et al. (1973, 1975, 1977 and 1980).

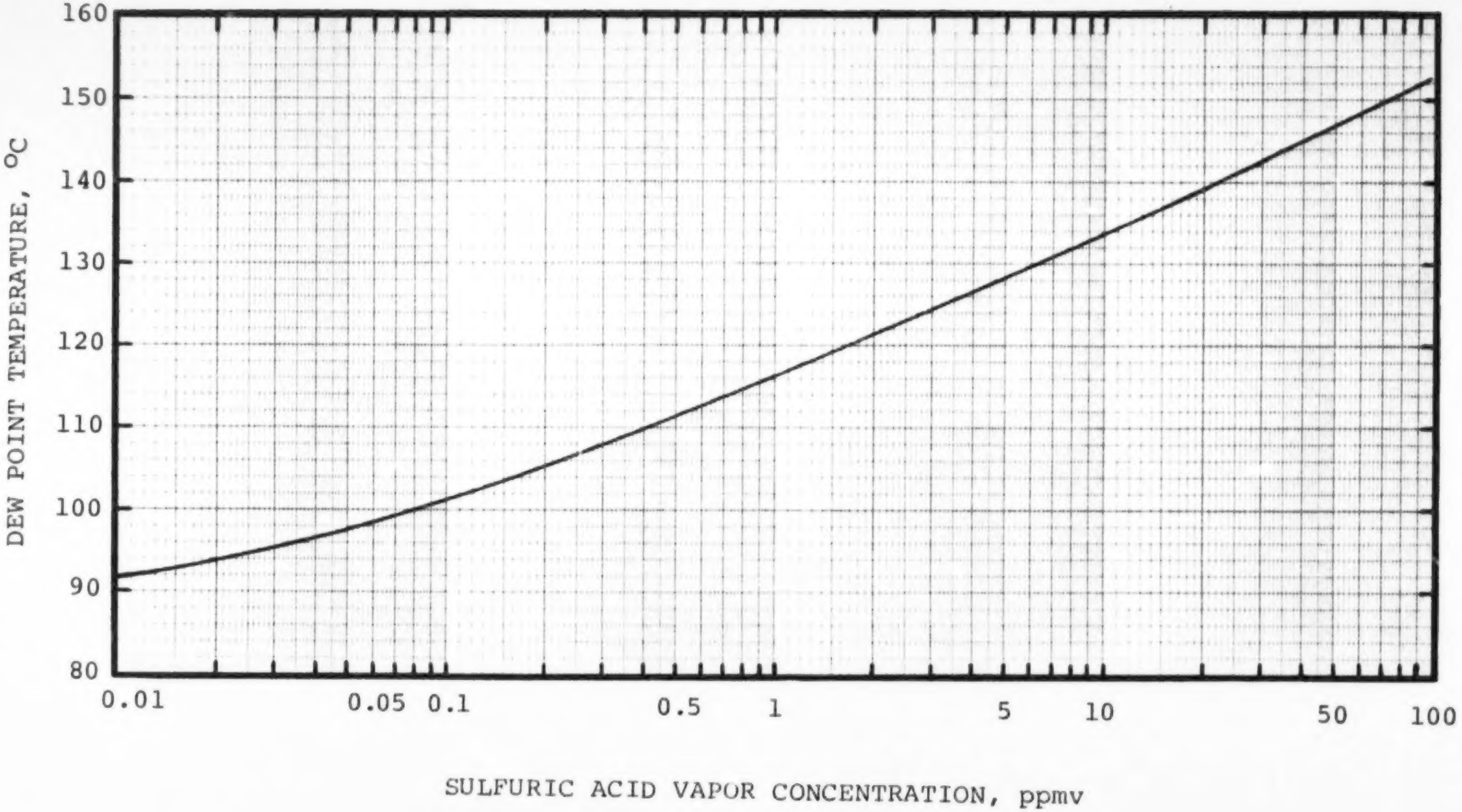

Figure 42. Dew point of sulfuric acid in flue gas.
(Lisle and Sensenbaugh, 1965)

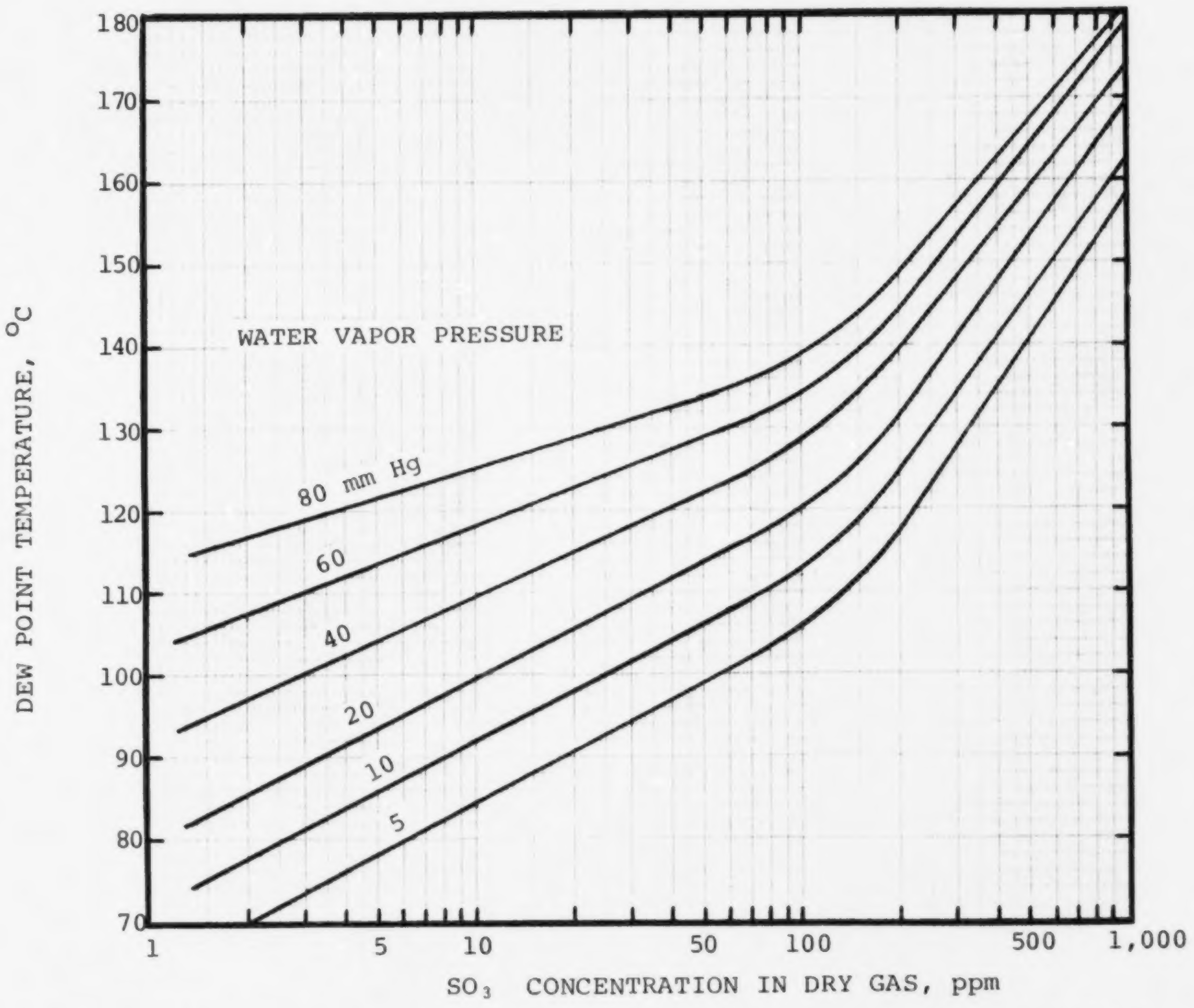

Figure 43. Dew points for dilute mixtures of sulfur trioxide in stack gases with various water contents. (Martin , et al. 1974)

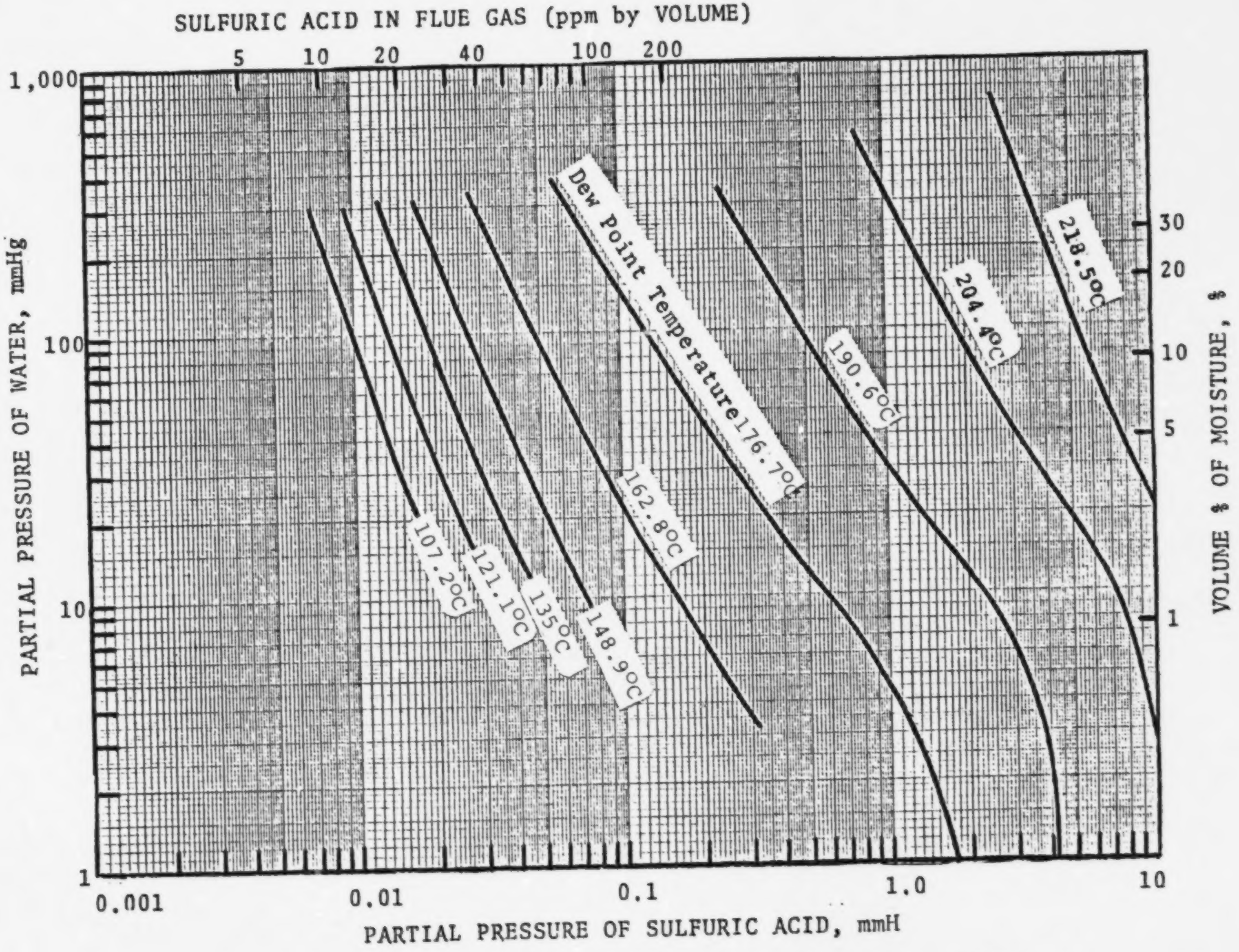

Figure 44. Acid dew point in flue gas (Müller, 1969)

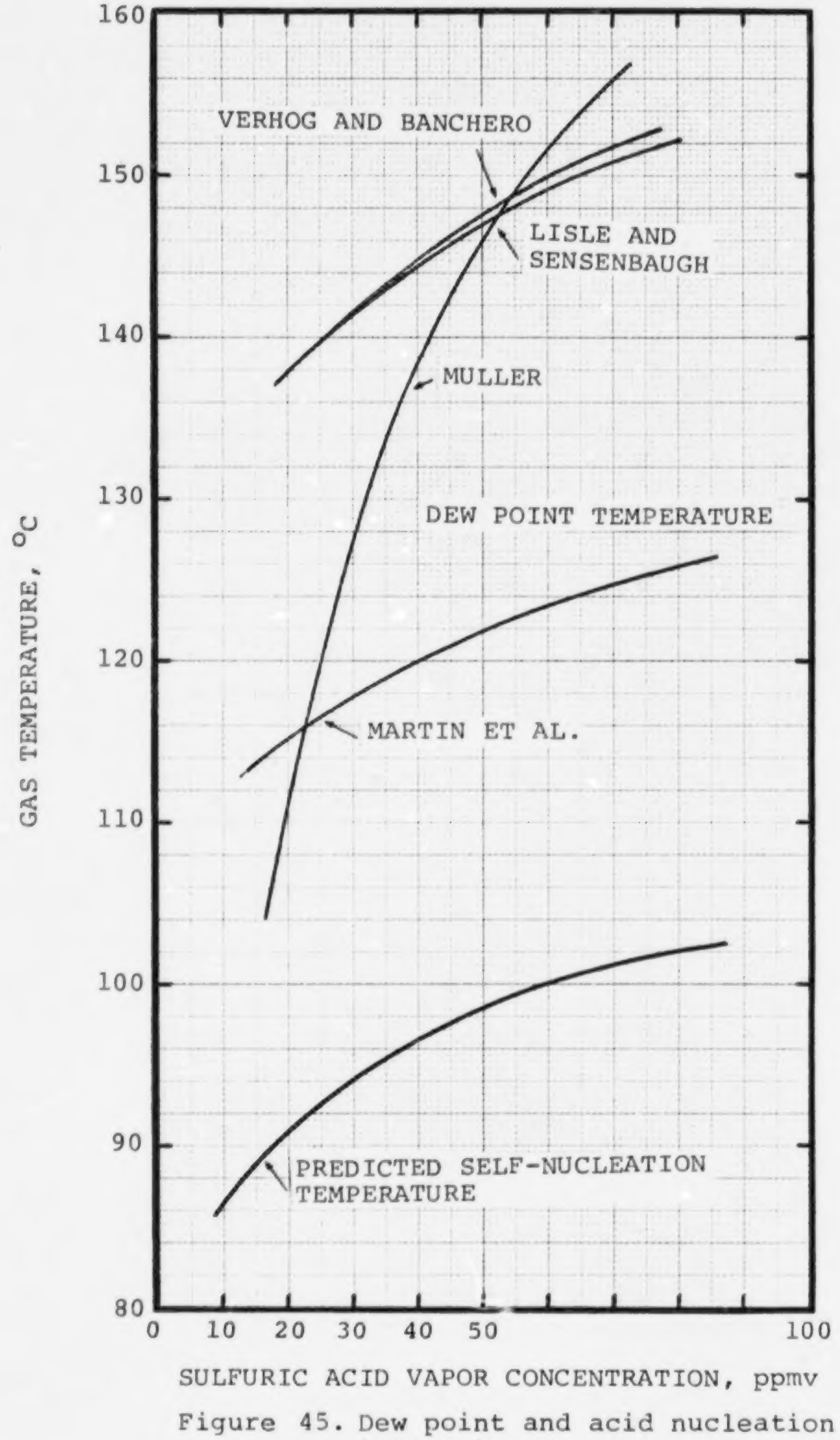

Figure 45. Dew point and acid nucleation temperatures.

FUTURE RESEARCH RECOMMENDATIONS

The temperature at which the self-nucleation of sulfuric acid mist starts is lower than the flue gas dew point temperature measured or predicted by other investigators. Thus, if the gas is cooled to between the dew point and the nucleation temperatures, it is possible to force the sulfuric acid vapor to condense out on surfaces rather than forming mist. It is recommended that additional research and pilot study be performed to demonstrate the feasibility of this method for sulfate particle emission control.

REFERENCES

Appel, R. B., Y. Tokiwa, S. M. Wall, M. Hik, E. L. Kothny, and J. J. Wesolowski, "Determination of Sulfuric Acid, Total Particle-Phase Acidity and Nitric Acid in Ambient Air", NTIS PB80-145980 (1979).

Azarniouch, M. K., A. J. Bobkowicz, N. E. Cooke, E. J. Farkas, "Growth of a Sulfuric Acid Droplet Exposed to Water Vapor", Can. J. Chem. Engr., 51, 590-595, (1973).

Barrie, L. A. and H. W. Georgii, "An Experimental investigation of the Absorption of Sulfur Dioxide by Water Drops Containing Heavy Metal Ions", Atmospheric Environment, 10, 743-749, (1976).

Barron, C. H. and H. A. O'Hern, "Reaction Kinetics of Sodium Sulfite Oxidation by the Rapid Mixing Method", Chem. Engr. Sci. 21: 397-404, (1966).

Becker, V. R. and W. Dooring, Annalen der Physik, 5: 719, (1935).

Beilke, S., D. Lamb, and J. Muller, "On the Uncatalyzed Oxidation of Atmospheric SO_2 by Oxygen in Aqueous Systems", Atmospheric Environment, 9, 1083-1090, (1975).

Beilke, S. and G. Gravenhorst, "Heterogeneous SO_2 Oxidation in the Droplet Phase", Atmospheric Environment, 12, 231-239, (1978).

Bird, R. B., W. E. Steward, E. N. Lightfoot, "Transport Phenomenon", John Wiley & Sons, Inc., New York, (1960).

Bracewell, J. M. and D. Gall, "The Catalytic Oxidation of Sulfur Dioxide in Solution at Concentrations Occurring in Fog Droplets", Proceedings of the Symposium on the Physio-Chemical Transformation of Sulfur Compounds in th Atmosphere and the Formation of Acid Smogs, Mainz, Germany (1967).

Brimblecombe, P. and D. J. Spedding, "The Catalytic Oxidation of Micromolar Aqueous Sulfur Dioxide - I. (Oxidation of Dilute Solutions of Iron (III), Atmospheric Environment, 8, 937-945, (1974).

Calvert, J. G., J. Su., J. W. Bottenheim, and O. P. Strang. Mechanism of the Homogeneous oxidation of Sulfur Dioxide in the Troposphere. Atmospheric Environment 12: 197-226, (1978).

Calvert, S. and R. D. Chimelewski, "Flux Force/Condensation Scrubber System for Collection of Fine Particulates Emissions from an Iron Melting Cupola", Final Report submitted to EPA, 1980.

Calvert, S. and S. Gandhi, "Fine Particle Collection by a Flux Force/Condensation Scrubber: Pilot demonstration", EPA 600/2-77-238, NTIS PB277-075, 1977.

Calvert, S., J. Goldsmid, D. Leith, and N. Jhaveri, "Feasibility of Flux Force/Condensation Scrubbing for Fine Particle Collection", EPA 650/2-73-036, NTIS PB227-307, 1973.

Calvert, S., N. Jhaveri, and T. Huisking, "Study of Flux Force/Condensation Scrubbing of Fine Particles", EPA 600/2-75-018, NTIS PB277-075, 1977.

Calvert, et al. "Scrubber Handbook" NTIS PB213-016, (1972).

Cantrell, B. K. and K. T. Whitby. Aerosol Size Distributions and Aerosol Volume Formation for a Coal-Fired Power Plant Plume. Atmospheric Environment 12, 323-34, 1978.

Cheney, J. L. and J. B. Homolya, "Characterization of Combustion Source Sulfate Emissions Using a Selective Condensation Sampling System", in Proceedings of the Workshop on Measurement Technology and Characterization of Primary Sulfur Oxides Emissions from Combustion Sources, April 24-26, 1978, NTIS PB-287436.

Cheney, J. l. and J. B. Homolya, "Sampling Parameters for Sulfate Measurements and Characterization," Environmental Science & Technology, 13: 584-588, May 1979.

Cheng, R. T., M. Corn, and J. O. Frohliger, "Contribution to the Reaction Kinetics of Water Soluble Aerosols and SO_2 in Air at ppm Concentration", Atmospheric Environment, 5, 987-1008, (1971).

Chun, K. C. and J. E. Quon, "Capacity of Ferric Oxide Particles to Oxidize Sulfur Dioxide in Air," Environ. Sci. Tech. 1: 532-538, 1973.

Cox, R. A. and S. A. Penkett, "Aerosol Formation from Sulfur Dioxide in the Presence of Ozone and Olefinic Hydrocarbons," J. Chem. Soc. 68: 1735-1753, 1972.

Davies, C. N. "Definitive Equation for the Fluid Resistance of Spheres", Proc. Phys. Soc. 57, (4): 1, 1923b.

Davies, C. N., ed., Aerosol Science, Academic Press, New York, (1966).

Davis, C. N., "Coagulation of Aerosols by Brownian Motion", J. Aerosol Sci., 10, 151-161, (1979).

Davis, D. D., G. Smith, and G. Klauber, "Trace Gas Analysis of Power Plant Plumes via Aircraft measurement," O_3, NO_x, SO_2 Chemistry. Science 186: 733-735, 1974.

Dennis, R., C. E. Billings, J. A. Record, P. Warneck, P. Arin, and M. L. Arin, "Measurements of Sulfur Dioxide Losses form Stack Plumes," Air Pollution Control Association 69th Annual Meeting, New York City, June 1969.

Doyle, G. J., J. Chem. Phys. 35, 795, (1961).

Driscoll, J. N. "Flue Gas Monitoring Techniques", Ann Arbor Science Publishers, 1974.

Easter, R. C. and P. Hobbs, "The Formation of Sulfates and the Enhancement of Cloud Condensation Nuclei in Clouds", J. Atm. Sci. 31, 1586-1594, (1974).

Eatough, D. J., S. izatt, J. Ryder, and L. D. Hansin, "Use of Benzaldehyde as a Selective Solvent for Sulfuric Acid: Interferences by Sulfate and Sulfite Salts", Environ. Sci. and Tech., 12, (12):1276-1278, (1978).

Fletcher, N. H. "The Physics of Rainclouds". Cambridge University Press. London, New York, 1962.

Flood, H. Z., Physic Chem. A170: 286, (1934).

Forrest, J. and L. Newman, "Further Studies on the Oxidation of Sulfur Dioxide in the Coal-Fired Power Plan Plumes", Atmospheric Environment 11: 465-474, 1974.

Foster, P. M., "The Oxidation of Sulfur Dioxide in Power Station Plumes", Atmospheric environment 3: 157-175, 1969.

Freiberg, J., "The Mechanism of Iron Catalyzed Oxidation of SO_2 in Oxygenated Solutions", Atmospheric Environment, 9: 661-672, (1974).

Freiberg, J., "Effects of Relative Humidity and Temperature on Iron-Catalyzed Oxidation of SO_2 in Atmospheric Aerosol," Environ. Sci. Tech. 8,731-734, 1974.

Frenkel, J. "Kinetic Theory of Liquids", Dover Publications, New York, 1955.

Friedlander, S. K. "Smoke, Dust and Haze", John Wiley and Sons, Inc., New York, (1977).

Fuchs, N. A. and A. G. Sutugin, "High-Dispersed Aerosols" in "Tropics in Current Aerosol Research", Hidy, G. M. and J. R. Brock, (eds) Pergamon, New York (1971).

Fuller, E. C. and R. H. Crist, "The Rate of Oxidation of Sulfute Ions by Oxygen", J. Am. Chem. Soc. 63, 1644-1650, (1941).

Gartrell, J. E., F. W. Thomas and S. B. Carpenter, "Atmospheric Oxidation of SO_2 in Coal-Burning Power Plant Plumes," Am. Ind. Hya. J. 24: 113-120, 1963.

Giauque, W. F., E. W. Hornung, J. E. Kunzler, And T. R. Rubin, "The Thermodynamic Properties of Aqueous Sulfuric Acid Solutions and Hydrates from 15 to 300°C". J. Am. Chem. Soc. 82: 62-70 (1960).

Gilliland, E. R., and T. K. Sherwood, Ind. Eng. Chem. 26: 516, (1934).

Gillani, N. V., R. Husar, D. E. Patterson and W. E. Wilson, Project MISTT: Kinetics of Particulate Sulfur Formation in a Power Plant Out to 300 km. Atmospheric Environment 13: 589-598.

Gmelin, Handbook Schwefel (Sulfur Handbook) 8th. Ed. (1963).

Gmitro, J. T. and T. Vermeulen. "Vapor-Liquid Equilibria for Aqueous Sulfuric Acid". AIChE. J. 10: 740-746, (1964a).

Gmitro, J.T. and T. Vermeulen. "Vapor-Liquid Equilibrium for Aqueous Sulfuric Acid". American Duplication Institute, Document 8041, Library of Congress, Washington, D.C., (1964b).

Green, H. L. and W. R. Lane. "Particulate Clouds: Dusts, Smokes, and Mists", 2nd. Ed. Van Nostrand, Princeton, N.J., (1964).

Hausen, Z. Ver. Deut. Ing. Beih. Verfahrenstech. 4: 91, Cited in Knudsen (1972) (1934).

Hegg, D. A. and P. V. Hobbs, "Measurements of Gas-to-Particle Conversion in The Plumes from Five Coal-Fired Electric Power Plants," Atmospheric Environment 14: 99-116, 1980.

Hidy, G. M. and J. R. Brock, "The Dynamics of Aerocolloidal System" Vol. 1., Pergamon Press, New York, 1970.

Hoather, R. C. and C. R. Goodeve, "The Oxidation of Sulfurous Acid. IV catalysis by a Glass Power Containing Manganese and Iron", Ind. Eng. Chem. 50: 1169-71 (1934).

Hobbs, P. V., D.A. Heg, M. W. Eltgroth and L. F. Radke, "Evolution of Particles in the Plumes of Coal-Fired Power Plants I. Deductions form Field Measurements, Atmospheric Environment 13: 935-951.

Hoffer, E. M., E. L. Kothny, and B. R. Appel, "Simple Method for Microgram Amounts of Sulfite in Atmospheric Particulates", Atmospheric Environment, 13, 303-306, (1979).

Homolya, J. B. and J. L. Cheney, "An Assessment of Sulfuric Acid and Sulfate Emissions from Combustion of Fossil Fuels" in Proceedings of the Workshop on Measurement Technology and Characterization of Primary Sulfur Oxides Emission from Combustion Sources, April 24-26, 1978, Southern Pines, NC.

Husar, R., D. Patterson, J. D. Husar, F. V. Gillani, and W. E. Wilson, "Sulfur Budget of a Power Plant Plume" Atmospheric Environment 12: 59-568, 1978.

Johnstone, H. F. and A. J. Moll, "Formation of Sulfuric Acid in Fog," Ind. Engr. Chem., 52: 861-863, 1960.

Junge, C. E. and T. G. Ryan, "Study of the SO_2-Oxidation in Solution and Its Role in Atmospheric Chemistry," Q. Jl. R. Met. Soc. 84: 46-55, (1958).

Karraker, D. G., "The Kinetics of the Reaction Betwen Sulfurous Acid an Ferric Ion", J. Phys. Chem. 67: 871-874, (1963).

Keenan, J. H., F. G. Keyes, P. G. Hill, and J. G. Moore, "Steam Tables." John Wiley & Sons, Inc., New York, (1969).

Kiang, C. S. nd D. Stauffer, "Chemical Nucleation for Various Humidities and Pollutants", Faraday Smyp. 7: 26-33, (1973).

Knudsen, J. G., "Heat Transfer by Convection". In: Chemical Engineers' Handbook, 5th. Ed., Chaper 10. J. H. Perry and C. H. Chilton, Edgs., McGraw-Hill Book Company, new York, New York, (1972).

Larson, T. V., N. R. Horike, and H. Harrison, "Oxidation of ulfur Dioxide by Oxygen and Ozone in Aqueous Solutions: A Kinetic Study with Significance to Atmospheric Rate Process". Atmospheric Environment, 12, 1597-1622, (1978).

Lisle, E. S. and J. D. Sensenbaugh, "The Determination of Sulfur Trioxide and Acid Dew Point in Flue Gases", Combustion, 12-16, January (1965).

Maddalone, R., N. Garner, "Process Measurement Procedures Sulfuric Acid Emissions," TRN Documnt No. 28055-6004-RU-00, February, 1977.

Maddelone, R. and N. Garmh, "Process Measurement Procedures: Sulfuric Acid Emissions", EPA 600/7-79-156, 1979.

Martin, R. R., F. S. manning, and E. D. Reed, "Watch for Elevated Dew Points in SO_3 Bearing Stack Gases", Hydrocarbon Processing, 143-144, June, (1974).

Matteson, M. J., W. Stober, and H. Luther, "Kinetics of the Oxidation of Sulfur Dioxide by Aerosols of Manganese Sulfate", I. & E. C. Fundam. 8: 677-687, (1969).

McCabe, W. L. and J. C. Smith. "Unit Operations of Chemical Engineering", 3rd. Ed. McGraw-Hill Company, New York, New York, (1976).

McKay, H. A. C., "The Atmospheric Oxidation of Sulfur Dioxide in Water Droplets in Presence of Ammonia", Atmospheric Environment, 5: 7-14, (1971).

Miller, J. M. and R. G. de Pena, "Contribution of Scavenged Sulfur Dioxide to the Sulfate Content of Rain Water", J. Geophys. Res. 77: 5905-5916, (1972).

Millikan, R. A. "Coefficients of Slip in Gases and the Law of Reflection of Molecules from the Surfaces of Solids and Liquids", Phys. Review 21 (3): 217, (1923a).

Millikan, R. A. "The General Law of Fall of a Small Spherical Body Through a Gas and its Bearing upon the Nature of Molecular Reflection from Surfaces", Phys. Review 22 (1): 1, 81923b).

Mirabel, P. and J. L. Katz, "Binary Homogeneous Nucleation as a Mechanism for the Formation of Aerosols", J. of Chem. Phys. 60 (3): 1138-1144, (1974).

Muller, P. Chem. Eng. Tech., 31: 345-351 (1969).

Nader, J. S., "Field Measurements and Characterization of Emissions from Coal-Fired Combustion Sources," Paper presented at the APCA 71st Annual Meeting, June 25-30, 1978, Houston, TX.

Nair, P. V. N. and K. G. Vohra, "Growth of Aqueous Sulfuric Acid Droplets as a Function of Relative Humidity," J. Aerosol Sci., 6, 265-271, (1975).

Newman, L., J. Forrest, and B. Manowitz, "The Application of an Isotopic Ratio Technique to a Study of the Atmospheric Oxidation of Sulfur Dioxide in the Plume from an Oil-Fired Power Plant", Atmospheric Environment 9: 959-977, 1975.

Novakov, T., S. K. Chang, and A. B. Harker, "Sulfates as Pollution Particles: Catalytic Formation on Carbon (Soot) Particles", Science 186: 259-261, 1974.

Patterson, R. G. and S. Calvert, "Submicron Particle Size Measurement with a screen Diffusion Battery", EPRI FP-840, Project 723. Electric Power Research Institute, Palo Alto, California, (1976).

Patterson, R. G., P. Riersgard, R. Parker, and S. Calvert, "Effects of Conditioning Agents on Emissions from Coal-fired Boilers: Test Report No. 1", EPA 600/7-79-104a, 1979.

Penkett, S. A. "Oxidation of SO_2 and Other Atmospheric Gases by Ozone in Aqueous Solutions", nature, 240: 105-106, (1972).

Penkett, S. A. and J. A. Garland, "Oxidation of SO_2 in Artificial Fogs by O_3", Tellus 26: 284-290, (1974).

Penkett, S. A., B. M. R. Jones and A. E. J. Eggleton, "The Importance of Atmospheric O_3 and H^2O^2 in Oxidizing SO_2 in Cloud and Rainwater", Atmospheric Environment, 13: 123-137, (1979).

Penkett, S. A., B. M. R. Jones and A. E. J. Eggleton, "A Study of SO_2 Oxidation in Stored Rainwater Samples", Atmospheric Environment, 13: 139-147, (1979).

Perry, J. H. and C. H. Chilton, Eds. "Chemical Engineers' Handbook". 5th. Ed. McGraw-Hill Book Co. New York. Pgs. 3-80, 81, (1972).

Rangaraj, C. N., "An In-Stack Diffusion Classifier for Aerosol Mass Distribution Measurements. M. E. Thesis. University of Florida. Gainesville, Florida, (1980).

Reid, W. T., "Basic Problems in Formation of Sulfate in Boiler Furnaces", J. Eng. for Power ASME Series A, p. 283, 1967.

Reiss, R. H., J. Chem. Phys. 18: 840, (1950).

Richards, L. W., K. R. Johnson, and L. S. Shepard, "Sulfate Aerosol Study", Rockwell International Report: AMC 8000. 13 FR (1978).

Sabinina, K. and L. Terpugov, "Die Oberflachenspannung des Systems Schwefelsaure-Wasser. (The Surface Tension of the System Sulfuric Acid-Water.)" Z. Phys. Che. A-137: 237-241, (1935).

Schroetter, L. C., "Kinetics of Air Oxidation of Sulfurous Acid Salts", J. Pharm. Sci. 52; 559-563, (1963).

Scott, W. D. and P. V. Hobbs, "The Formation of Sulfate in Water Droplets", J. Atm. Sci. 24: 54-57, (1967).

Sem, G. J. "Submicron particle Sizing Experience on A smoke Using the Electrical Aerosol Size Analyzer", paper in Proceedings: Seminar on In-Stock Particle Sizing for Particulate Control Device Evaluation," D. V. Osdell Compiler, EPA-600/2-77-060, NTIS PB266103, February, 1977.

Shen, T. T., L. G. Ayer, "Determination of SO_2 Emission from Oil Combustion Sources by Fuel Analysis and SO_2/CO^2 Relations", JAPCA 25: 851, August, 1975.

Sherwood, T. K., R. L. Pigford, and C. R. Wilke, "Mass Transfer". McGraw-Hill Book Company, New York, New York, (1975).

Shugard, W. J. and R. H. Heist, and H. Reiss, "Theory of Vapor Phase Nucleation in Binary Mixtures of Water and Sulfuric Acid" J. of Chem. Phys. 61 (12): 5298-5305, (1974).

Sieder, E. N. and G. E. Tate, Ind. Eng. Chem. 28: 1429, (1936).

Sillen, L. G., "Stability Constant of Metal-Ion Complexes, Section 1 - Inorganic Liquids", 2nd. Ed., Chem. Soc. (London), Special Publication no. 17, (1964).

Stauffer, D., V. A. Mohnen, and C. S. Kiang, "Hetermolecular Condensation Theory Applied to Particle Growth", Aerosol Science 4: 461-471, 1973.

Stephens, W. T. and R. O. McCaldin, "Attenuation of Power Station Plumes as Determined by Instrumental Aircraft", Environ. Sci. Tech. 5: 615-621, 1971.

Sutherland, in Hegg, D. A. and P. V. Hobbs, "Oxidation of Sulfur Dioxide in Aqueous Systems with Particular Reference to the Atmosphere", Atmospheric Environment 12: 241-253, (1978).

Takahashi, M. Kasohara, and M. Itoh, "A kinetic Model of Sulfuric Acid Aerosol Formation from Photochemical Oxidation of Sulfur Dioxide Vapor", Aerosol Science, 6: 45-55, (1975).

Tanner, R. L., R. Cederwall, R. Carber, D. Leahy, W. Monlow, R. Meyers, M. Phillips, and L. Newman, "Separation and Analysis of Aerosol Sulfate Species at Ambient Concentrations", Atmospheric Environment, 11: 955-966, (1977).

Tomasi, C., R. Guzzi, and Vittori, The SO_2-NH_3-Solution Droplet System in an Urban Atmosphere", J. Atm. Sci. 32: 1580-1586, (1975).

Treybal, R. E., "Mass Transfer Operation", 2nd. Ed., mcGraw-Hill Book Company, New York, New York, (1968).

Urone, P., R. A. Lucas, "A Specific Method for the Determination of Sulfuric Acid Emissions from Cobustion Sources", Workshop Proceedings on Primary Sulfate Emissions from Combustion Sources, EPA-600/9-79-020a, p. 63, August, 1978.

Urone, P., H. Lutsep, C. M. Noyes, and J. F. Parcher, "Static Studies of Sulfur Dioxide Reactions in Air", Environ. Sci. Tech. 2, 611-618, 1968.

Ursenbach, W. O., A. C. Hill, W. H. Edwards, and S. M. Kunen, "Conversion Rate of SO_2 to Submicron Sulfate in the Plumes of a Coal-Fired Power Plant in the Wetern United States. Presented at 70th. Annual Meeting of the Air Pollution Control Association, Toronto, Canada, June 20-24, 1977.

Van den Heuvel, A. P. and B. J. Mason, "The Formation of Ammonium Sulfate in Water Droplets Exposed to Gaseous Sulfur Dioxide and Ammonia", Q. Jl. R. Met. Soc. 89: 271-275, (1963).

Verhoff, F. H. and J. T. Banchero, "Predicting Dew Points of Flue Gases", Chem. Eng. Progress, 70: 71-72, August, (1974).

Weber, E., "Contribution to the Residence Time of Sulfur Dioxide in a Polluted Atmosphere", J. Geophys. Res. 75: 2909-2915, 1970.

Winkelmann, D., "Die Elektrochemische Messung der Oxidationsgeschwindigkeit von Na_2 durch gelosten Sauerstoff", 7, Elektrochemie, 59: 891-895, (1955).

Yue, G. K., "A Quick Method for Estimating the Equilibrium Size and Composition of Aqueous Sulfuric Acid Droplets," J. Aerosol Sci., 10: 75-86, (1979).

Yue, G. K., and P. Hamill, "The Homogeneous Nucleation Rates of H_2SO_4-H_2O Aerosol Particles in Air", J. Aerosol Science, 10: 609-614, (1979).

Zoldovich, J. B., J. Exptel. Theoret. Phys. (U.S.S.R.) 2: 525, (1942).

APPENDIX "A"

COMPUTER PROGRAM LISTINGS

```
C
C     .................................................................
C        A.P.T.  PROJECT 76 (EPA 68-02-3650)
C        BINARY CRITICAL NUCLEATION TEMPERATURE
C
C        PURPOSE
C           GIVEN THE GAS PHASE MOLE FRACTIONS OF H2SO4 AND H2O, AND
C           THE PREVAILING TEMPERATURE, THIS PROGRAM CALCULATES THE
C           RATE OF SULFURIC ACID NUCLEUS FORMATION.
C
C        REMARKS
C           NONE
C
C        SUBROUTINES AND FUNCTION SUBPROGRAMS REQUIRED
C           SA (ACID SATURATION RATIO OVER A GIVEN NUCLEUS COMPOSITION)
C           PA (VAPOR PRESSURE OF ACID OVER GIVEN NUCLEUS COMPOSITION)
C           PW (VAPOR PRESSURE OF WATER OVER GIVEN NUCLEUS COMPOSITION)
C           RHO (DENSITY OF SULFURIC ACID)
C           SIGMA (SURFACE TENSION OF SULFURIC ACID)
C           ALI (AITKEN-LAGRANGE INTERPOLATION)
C           ATSM (AITKEN TABLE SEARCH, MONOTONIC)
C           DGT3 (DERIVATIVE OF A GENERAL TABLE, 3 POINT METHOD)
C
C        METHOD
C           THE RATE OF NUCLEATION IS CALCULATED BY THE GENERALIZED
C           KINETIC THEORY EQUATION (STAUFFER AND KIANG, 1973).  THE
C           NUCLEUS COMPOSITION IS CALCULATED BY YUE'S (1979) METHOD.
C           VAPOR PRESSURE DATA IS FITTED AS LN P VS 1/T FROM THE
C           DATA OF GMITRO AND VERMEULEN (1964).  SURFACE TENSION
C           IS FROM SABININA AND TERPUGOV (1935) BELOW 50 C.  SURFACE
C           TENSION DATA IS LINEARLY EXTRAPOLATED ABOVE THAT TEMPE-
C           RATURE.  DENSITY IS FROM PERRY AND CHILTON (1972).  IT IS
C           EXTRAPOLATED ABOVE 100 C.
C
C        REFERENCES
C           GMITRO, J. I., AND T. VERMEULEN.  1964.  AICHE J.
C              10:740-746.
C           PERRY J. H., AND C. H. CHILTON, EDS.  1972.  CHEMICAL
C              ENGINEERS' HANDBOOK, 5TH ED. MCGRAW-HILL, N.Y.
C              PP. 3-80,81.
C           SABININA, L., AND L. TERPUGOV.  1935.  Z. PHYS. CHEM.
C              A173:237-241.
C           C. S. KIANG, AND D. STAUFFER.  1973.  FARADAY SYMP.
C              7:26-33.
C           YUE, G. K.  1979.  J. AEROSOL SCI. 10:75-86.
C
C     .................................................................
C
      REAL MA,MW,KB,LNS,ISTAR,ISTARR,NT,NA,NSTAR
      DIMENSION SAL(15),SAU(15)
C
C        INITIALIZE CONSTANTS
C
      COMMON /T/ T /MA/ MA /MW/ MW /SWG/ SWG /PA0/ PA0 /PW0/ PW0
      COMMON /R/ R /DR/ DR /S/ S /DS/ DS /AW/ AW
```

```
C
C         ALL CONSTANTS IN SI UNITS
C
      DATA PT,RG,KB,MA,MW /101325.,8.3143,1.3806E-23,0.1,0.018/
      PI=4.*ATAN(1.)
C
C         INPUT DATA
C
      WRITE (1,190)
      WRITE (2,190)
      WRITE (1,220)
      READ (1,210) YW
      WRITE (2,230)
   90 WRITE (1,200)
      READ (1,210) YAD
  100 WRITE (1,240)
      READ (1,250) T
      IF (T.LE.0.) GOTO 185
C
C         PREPARATORY CALCULATIONS
C
      TK=T+273.15
      YA=YAD*1.E-6
      PA0=PA(1.,T)
      PW0=PW(0.,T)
      SAG=YA*PT/PA0
      SWG=YW*PT/PW0
      J=1
      K=1
      XUU=0.82
      XLL=0.69
      X=0.75
C
C         CALCULATE EQUILIBRIUM DROP COMPOSITION FOR GIVEN CONDITIONS
C
      DO 170 I=1,15
       GO TO (110,120),I
       GO TO 130
  110  SALL=SA(XLL)
       SAL(1)=SALL
       GO TO 170
  120  SAUU=SA(XUU)
       SAU(1)=SAUU
       GO TO 170
  130  SAC=SA(X)
       IF (ABS(ALOG(SAC/SAG)).LT.0.001) GO TO 180
       IF (ALOG(SAC/SAG)) 140,180,150
  140  J=J+1
       SAL(J)=SAC
       IF (SAL(J).LE.SALL) GO TO 160
       SALL=SAL(J)
       XLL=X
       GO TO 160
  150  K=K+1
       SAU(K)=SAC
       IF (SAU(K).GE.SAUU) GO TO 160
       SAUU=SAU(K)
       XUU=X
  160  X=XLL+ALOG(SAG/SALL)/ALOG(SAUU/SALL)*(XUU-XLL)
C      SAC2=SA(X)
C      WRITE (1,165) XLL,XUU,X,SALL,SAUU,SAG,SAC2
C 165  FORMAT (7(2X,1PE10.3))
  170 CONTINUE
  180 XSTAR=X
C
C        CALCULATE THE CRITICAL DROP RADIUS
C
      RK=2.*MW*S/R/RG/TK/ALOG(SWG/AW)
      FPROP=1.+XSTAR/R*DR-1.5*XSTAR/S*DS
      LNS=ALOG(SWG/AW)
C     WRITE (1,179) LNS,RK,FPROP
C 179 FORMAT (3(6X,1PE10.3))
      RSTAR=RK*FPROP
C
C        CALCULATE NUCLEATION CURRENT
C
      XSECT=4.*PI*RSTAR**2.
      DELG=XSECT*S/KB/TK
      NT=PT/KB/TK
      VM=SQRT(RG*TK/2./PI/MA)
      NA=NT*YA
      NSTAR=NT*YW*EXP(-1./3.*DELG)
C     WRITE (1,181) XSECT,DELG,NT,VM,NA,NSTAR
C 181 FORMAT (6(3X,1PE10.3))
      ISTAR=NA*VM*XSECT*NSTAR
C
C        OUTPUT RESULTS
C
      YAA=1.E6*YA
      XA=1.E2*XSTAR
      RSTARA=1.E10*RSTAR
      ISTARR=1.E-6*ISTAR
      WRITE (1,230)
      WRITE (1,260) YW,YAA,T,XA,RSTARA,ISTARR
      TOLD=T
      GO TO 100
  185 WRITE (2,260) YW,YAA,TOLD,XA,RSTARA,ISTARR
      WRITE (1,200)
      READ (1,210) YAD
      IF (YAD.GT.0.) GOTO 100
  186 WRITE (1,220)
      READ (1,210) YW
      IF (YW.GT.0.) GOTO 90
      STOP
  190 FORMAT (1H0,15X,'APT PROJECT 76--EPA 68-02-3650'/
     1            16X,'NUCLEATION TEMPERATURE PROGRAM'//)
  200 FORMAT (1H ,'ENTER GAS PHASE H2SO4 CONCENTRATION (PPMV)
     1 (E10.3)',10X)
  210 FORMAT (E10.3)
  220 FORMAT (1H0,'ENTER GAS PHASE WATER VAPOR CONTENT (VOLUME
     1FRACTION) (E10.3)',4X)
  230 FORMAT (//,8X,'YW',7X,'YA (PPMV)',5X,'TG (C)',7X,'X* (%WT)',
     1        5X,'R* (A)',3X,'I* (PER CC-SEC)'//)
  240 FORMAT (1H0,'ENTER SYSTEM TEMPERATURE (CELSIUS) (F6.1)',7X)
  250 FORMAT (F6.1)
  260 FORMAT (6(3X,1PE10.3))
      END
C
C
C
C     ..............................................................
C
C        FUNCTION SA(X)
C
C        PURPOSE
C           THIS FUNCTION CALCULATES THE EQUILIBRIUM SPECIFIC ACIDITY
C           (SULFURIC ACID SATURATION RATIO) FOR A GIVEN HUMIDITY,
C           TEMPERATURE, AND CRITICAL NUCLEUS COMPOSITION.
C
C        USAGE
C           SAC=SA(XGUESS)
C
C        DESCRIPTION OF PARAMETERS
C           SAC   - CALCULATED SPECIFIC ACIDITY
C           XGUESS- GUESSED ACID NUCLEUS COMPOSITION
C
C        REMARKS
C           THE CALCULATION ASSUMES A GIVEN TEMPERATURE AND SPECIFIC
C           HUMIDITY.
C
C        SUBROUTINES AND FUNCTIONS REQUIRED
C           RHO
C           SIGMA
C           PA
C           PW
C
C        METHOD
C           THE METHOD OF YUE (1979) IS USED.  YUE NOTICED THAT THE
C           GENERALIZED KELVIN EQUATIONS AS GIVEN BY NAIR AND VOHRA
C           (1973) ARE STRAIGHT LINES WHEN PLOTTED WITH THE PROPER
C           AXES.
C
C        REFERENCES
C           NAIR, P. V. N., AND K. G. VOHRA.  1975.  J. AEROSOL SCI.
C              6:265-271.
C           YUE, G. K.  1979.  J.AEROSOL SCI. 10:75-86.
C     ..............................................................
C
      FUNCTION SA(X)
      REAL MA,MW
      COMMON /T/ T /MA/ MA /MW/ MW /SWG/ SWG /PW0/ PW0 /PA0/ PA0
      COMMON /R/ R /DR/ DR /S/ S /DS/ DS /AW/ AW
      ALPHA(X,R,DR,S,DS)=(1.-(1.-X)/R*DR+1.5*(1.-X)/S*DS)/
     1                    (1.+X/R*DR-1.5*X/S*DS)
      CALL RHO(X,T,R,DR)
CALL SIGMA(X,T,S,DS)
ALPHAX=ALPHA(X,R,DR,S,DS)
AA=PA(X,T)/PA0
AW=PW(X,T)/PW0
SA=AA*EXP(MA/MW*ALPHAX*ALOG(SWG/AW))
RETURN
END
```

```
C
C
C     ..............................................................
C
C        FUNCTION PA(X,T)
C
C        PURPOSE
C           THIS FUNCTION CALCULATES THE VAPOR PRESSURE OF H2SO4
C           ABOVE SULFURIC ACID.
C
C        USAGE
C           PAC=PA(X,T)
C
C        DESCRIPTION OF PARAMETERS
C           PAC   - CALCULATED VAPOR PRESSURE OF H2SO4
C           X     - WEIGHT FRACTION H2SO4 IN SOLUTION
C           T     - TEMPERATURE
C
C        REMARKS
C           THE TEMPERATURE RANGE IS 50-200 CELSIUS.  THE ACCURACY
C           OF THE LINEAR LN P VS 1/T FIT IS 10%.
C
C        SUBROUTINES AND FUNCTIONS REQUIRED
C           ATSM
C           ALI
C
C        METHOD
C           THE TEMPERATURE VARIATION OF THE DATA OF GMITRO AND
C           VERMEULEN (1964) WAS FIT AS LN P VS 1/T.  SUBROUTINES
C           ATSM AND ALI FROM THE IBM SCIENTIFIC SUBROUTINE
C           PACKAGE (1970) WERE INVOKED TO INTERPOLATE FOR COMPO-
C           SITION.
C
C        REFERENCES
C           GMITRO, J. I., AND T. VERMEULEN.  1964.  AIChE J.
C                 10:740-746.
C           I. B. M. CORP.  1970.  SYSTEM/360 SCIENTIFIC SUBROUTINE
C                 PACKAGE.  VERSION III.  5th ED.  GH20-0205-4.
C                 INTERNATIONAL BUSINESS MACHINES CORP., WHITE PLAINS,
C                 NEW YORK.
C
C     ..............................................................
C
C
      FUNCTION PA(X,T)
      REAL M(20)
      DIMENSION Z(20),F(20),B(20),ARG(10),VAL(10)
C
C        Z IS THE VECTOR OF H2SO4 WEIGHT FRACTIONS
C        M IS THE VECTOR OF SLOPES OF LN PA VS 1/TABS,
C           PA IN PA, T IN K.
C        B IS THE VECTOR OF INTERCEPTS OF THE LN PA VS 1/TABS
C           LINES.
C
      DATA Z/0.5,0.6,0.7,0.72,0.74,0.76,0.78,0.8,0.82,0.86,0.9,0.92,
     1        0.94,0.96,0.98,0.99,0.995,0.998,0.999,1./
      DATA M/-5624.1145,-5052.9897,-4857.3888,-4866.5577,-4715.4360,
     1        -4527.5525,-4508.6673,-4337.8722,-4297.9535,-3776.2812,
     2        -3955.0535,-3736.2152,-3109.3157,-3432.5217,-3363.2735,
     3        -2914.6968,-2919.0985,-2922.4874,-2839.1437,-3770.0445/
      DATA B/11.659114,11.318657,11.779284,12.000124,11.844194,
     1        11.604006,11.751047,11.535394,11.631277,10.735882,
     2        11.442977,10.940634,9.624158,10.476220,10.389028,
     3         9.389026,9.416559,9.434403,9.267724,11.497936/
C
C        FOR A GIVEN TEMPERATURE GENERATE THE VECTOR OF PRESSURE
C        NODE POINTS
C
      TK=T+273.15
      DO 1 I=1,20
       F(I)=M(I)/TK+B(I)
    1 CONTINUE
C
C        INTERPOLATE ALONG THE CURVE OF PA(X) AT CONSTANT T
C
      CALL ATSM(X,Z,F,20,1,ARG,VAL,10)
      CALL  ALI(X,ARG,VAL,Y,10,0.005,IER)
C
C        CONVERT BACK TO CARTESIAN COORDINATES
C
      PA=EXP(ALOG(10.)*Y)
      RETURN
      END
C
C     ..................................................................
C
C        FUNCTION PW
C
C        PURPOSE
C           THIS FUNCTION CALCULATES THE VAPOR PRESSURE OF H2O ABOVE
C           SULFURIC ACID SOLUTION.
C
C        USAGE
C           PWC=PW(X,T)
C
C        DESCRIPTION OF PARAMETERS
C           PWC   - CALCULATED VAPOR PRESSURE OF H2O, Pa
C             X   - SOLUTION COMPOSITION, WT. FRACTION H2SO4
C             T   - TEMPERATURE, CELSIUS
C
C        REMARKS
C           THE TEMPERATURE RANGE IS 50-200 CELSIUS.  THE ACCURACY
C           OF THE LINEAR LN P VS 1/T FIT IS 10%.
C
C        SUBROUTINES AND FUNCTION SUBPROGRAMS REQUIRED
C           ATSM (AITKEN TABLE SEARCH, MONOTONIC)
C           ALI  (AITKEN-LAGRANGE INTERPOLATION)
C
C        METHOD
C           THE TEMPERATURE VARIATION OF THE DATA OF GMITRO AND
```

```
C          VERMEULEN (1964) AND KEENAN et al. (1969) WAS FIT AS
C          LN P VS 1/T.  SUBROUTINES ATSM AND ALI FROM THE IBM
C          SCIENTIFIC SUBROUTINE PACKAGE WERE INVOKED TO INTERPOLATE
C          FOR COMPOSITION.
C
C       REFERENCES
C          GMITRO, J.I., AND T. VERMEULEN (1964) AIChE J. 10:740-746.
C          I. B. M. CORP.  1970.  SYSTEM/360 SCIENTIFIC SUBROUTINE
C                PACKAGE.  VERSION III.  5th ED.  GH20-0205-4.
C                INTERNATIONAL BUSINESS MACHINES CORP., WHITE PLAINS,
C                NEW YORK.
C          KEENAN,J.H., F.G. KEYES, P.G. HILL, AND J.G. MOORE.  1969.
C                STEAM TABLES.  JOHN WILEY & SONS, INC., NEW YORK,
C                NEW YORK.
C
C     .....................................................................
C
C
      FUNCTION PW(X,T)
      REAL M(34)
      DIMENSION Z(34),F(34),B(34),ARG(10),VAL(10)
C
C        Z IS THE VECTOR OF H2SO4 WEIGHT FRACTIONS
C        M IS THE VECTOR OF SLOPES OF LN PA VS 1/TABS,
C           PA IN PA, T IN K.
C        B IS THE VECTOR OF INTERCEPTS OF THE LN PA VS 1/TABS
C           LINES.
C
      DATA Z/0.,0.3,0.35,0.4,0.45,0.5,0.55,0.6,0.65,0.7,0.72,0.74,0.76,
     1      0.78,0.8,0.82,0.84,0.86,0.88,0.9,0.91,0.92,0.93,0.94,0.95,
     2      0.96,0.97,0.98,0.985,0.99,0.995,0.998,0.999,1./
      DATA M/-2168.945958,-2197.207388,-2212.756088,-2237.438547,
     1      -2271.399770,-2316.514300,-2370.307991,-2433.037812,
     2      -2518.307053,-2635.040052,-2692.454451,-2756.425485,
     3      -2828.733666,-2911.199984,-3007.756126,-3114.106427,
     4      -3213.158275,-3301.870770,-3400.437567,-3494.147784,
     5      -3544.417491,-3598.509274,-3647.343587,-3683.049838,
     6      -3738.743619,-3788.352356,-3827.128187,-3899.926919,
     7      -3944.894872,-3903.160331,-4062.515413,-4445.443303,
     8      -4741.096955,-4920.147464/
      DATA B/10.80085,10.769469,10.769193,10.781296,10.803889,10.847749,
     1     10.869256,10.892628,10.933958,11.007144,11.050274,11.100038,
     2     11.160581,11.235104,11.334218,11.446489,11.520699,11.550587,
     3     11.601769,11.624455,11.641614,11.663854,11.663381,11.618861,
     4     11.605811,11.550045,11.430249,11.311767,11.211946,10.820317,
     5     10.742814,11.172975,11.615409,11.728771/
C
C        GENERATE THE VECTOR OF PRESSURE VALUES FOR THE GIVEN
C        TEMPERATURE
C
      TK=T+273.15
      DO 1 I=1,34
       F(I)=M(I)/TK+B(I)
    1 CONTINUE
C
```

```
C        INTERPOLATE ALONG THE CURVE OF PW(X) AT CONSTANT T
C
      CALL ATSM(X,Z,F,34,1,ARG,VAL,10)
      CALL  ALI(X,ARG,VAL,Y,10,0.005,IER)
C
C        CONVERT BACK TO CARTESIAN COORDINATES
C
      PW=EXP(ALOG(10.)*Y)
      RETURN
      END
C
C     ..................................................................
C
C        SUBROUTINE RHO
C
C        PURPOSE
C           THIS SUBPROGRAM CALCULATES THE DENSITY OF SULFURIC ACID
C           SOLUTION FOR A GIVEN TEMPERATURE AND COMPOSITION.  ALSO IT
C           CALCULATES THE SLOPE OF THE DENSITY VS. COMPOSITION VALUE
C           AT THE GIVEN TEMPERATURE AND COMPOSITION.
C
C
C        USAGE
C           CALL RHO (X,T,R,DRDX)
C
C        DESCRIPTION OF PARAMETERS
C              X -  ACID SOLUTION COMPOSITION, WT. FRACTION H2SO4
C              T -  TEMPERATURE, CELSIUS
C              R -  INTERPOLATED VALUE OF DENSITY, KG/M3
C           DRDX -  OUTPUT VALUE OF SLOPE OF DENSITY VS COMPOSITION
C                   CURVE, KG/M3
C
C        REMARKS
C           DATA WAS AVAILABLE ONLY UP TO 100 CELSIUS.  FOR TEMPERATURES
C           ABOVE THAT, LINEAR EXTRAPOLATION WAS USED.
C
C        SUBROUTINES AND FUNCTION SUBPROGRAMS REQUIRED
C           ATSM (AITKEN TABLE SEARCH, MONOTONIC)
C           ALI  (AITKEN-LAGRANGE INTERPOLATION)
C           DGT3 (DERIVATIVE OF A GENERAL TABLE, PARABOLIC FIT)
C
C        METHOD
C           THE TEMPERATURE VARIATION OF THE DATA OF PERRY AND
C           CHILTON (1972) WAS FIT AS LN P VS 1/T.  SUBROUTINES ATSM
C           AND ALI FROM THE IBM SCIENTIFIC SUBROUTINE PACKAGE (1970)
C           WERE INVOKED TO INTERPOLATE FOR COMPOSITION.  IBM
C           SUBROUTINE DGT3 WAS THEN USED TO DIFFERENTIATE THE TABLE
C           VALUES.
C
C        REFERENCES
C           I. B. M. CORP.  1970.  SYSTEM/360 SCIENTIFIC SUBROUTINE
C                 PACKAGE.  VERSION III.  5th ED.  GH20-0205-4.
C                 INTERNATIONAL BUSINESS MACHINES CORP., WHITE PLAINS,
C                 NEW YORK.
C           PERRY, J.H. AND C.H. CHILTON, Eds.  1972.  CHEMICAL
```

```
C                  ENGINEERS' HANDBOOK.  5th Ed.  McGRAW-HILL BOOK CO.
C                  NEW YORK, NEW YORK.
C
C     ..................................................................
C
C
      SUBROUTINE RHO(X,T,R,DR)
      REAL M(11)
      DIMENSION Z(11),F(11),B(11),DF(11),ARG(11),VAL(11)
C
C        Z IS THE VECTOR OF H2SO4 WEIGHT FRACTIONS
C        M IS THE VECTOR OF SLOPES OF RHO VS T, RHO IN KG/M**3,
C            T IN DEG. C.
C        B IS THE VECTOR OF INTERCEPTS OF THE RHO VS T LINES.
C
      DATA Z/0.,0.3,0.4,0.5,0.6,0.7,0.8,0.9,0.95,0.99,1./
      DATA M/-0.74791,-0.6925,-0.7275,-0.7535,-0.7895,-0.8595,
     1      -0.9735,-1.0170,-0.9820,-0.9602,-0.9580/
      DATA B/1025.55,1232.77,1317.15,1409.85,1513.83,1627.21,
     1      1746.15,1834.26,1853.16,1853.15,1849.36/
C
C        FOR A GIVEN TEMPERATURE, GENERATE THE VECTOR OF DENSITIES
C
      DO 1 I=1,11
       F(I)=M(I)*T+B(I)
    1 CONTINUE
C
C        INTERPOLATE ALONG THE CURVE OF DENSITY VERSUS COMPOSITION
C        AT CONSTANT TEMPERATURE
C
      CALL ATSM(X,Z,F,11,1,ARG,VAL,6)
      CALL  ALI(X,ARG,VAL,Y,6,0.5,IER1)
C
C        CALCULATE THE DERIVATIVES AT THE NODE POINTS
C        INTERPOLATE FOR THE DERIVATIVE AT THE COMPOSITION OF INTEREST
C
      CALL DGT3(Z,F,DF,11,IER2)
      CALL ATSM(X,Z,DF,11,1,ARG,VAL,6)
      CALL  ALI(X,ARG,VAL,DY,6,0.5,IER3)
C
C        OUTPUT DESIRED DENSITY AND SLOPE
C
      R=Y
      DR=DY
      RETURN
      END
C
C
C     ..................................................................
C
C        SUBROUTINE SIGMA
C
C        PURPOSE
C           THIS SUBPROGRAM CALCULATES THE SURFACE TENSION OF SULFURIC
C           ACID SOLUTION FOR A GIVEN TEMPERATURE AND COMPOSITION.  THE
```

```
C        SLOPE OF THE SURFACE TENSION VS COMPOSITION CURVE IS ALSO
C        CALCULATED.
C
C     USAGE
C        CALL SIGMA (X,T,S,DSDX)
C
C     DESCRIPTION OF PARAMETERS
C           X -  ACID SOLUTION COMPOSITION, WT. FRACTION H2SO4
C           T -  TEMPERATURE, CELSIUS
C           S -  INTERPOLATED VALUE OF SURFACE TENSION, J/M**2
C        DSDX -  OUTPUT VALUE OF SLOPE OF THE SURFACE TENSION VS
C                COMPOSITION CURVE, J/M**2
C
C     REMARKS
C        DATA WAS AVAILABLE ONLY UP TO 50 CELSIUS.  FOR TEMPERATURES
C        ABOVE THAT, LINEAR EXTRAPOLATION WAS USED. THE DATA IS
C        STORED BELOW IN UNITS OF DYNE/CM.
C
C     SUBROUTINES AND FUNCTION SUBPROGRAMS REQUIRED
C        ATSM (AITKEN TABLE SEARCH, MONOTONIC)
C        ALI  (AITKEN-LAGRANGE INTERPOLATION)
C        DGT3 (DERIVATIVE OF A GENERAL TABLE, PARABOLIC FIT)
C
C     METHOD
C        THE TEMPERATURE VARIATION OF THE DATA OF SABININA AND
C        TERPUGOV (1935) WAS LINEARLY FIT.  SUBROUTINES ATSM
C        AND ALI FROM THE IBM SCIENTIFIC SUBROUTINE PACKAGE (1970)
C        WERE INVOKED TO INTERPOLATE FOR COMPOSITION.  IBM
C        SUBROUTINE DGT3 WAS THEN USED TO DIFFERENTIATE THE TABLE
C        VALUES.
C
C     REFERENCES
C        I. B. M. CORP.  1970.  SYSTEM/360 SCIENTIFIC SUBROUTINE
C              PACKAGE.  VERSION III.  5th ED.  GH20-0205-4.
C              INTERNATIONAL BUSINESS MACHINES CORP., WHITE PLAINS,
C              NEW YORK.
C        SABININA, L. AND L. TERPUGOV.  1935.  Z. PHYS. CHEM.
C              A173:237-241.
C
C  ............................................................
C
C
      SUBROUTINE SIGMA (X,T,S,DS)
      REAL M(15)
      DIMENSION Z(15),F(15),DF(15),B(15),ARG(11),VAL(11)
C
C        Z IS THE VECTOR OF H2SO4 WEIGHT FRACTIONS
C        M IS THE VECTOR OF SLOPES OF SIGMA VS TEMPERATURE LINES,
C        DYNE/(CM-C)
C        B IS THE VECTOR OF INTERCEPTS OF THE SIGMA VS T LINES, DYNE/CM
C
      DATA Z/0.,0.2418,0.3851,0.4113,0.4584,0.5344,0.5677,0.6034,
     1          0.6669,0.7350,0.7976,0.8616,0.9190,0.9771,1./
      DATA M/-0.1675,-0.0985,-0.0875,-0.0821,-0.0755,-0.0524,-0.0409,
     1       -0.0359,-0.0318,-0.0259,-0.0268,-0.0270,-0.0277,-0.0303,
     2      -0.0304/
      DATA B/76.000,76.485,77.971,78.067,78.135,77.620,77.167,76.779,
     1      75.812,74.241,72.058,68.256,62.535,55.491,53.182/
      DO 1 I=1,15
       F(I)=M(I)*T+B(I)
    1 CONTINUE
C
C        FIRST INTERPOLATE BETWEEN CONSTANT X LINES
C
      CALL ATSM(X,Z,F,15,1,ARG,VAL,6)
      CALL  ALI(X,ARG,VAL,Y,6,0.1,IER1)
C
C        THEN DIFFERENTIATE ALONG X AND INTERPOLATE THESE VALUES
C
      CALL DGT3(Z,F,DF,15,IER2)
      CALL ATSM(X,Z,DF,15,1,ARG,VAL,6)
      CALL  ALI(X,ARG,VAL,DY,6,0.1,IER3)
C
C        A FACTOR OF 1.E-3 IS REQUIRED TO CHANGE THE UNITS OF SIGMA FROM
C        DYNE/CM TO J/M**2
C
      S=Y*1.E-3
      DS=DY*1.E-3
      RETURN
      END
```